UNIVERSITY OF CALIFORNIA,
IRVINE

The modulating effect of ocean thermal forcing on the retreat of Greenland's marine-terminating glaciers

DISSERTATION

submitted in partial satisfaction of the requirements
for the degree of

DOCTOR OF PHILOSOPHY

in Earth System Science

by

Michael Wood

Dissertation Committee:
Professor Eric Rignot, Chair
Professor Mathieu Morlighem
Professor Isabella Velicogna

2019

DEDICATION

In memory of Samuel "Samwise" Boldissar

Climb on my friend.

TABLE OF CONTENTS

LIST OF FIGURES

LIST OF TABLES

ACKNOWLEDGMENTS

I would like to thank my Ph.D. advisor Dr. Eric Rignot for taking me on as a Ph.D. student in 2014 when I had little background in glaciers and ice sheets. I am immensely grateful for his endless support of my projects, my travel to conferences and several field seasons in Greenland, and my professional development activities. The time he has spent arduously reviewing countless reports, manuscripts, slides and other ideas has supported my growth as a researcher and helped me build a foundation for the rest of my scientific career. I especially appreciate the balance he struck between being patient with my development as a graduate student and pushing me when I needed it.

This work would have also been impossible without all of the additional help and support I've received from my faculty mentors, collaborators, and fellow graduate students at UCI. I appreciate the time and support my Ph.D. committee members Dr. Isabella Velicogna and Dr. Mathieu Morlighem have provided for me over the years, both in comments, suggestions, and criticisms of my work, as well as extracurricular support outside of the office. I've had the pleasure to work under their mentorship on the work outlined in this dissertation as well as other projects to progress our understanding of processes contributing to past, present, and future changes on the ice sheet. I also have an immense amount of gratitude for Drs. Jérémie Mouginot and Bernd Scheuchl, two amazing research associates who took me under their wing when I was a wide-eyed, first-year graduate student and helped get me on track to become a successful researcher. I am also grateful for the helpful contributions and support that my fellow graduate students and postdocs have provided including Lu An, Virginia Brancato, Cilan Cai, Emily Kane, Xin Li, Romain Millan, and Hongju Yu. I have also enjoyed working and spending time with Yara Mohajerani whose insightful world view has consistently changed my prospective of science and life in general.

I have also received help and insight from lots of collaborators at other institutions and abroad. My involvement with NASA's Ocean Melting Greenland campaign has formed the backbone and motivation for this Ph.D. project, and I am deeply appreciative of Steve Dinardo, Ian Fenty, and Josh Willis for including me in this project and being patient with my work as I progressed through my graduate program. Ian, along with Dimitris Menemenlis, also consistently provided support and guidance with the ECCO simulations that were instrumental in this project. I am also thankful for the help and guidance of Anders Bjørk who, in addition to helping with my research, is probably the coolest scientist I have ever met. Finally, I'd like to thank the crew members on the MV Cape Race, the RV Neptune, and the SY Ivilia; Chris Kemp and the folks at Terrasond; and Nolwenn Chauché, Pauline Chauché, and James Killingbeck from Access Arctic for helping to collect key data around Greenland and getting us through rough conditions in one piece.

Outside of research, I'd like to thank those who have helped me develop as an instructor in the classroom including my mentors in the Earth System Science department and the folks at the Division of Teaching Excellence and Innovation. I appreciate the time Drs. Julie Ferguson and Elizabeth Crook have spent reviewing my teaching materials and allowing me to practice facilitating lectures in their courses. I am also thankful for the guidance of Drs. De Gallow, Danny Mann, and Matthew Mahavongtrakul and the support of the past and present Pedagogical Fellows for reshaping my prospective of teaching and allowing me to develop within a safe learning space.

Last but not least, I'd like to thank my friends, family, and girlfriend for their help and encouragement while I have undertaken this journey. I can't imagine going through this program without their support. They have been endlessly enthusiastic about my work and have gone out of their

way to help me, whether it was a short drive in California or via encouraging emails sent to boost my morale in the field. I can't begin to express my gratitude for this love.

This work was performed in the Department of Earth System Science at the University of California, Irvine, with funding from NASA's Oceans Melting Greenland campaign. The ESS department has been an incredible place to pursue a doctorate degree from the faculty members and graduate students to the staff making it all happen. The student affairs managers who have headed our department in my time here, including Morgan Sibley Jaycee Chu, and Melanie Nakanishi, have always made ESS feel like a home for me. And Elliot McCollum, I can't thank you enough for all of the logistics you've helped organize over the past few years – I don't know how the department would function without you.

CURRICULUM VITAE

Michael Wood

EDUCATION

Doctor of Philosophy in Earth System Science **2019**
University of California, Irvine *Irvine, CA*

Bachelor of Science in Mathematical Sciences **2013**
University of California, Santa Barbara *Santa Barbara, CA*

RESEARCH EXPERIENCE

Graduate Research Assistant **2014–2019**
University of California, Irvine *Irvine, California*

TEACHING EXPERIENCE

Teaching Assistant **2015–2018**
University of California, Irvine *Irvine, CA*

Instructor of Record **Summer 2018**
University of California, Irvine *Irvine, CA*

Pedagogical Fellow **2017**
University of California, Irvine *Irvine, CA*

JOURNAL PUBLICATIONS

Forty-six years of Greenland Ice Sheet mass balance from 1972 to 2018 **2019**

Jérémie Mouginot, Eric Rignot, Anders Bjørk, Michiel van den Broeke, Romain Millan, Mathieu Morlighem, Brice Noël, Bernd Scheuchl, **Michael Wood**

Proceedings of the National Academy of Sciences

Modeling the response of Northwest Greenland to enhanced ocean thermal forcing and subglacial discharge **2019**

Mathieu Morlighem, **Michael Wood**, Helene Seroussi, Youngmin Choi, Eric Rignot

The Cryosphere

Detection of Glacier Calving Margins with Convolutional Neural Networks: A Case Study **2019**

Yara Mohajerani, **Michael Wood**, Eric Rignot, Isabella Velicogna

Remote Sensing

Control of ocean temperature on Jakobshavn Isbræs present and future mass loss **2018**

Johannes Bondzio, Mathieu Morlighem, Helene Seroussi, **Michael Wood**, Jeremie Mouginot

Geophysical Research Letters

Ocean-induced melt triggers glacier retreat in Northwest Greenland **2018**

Michael Wood, Eric Rignot, Ian Fenty, Dimitris Menemenlis, Romain Millan, Mathieu Morlighem, Jeremie Mouginot, Helene Seroussi

Geophysical Research Letters

Vulnerability of Southeast Greenland Glaciers to Warm Atlantic Water From Operation IceBridge and Ocean Melting Greenland Data **2018**

Romain Millan, Eric Rignot, Jeremie Mouginot, **Michael Wood**, Anders Anker Bjørk, Mathieu Morlighem

Geophysical Research Letters

Comparison of four calving laws to model Greenland outlet glaciers **2018**

Youngmin Choi, Mathieu Morlighem, **Michael Wood**, Johannes H Bondzio

The Cryosphere

Modeling the Response of Nioghalvfjerdsfjorden and Zachariae Isstrøm Glaciers, Greenland, to Ocean Forcing Over the Next Century **2017**

Youngmin Choi, Mathieu Morlighem, Eric Rignot, Jérémie Mouginot, **Michael Wood**

Geophysical Research Letters

BedMachine v3: Complete bed topography and ocean bathymetry mapping of Greenland from multibeam echo sounding combined with mass conservation **2017**

Mathieu Morlighem, Chris Williams, Eric Rignot, Lu An, Jan Erik Arndt, Jonathan Bamber, Ginny Catania, Nolwenn Chauché, Julian Andrew Dowdeswell, Boris Dorschel, Ian Fenty, Kelly Hogan, Ian Howat, Alun Hubbard, Martin Jakobsson, Tom M Jordan, Kristian Kjellerup Kjeldsen, Romain Millan, L Mayer, Jérémie Mouginot, Brice PY Noël, Colm OCofaigh, Steven Palmer, Soren Rysgaard, Helene Seroussi, Martin Siegert, Patricia Slabon, Fiamma Straneo, Michiel van den Broeke, Wilhelm Weinrebe, **Michael Wood**, Karl Brix Zinglersen

Geophysical Research Letters

SELECTED CONFERENCE PRESENTATIONS

Assessing the role of the ocean in the widespread retreat of Greenland's tidewaters glaciers over the past three decades (Talk) **2018**

American Geophysical Union Fall Meeting, Washington D.C.

On the ocean-induced retreat of northwest Greenland glaciers: Insights from Oceans Melting Greenland (OMG) bathymetric mapping in 2017 (Talk) **2018**

NASA Program for Arctic Regional Climate Assessment, Greenbelt, MD

Increased ocean-induced melt triggers glacier retreat in northwest and southeast Greenland (Talk) **2017**

American Geophysical Union Fall Meeting, New Orleans, LA.

Oceans Melting Greenland (OMG) mapping of northwest Greenland via ship-based echo-sounding and airborne gravity, with insights into the recent behavior of its glaciers (Poster) **2017**

NASA Program for Arctic Regional Climate Assessment, Greenbelt, MD

On the response of northwest Greenland glaciers to ocean thermal forcing (Poster) **2016**
American Geophysical Union Fall Meeting, San Francisco, CA

Oceans Melting Greenland: Season 2015 (Talk) **2016**
NASA Program for Arctic Regional Climate Assessment, Greenbelt, MD

Oceans Melting Greenland (OMG) bathymetric mapping of northwest Greenland and implications for the recent evolution of its glaciers (Poster) **2015**
American Geophysical Union Fall Meeting, San Francisco, CA

ABSTRACT OF THE DISSERTATION

The modulating effect of ocean thermal forcing on the retreat of Greenland's marine-terminating glaciers

By

Michael Wood

Doctor of Philosophy in Earth System Science

University of California, Irvine, 2019

Professor Eric Rignot, Chair

In recent decades, tidewater glaciers in Greenland have exhibited a complex spatial pattern of retreat and contributed significantly to sea level rise. This development has been coincident with the warming of ocean waters around Greenland's continental shelf and within its fjords. Here, I use a combination of regional ocean state estimates, remotely-sensed data of glacier evolution, and novel observations of bathymetry and water temperature from NASA's Ocean Melting Greenland mission to quantify the role of warm, salty Atlantic Water in controlling the retreat of 226 marine-terminating glaciers from 1985 to present. Modeled ocean-induced undercutting of calving margins compared with ice advection and ice front change indicates that glacier perturbations are largely triggered by excess melt by the ocean. Subsequent ice front retreat is determined by the bed geometry underneath the ice and the progression of ice front undercutting after retreat: Shallow protrusions, submerged sills and colder, fresher water act to stabilize ice fronts, while deeper, warmer fjords tend to enhance retreat. Despite the role of the ocean in inducing the inland migration of glacier margins, calving processes still dominate the total ablation on the periphery of the ice sheet. This work highlights the role of ocean temperature variability in modulating the retreat of Greenland's glaciers.

Chapter 1

Introduction

1.1 Recent Evolution of the Greenland Ice Sheet

The Greenland Ice Sheet (GrIS) contains approximately 3.0×10^6 km^3 (2.7×10^6 Gt) of ice [Morlighem et al., 2017] – the equivalent of approximately 7.4 m of sea level rise or 6.7% of the total freshwater on Earth. In recent decades, the GrIS has been losing mass at an accelerating rate, contributing to global sea level rise at 0.38 mm/decade between 1972 and 1992 and 5.04 mm/decade between 1992 and 2018 [Mouginot et al., 2019]. The ice sheet loses mass in two main processes: negative surface mass balance anomalies and increased ice dynamics.

Surface mass balance (SMB) reflects the balance of accumulation and ablation processes on the surface of the ice sheet. The ice sheet accumulates mass as precipitation in the form of snow or refrozen rain (P), and loses mass by evaporation (E), sublimation (S), and runoff (R) into the surrounding ocean, i.e.

$$SMB = P - E - S - R \text{ [Gt/yr]} \tag{1.1}$$

SMB is positive in Greenland as accumulation via snow and rain exceeds that which is lost through ablation processes. However, runoff from the ice sheet has increased within the past two decades,

yielding a negative anomaly in SMB (Figure 1.1).

Ice dynamics represents the interrelated changes in glacier length, ice thickness, and flow speed at the 260+ glaciers which flow from the interior ice divide of the GrIS to the periphery. Marine-terminating glaciers (or "tidewater" glaciers) represent the largest and fastest-flowing glaciers on the ice sheet: by width, the largest glacier in Greenland is Humboldt Glacier (∼100 km wide) in the northern sector of the ice sheet, while by ice flux, the most significant glacier is Jakobshavn Isbræ (∼33 Gt/yr) in the central west sector. Mirroring the effect of SMB, ice discharge (D) through Greenland's glaciers has increased substantially over the past several decades (Figure 1.1). The total mass balance (MB) of the ice sheet is determined by both SMB and D:

$$MB = SMB - D \text{ [Gt/yr]} \tag{1.2}$$

The negative anomaly in SMB and the increases in D over the past several decades have yielded an increasingly negative MB on the ice sheet (Figure 1.1)

Coincident with this mass loss, the ice margins of marine-terminating glaciers have retreated inland [Moon and Joughin, 2008, Murray et al., 2015, Hill et al., 2018b, Wood et al., 2018]. Glacier retreat has been most extensive in the northwest and southeast sectors – the two areas constituting the highest increase in discharge rates – yet all sectors have instances of observed glacier retreat. While the area of ice lost at glacier margins is negligible in comparison to the total area of the ice sheet, the loss of grounded ice plays an important role in its overall mass balance because ice at glacier termini provides a buttressing force against ice upstream and keeps the flow speed of the glaciers consistent through time [Meier and Post, 1987]. When this ice is removed, the glaciers will flow faster and lead to increased ice discharge – the same phenomenon observed on the ice sheet over the past four decades. The loss of floating ice attached to the front of glaciers may additionally provide a small buttressing force through friction on its shear margins, but substantial floating extensions ($>$ 5 km) are rare in Greenland: only 10 glaciers have maintained such extensions, and 6 of these have broken up since the year 2003 [e.g. Podlech and Weidick [2004]]. Thus, while the glaciers with floating extensions may be much larger and have higher absolute discharge rates, their effect on mass loss from the ice sheet may be outweighed by the vast quantity of other glaciers losing

grounded ice from the ice sheet margins.

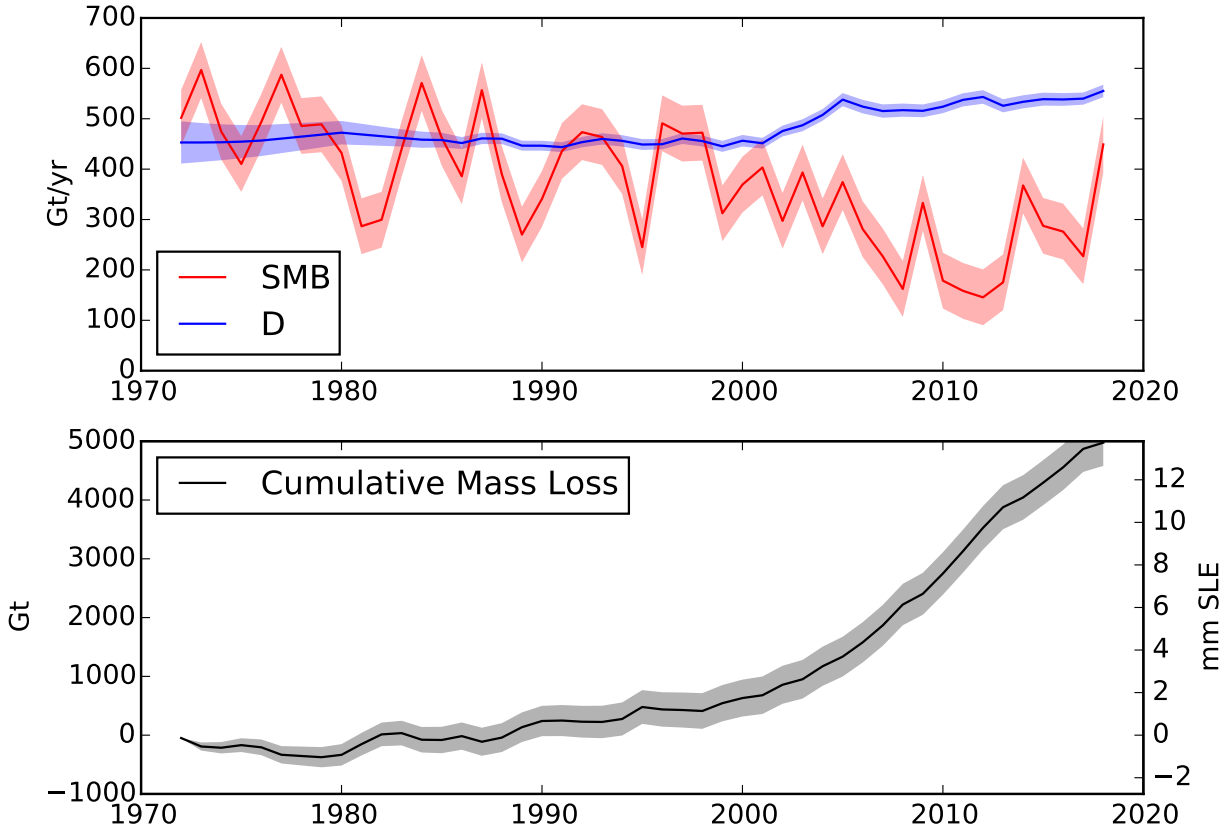

Figure 1.1: Mass Balance of the Greenland Ice Sheet 1972-2018

The annual surface mass balance and discharge estimates from Mouginot et al. [2019], yielding an accelerating mass loss from the Greenland Ice Sheet over the past 46 years.

1.2 Oceanographic Setting of Greenland

Greenland is bordered by the Subpolar Gyre of the North Atlantic Ocean to its south, Baffin Bay to its west, the Arctic Ocean to its north, and the Greenland Sea to its east (Figure 1.2). The water masses reaching Greenland's coastline can be broadly split by their source currents: The North Atlantic Current and the Transpolar Current.

The North Atlantic Current flows northwest toward Ireland where the flow splits into one branch moving northwest toward Iceland and another flowing north along Norway toward Svalbard, form-

Figure 1.2: Overview of Greenland and Surrounding Oceans

ing the Norwegian Current. The Iceland-bound current flows on the southern boundary of Iceland, around the shallow Mid-Atlantic Ridge, and then southwest toward Greenland, forming the Irminger Current (IC). When this southwesterly current meets the cold, fresh, southward-flowing East Greenland Current (EGC), the warm and salty water within the IC subducts the EGC, providing warm water below approximately 200 m. At the southern tip of Greenland, the IC turns north and flows along the southwest coast, forming the West Greenland Current (WGC). When the WGC reaches Davis Straight, the flow bifurcates with one portion moving east in the Labrador Sea and into the western lobe of the subpolar gyre, and the other portion moving north through Davis Straight. The WGC is the primary supplier of heat to Baffin Bay and the west coast of Greenland, which largely occurs via eddies on the eastern boundary of the passage. In Baffin Bay, there is an anti-cyclonic circulation, with a net northward movement on the eastern side of the basin, and southward return flow on the west side of the basin.

The Transpolar Current flows southward from the Arctic Ocean toward Greenland, with the main branch flowing toward the Greenland Sea. This flow meets the northern end of the Norwegian current on the southern boundary of Svalbard. These two currents flow south along Greenland's east coast with the cold water from the transpolar current constituting the EGC.

Figure 1.3 depicts the approximate current directions described here.

1.2.1 Historical Oceanographic and Hydrographic Observations

The common method for sampling ocean waters around Greenland is to use conductivity-temperature-depth (CTD) sensors to observe the variation of salinity and temperature with depth. Historical CTDs are compiled in the World Ocean Database [Levitus et al., 2013] and the International Council for the Exploration of the Seas Database (http://ices.dk). Due to difficulties in navigating sea ice and icebergs around the continent which increase with latitude, historical observations of Greenland's surrounding waters have been fairly sparse, and conversely decrease in availability with latitude (Figure 1.4). While some observations near northern glaciers exist, the southwest and central west regions are the best-sampled regions due to their proximity to the major towns

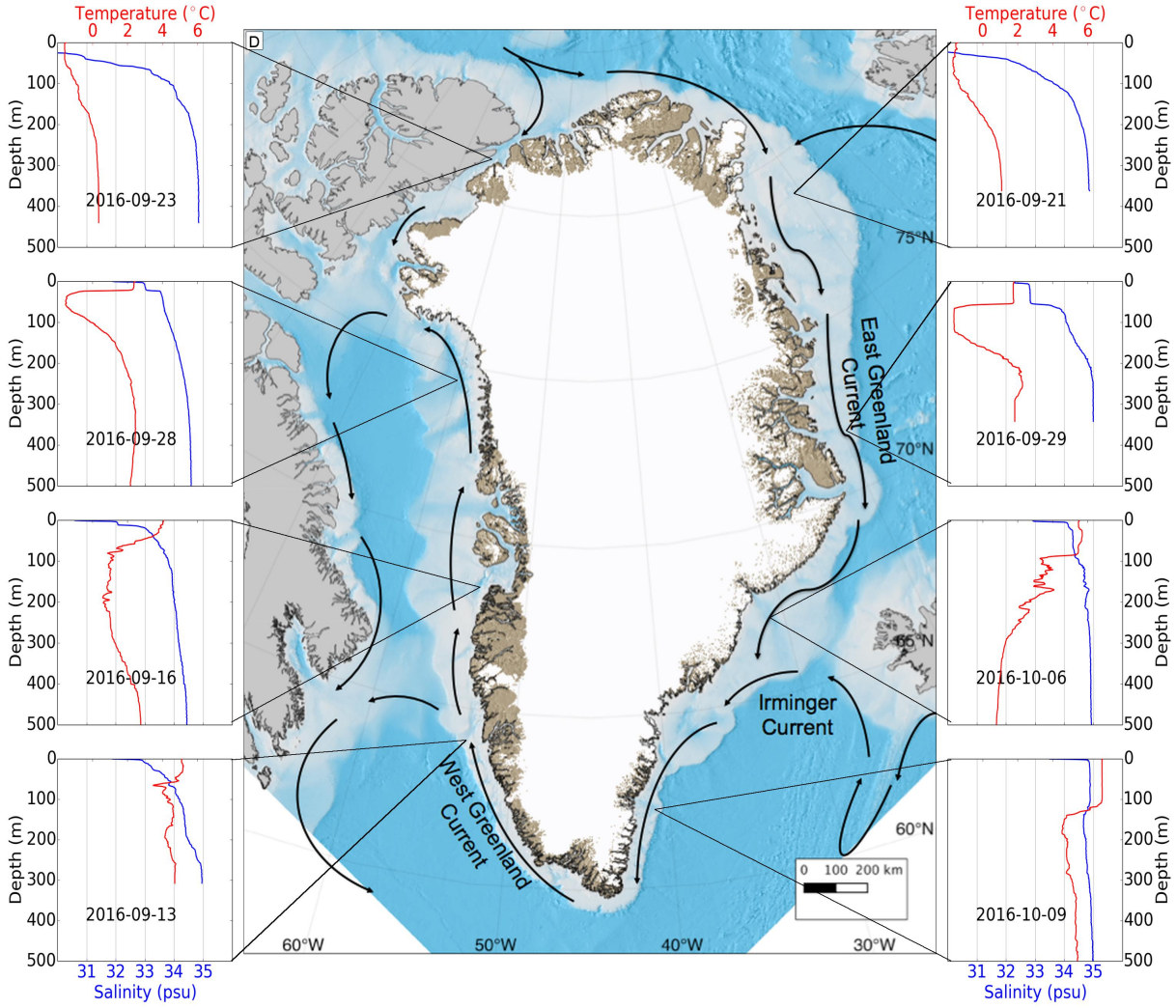

Figure 1.3: Overview of Ocean Currents and Representative Observations

Selected CTDs depicting the variation of water temperature and salinity with depth and latitude. Note that waters are typically warmer and saltier at lower latitudes, consistent with their relative distance from the North Atlantic Ocean.

and research centers on the continent. Disko Bay has been surveyed each year since 2000 by the Danish Meteorological Institute (DMI), primarily due to its relative ease of access and its close location relative to the medium-sized towns of Illullisat and Aasiaat, and the prominent glacier Jakobshavn Isbræ. DMI has also consistently sampled Godthåbsjord since 2006, which is adjacent to the Greenland Institute of Natural Resources in Nuuk and contains three large glaciers which terminate in the fjord. Other observations around Greenland have been made by smaller research excursions [e.g. Mayer et al. [2000]] and instruments on industrial fishing operations [e.g. Holland et al. [2008]]

These historical observations reveal a water column which typically consists of a cold, fresh layer of Arctic origin between the surface and 100 m (Polar Water, PW), a warm, salty layer of Atlantic origin below 200 m (Atlantic Water, AW), and a mixed transition zone in between. The warmest waters – between 6 and 9°C – are found in the southeast sector of the ice sheet where the IC delivers water from the North Atlantic Current. As the IC mixes with the EGC and ice sheet runoff along the King Christian IV coast and later in southwest Greenland, the temperature declines 1-2°C and a prominent fresh layer develops near the surface. Temperatures decline further with latitude as cold, PW is mixed within the water column, yielding a temperature range of -1 to 4°C in central west and northwest Greenland. The same latitudinal temperature gradient is observed on the east coast of Greenland with waters near the Northeast Greenland Ice Stream between -2 and 1°C. See Figure 1.3 for example CTD profiles obtained in September and October of 2016 that exemplify these latitudinal trends. Despite the mixing of PW and AW with latitude, and the modulation of these waters by ice sheet runoff and glacial melt within fjords, the deep AW layer is nonetheless a prominent feature near glacier margins. The signature of AW is most prominent in fjords closer to the IC, but is still identifiable in the few observations available for Greenland's northern-most fjords [Straneo et al., 2012].

For bathymetry, the most accurate measurements of sea floor depth come from single- and multi-beam echo sounders (SBES and MBES, respectively). Mirroring the availability of oceanographic observations, MBES measurements of bathymetry both on the continental shelf and within the fjords have primarily been limited to the subpolar gyre, a handful of regions on the continental

shelf, and a few select fjords. SBES measurements, such as those provided by fishing vessels, are more abundant and make up the majority of measurements around Greenland. These hydrographic measurements of Greenland's surrounding ocean are compiled in the International Bathymetric Chart of the Arctic Ocean [IBCAO, Jakobsson et al. [2012]].

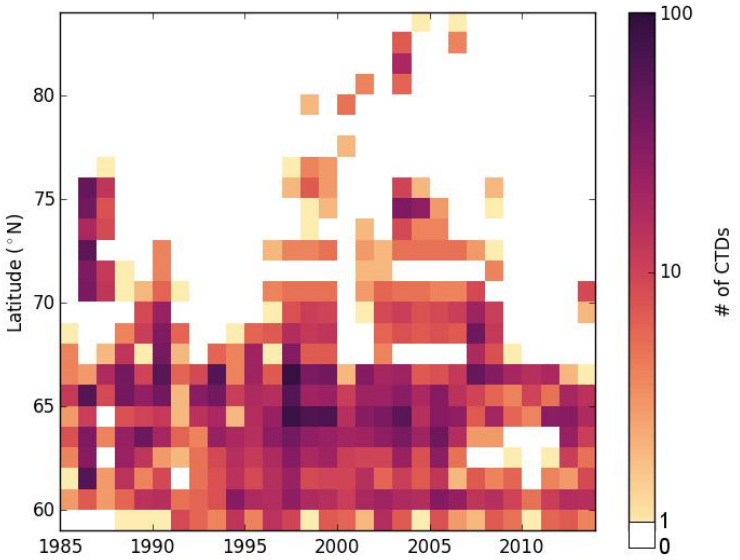

Figure 1.4: Availability of Historical CTDs around Greenland

Historical observations have been most abundant south of 68°N but some observations north of this parallel exist. The search domain for this plot is reflected in 1.2

1.2.2 ECCO Simulations

To investigate the temperature and salinity trends in other regions of Greenland where observations are less abundant, it is necessary to use ocean models which simulate the transport of heat and salt through the network of ocean currents described above. The project described herein uses ocean state estimates from the Estimating the Circulation and Climate of the Ocean (ECCO) consortium. ECCO provides products which range from data-constrained global state estimates to high-resolution simulations run from an initial (data-constrained) ocean state.

Within the ECCO framework, Rignot et al. [2012] provide a regional "Arctic Solution" which simulates the circulation around Greenland 1992-2011 at a 4 km resolution – a scale required to capture the transport of heat by eddies. Another simulation from Zhang et al. [2018] – the "LLC270

Solution" – is provided 2001-2017 at a more coarse (∼25 km) resolution constrained by observations. Together, these simulations indicate a warming of ocean waters around Greenland between 1997 and 2008 via the advection of heat anomalies from the subpolar gyre. The largest warming signal of approximately 3°C is observed in Baffin Bay, yet warming is observed along all coastlines of the ice sheet. After 2008, all regions except the northeast and central east experienced a 1-2°C cooling which persisted until the end of the simulation period. Figure 1.5 depicts the mean trends at 250 m depth for the 7 regions of Greenland as simulated in these two ocean model estimates.

Although the Arctic and LLC270 Solutions are useful for estimating temperature and salinity variability on Greenland's continental shelf and surrounding seas, they are not able to simulate circulation within fjords and the heat transport directly to the glacier terminus regions. Glacier fjords are typically 5-20 km wide which cannot be effectively captured at the resolution of these two simulations. Moreover, the models rely on the bathymetry from IBCAO which contains little information on the depth of Greenland's fjords due to a lack of hydrographic measurements. A detailed description of the model errors, the adjustments of the solutions for use within glacier fjords, and the merging procedure is provided in Section 2.3.3.

While the dearth of oceanographic and hydrographic measurements has limited the ability of these models to represent oceanographic properties and trends in close proximity to the glacier fronts, new measurements collected during the course of this project will help elucidate circulation within fjords and improve our understanding of processes directly impacting glacier stability.

1.3 Role of Ice-Ocean Interactions

The importance of a glacier's fjord environment in determining its front position was first described as a major contributor to ice front stability for Alaskan glaciers where glaciers terminating in deeper fjords were observed to retreat faster than those in shallow fjords [Post, 1975]. Ice front retreat is further enhanced if the ice front retreats into deep waters where the effective pressure-dependent melting point declines and the glacier is in contact with warmer, saltier water at depth [Meier and Post, 1987].

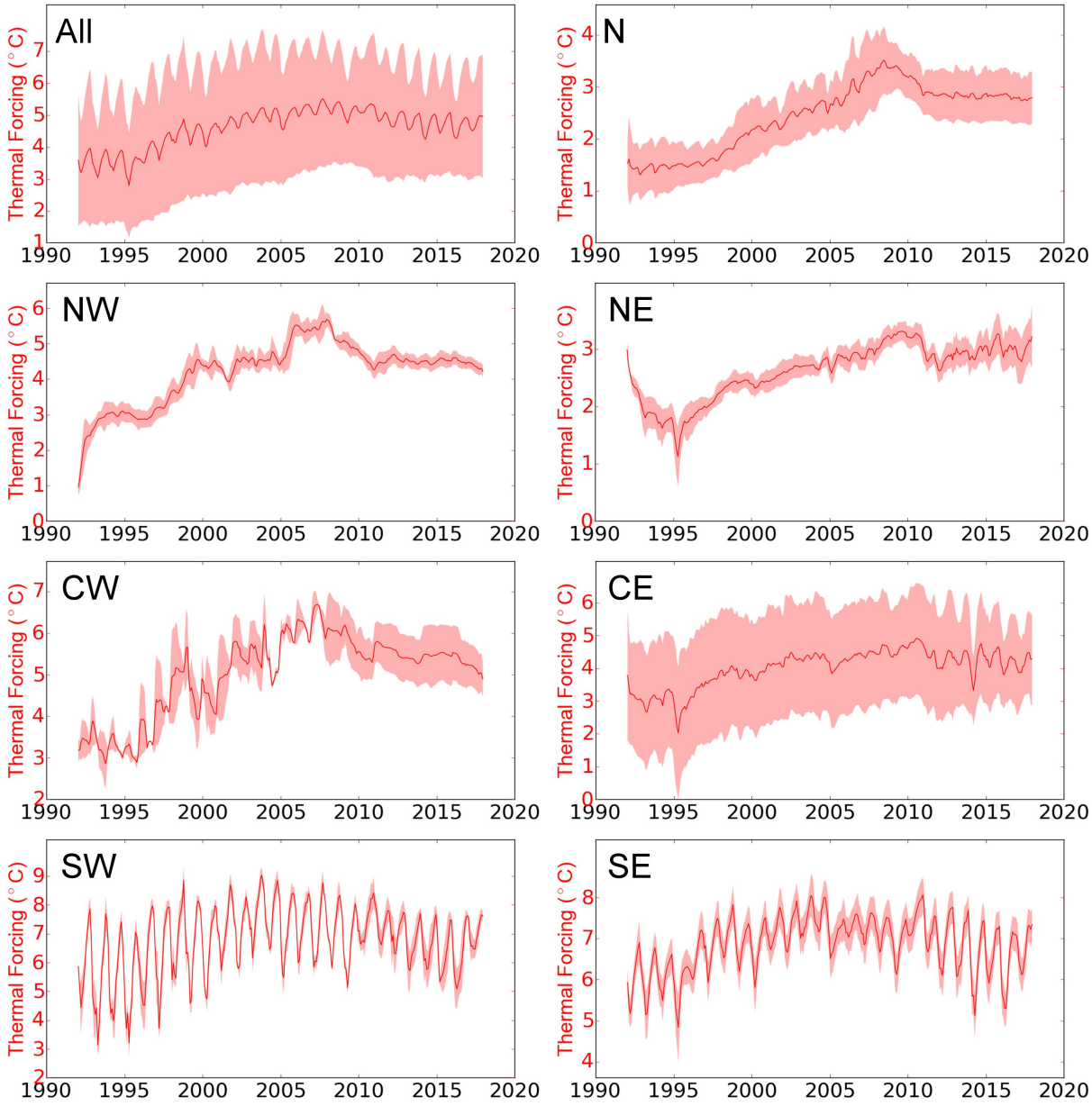

Figure 1.5: Simulated Ocean Temperature around Greenland 1992-2011

The mean temperature in the 7 sectors of the ice sheet. The shaded envelope represents one standard deviation of the sampled temperature in each of the sample areas defined in Section 2.3.3

In Greenland, ice discharge rates are typically much higher than in Alaska, and the difficulty of conducting oceanographic observations within ice-choked fjords has largely obscured the understanding of how ocean warming impacts glacier terminus stability [Joughin et al., 2012, Straneo and Heimbach, 2013]. Nonetheless, the correlative timing of ocean warming on Greenland's continental shelf and increased ice discharge from marine-terminating glaciers has suggested a strong link between the two processes. For example, warmer ocean waters advected from the subpolar gyre through Davis Straight and into Disko Bay were observed to play a critical role in the break-up of Jakobshavn Isbræ's 10 km-long floating ice extension in 2003, leading to a 100% increase in ice speed [Holland et al., 2008]. The recent slowdown and re-advance concurrent with colder waters in Disko Bay after 2015 [Khazendar et al., 2019] has provided further evidence that ocean forcing is a key factor in modulating the front positions of marine-terminating glaciers. Regional observations and ocean model estimates on the east coast of Greenland have also identified a strong relation between ice front retreat, thinning, and acceleration, and warmer ocean waters in the Greenland and Irminger Seas [Murray et al., 2010, Seale et al., 2011].

While there is substantial evidence that ocean temperature variability plays a key role in the observed evolution of Greenland glaciers, estimates of ocean-induced melt rates have been relatively sparse. Existing measurements indicate substantial melt rates between 1 and 5 m/d, which is the same order of magnitude as ice flow speeds. For example, In Torssukataq Fjord, Disko Bay, CTD measurements near 4 glaciers revealed substantial melt rates up to 3.9 m/d [Rignot et al., 2010] which compares well with ice velocities between 5 and 6 m/d. Similarly, at Saqqarliup Sermia in Illullisat Isfjord, ice melt rates were estimated at 0.5 m/d [Slater et al., 2018] which is nearly equivalent to the ice flow speed. Melt rates of the same magnitude are estimated on the east coast of Greenland: for instance, submarine melt at Helheim Glacier has been estimated at 1.8 m/d during the summer [Sutherland and Straneo, 2012]. Finally, for 13 glaciers glaciers with floating extensions, remotely-sensed estimates of ice flux and frontal ablation demonstrated melt rates of 1-3 m/d with the highest rates observed in central west Greenland [Enderlin and Howat, 2013].

Marine-terminating glaciers on the Greenland Ice Sheet form englacial hyrologic networks which transport surface melt water at inland locations to the base of the glacier terminus. This fresh

water is combined with basal melting underneath the ice and discharged at the base of the glacier terminus. Since the discharge is less dense than the surrounding fjord waters, it quickly rises toward the surface, entraining dense fjord water from depth along the way. Melt within these rising plumes reaches a maximum near the base of the glacier acting to undercut the ice front. While direct melt outside of the entrainment plumes can be substantial [Chauche, 2016, Slater et al., 2018], the intense melting at the base acts to retreat the grounding line, and small floating extensions are quickly calved off from the front. In this framework, ablation processes can be divided into melt at the base and any residual ice blocks which subsequently calve off, and iceberg calving which occurs via other processes.

There have been three main methods to infer ice front melt by the ocean within subglacial discharge plumes: conservation of mass, salt, and heat from inner-fjord CTDs, plume theory, and the parameterization model experiments. Conservation equations have been used successfully for glaciers in central west Greenland fjords [Rignot et al., 2010] although this approach requires several CTDs in close proximity to the calving front and an assumption on the circulation pattern within the fjord, yielding considerable uncertainty. Plume theory has been applied successfully in a number of fjords (e.g. Illullisat Isfjord [Slater et al., 2018, Khazendar et al., 2019]) but requires additional assumptions about the circulation within the fjord. In both of these approaches to estimating the impact of melt on the ice front location of the glacier, the exact location of ocean melt on the ice face is not determined, but rather an average is calculated. Instead, the project herein will rely on the parameterization of maximal melt near the grounding line as derived from high-resolution modeling experiments. These experiments were first carried out in 2 dimensions [Xu et al., 2012] and later in 3 dimensions [Xu et al., 2013] for melt on Store glacier in central west Greenland. Later, these model experiments were expanded to include a number of different glacier geometries [Rignot et al., 2016].

Estimates of ice front melt are critical to quantifying the impact of ocean temperature variability on the evolution of the ice sheet, both in the recent past and in projections of Greenland mass loss in the coming century. While the estimates above have provided a snapshot of this impact within specific seasons and temperature regimes, a full quantification of ocean melt around Greenland is

still lacking.

1.4 Research Objectives

The collective observations of recent glacier retreat and mass loss, estimates of ocean warming around Greenland, and the existing literature on ice-ocean interactions have provided a broad body of evidence suggesting ocean-induced melt plays a significant role in modulating the evolution of glaciers on the ice sheet. However, the relatively few studies which have attempted to quantify the magnitude of ocean melt and its role in driving changes on the ice has left the extent to which the ocean modulates mass loss from the ice sheet unclear.

The goal of the research described herein is to quantify the extent by which ocean temperature variability in the waters around Greenland has modulated the ice front positions and dynamics of the 226 marine-terminating glaciers discharging ice from the GrIS between 1992 and 2018. The central hypothesis is that increased melt on the periphery of the ice sheet removes grounded ice at glacier terminus region, leading to the retreat of ice margins and the acceleration of ice toward the ocean. Specifically, the science objectives of this project are as follows:

1) For each of Greenland's 226 marine-terminating glaciers:
    i. Reconstruct the history of ice margin positions and glacier flow speeds from remotely-sensed data
    ii. Estimate the variation in ocean-induced melt on the ice terminus using ocean state estimates and modeled fjord circulation regimes
    iii. Quantify the proportion of ice retreat attributed to ocean variability
2) Delineate categorizations for the response of glaciers to ocean temperature variability
3) Assess the proportion of recent ice sheet change which has been induced by ocean warming within the past several decades

Chapter 2

Methodology

2.1 Glacier Terminus Location

The location of a glacier's terminus is determined by the balance between the advection of ice from upstream (q_f) and the total ablation at the terminus [Rignot et al., 2016]. For marine-terminating glaciers, the two dominant ablation processes are iceberg calving (q_c) and direct melt by the ocean (q_m). Letting q_r represent the change in the glacier grounding line position, conservation of mass yields

$$q_r = q_f - q_c - q_m \text{ [m/d]} \tag{2.1}$$

where q_r is oriented to be positive in the direction of ice flow. In this framework, a glacier front will retreat (advance) if the combination of q_m and q_c are greater (less) than q_f. Figure 2.1 depicts these processes.

As described in below, the sources of q_r, q_f and q_m are derived from a combination of remotely-sensed measurements, models, and in situ observations, while q_c is inferred as the residual term in equation 2.1.

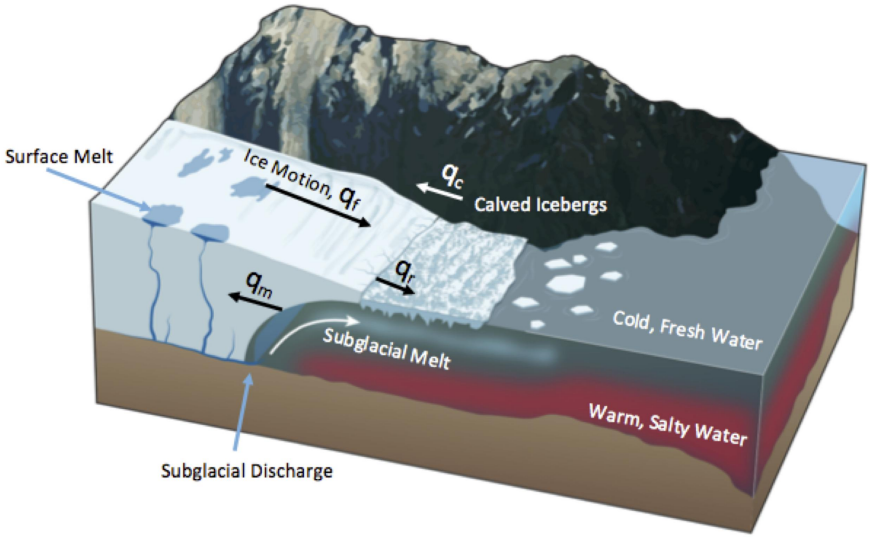

Figure 2.1: Glacier Flux Balance Diagram

Figure adapted from Straneo and Heimbach [2013]

Data Sources Glacier terminus locations are determined from historical satellite imagery from a variety of optical- and radar-based sensors. In the project described herein, imagery from Landsat 5 (1985-1998), Landsat 7 (1999-2012), and Landsat 8 (2013-2019) are utilized to derive a historical record of ice front positions. These scenes are provided by NASA and the United States Geological Survey through the "Earth Explorer" web portal (earthexplorer.usgs.gov). The resolution of these images vary from 30 m for Landsat 5, and 15 m for Landsat 7 and Landsat 8. The "green" band (Band 3, 0.52 - 0.60 μm) is used for Landsat 5 scenes while the "panchromatic" band is used for Landsat 7 (Band 8, 0.52 - 0.90 μm) and Landsat 8 (Band 8, 0.503 - 0.676 μm) scenes.

As ice front positions serve as a proxy for ice sheet flux, several datasets exist which describe their historical locations. Murray et al. [2015] digitized front positions for 199 tidewater glaciers between 2000 and 2010 from Landsat 7 imagery, providing several fronts per year during the northern hemisphere summer. Moon and Joughin [2008] digitize front positions for 203 glaciers between 2000 and 2018 from ERS-1, RADARSAT-1, Landsat-8 and Sentinel-1A/B data, providing one front per year during the northern hemisphere winter. Hill et al. [2018b] provide a longer historical record for 18 glaciers in northern Greenland from the early 1990's to present using a variety of aerial and satellite sources. These datasets are used to supplement the records generated in this

Table 2.1: UTM Zone Longitude Ranges near Greenland

UTM Zone	Longitude Range
19	72°W – 66°W
20	66°W – 60°W
21	60°W – 54°W
22	54°W – 48°W
23	48°W – 42°W
24	42°W – 36°W
25	36°W – 30°W
26	30°W – 24°W
27	24°W – 18°W

UTM zones define projections which are optimized for distance and area calculations. For integrated values, the zone corresponding to a glacier's location is used for calculations.

study.

Methods To construct records of ice front change, glacier margins are manually digitized using the open source geographical information software QGIS. Fronts are digitized and stored in polar stereographic coordinates (ESPG: 3413).

To deduce the retreat or advance of a glacier ice front between two time periods, the total change in area is calculated between the two front positions. For a linear retreat metric, the front area change is divided by the average width of all available ice fronts. This is similar to the "Box Method" [Moon and Joughin, 2008] in which the the width and orientation are chosen by hand.

Numerical Implementation To calculate the front area change for a glacier, first a sample area is defined which encompasses the front area region and an arbitrary section of the glacier upstream. Then, to calculate the area change between two observations, the front positions are used to portion the sample area into the region of the glacier delineated by the front. For efficiency, the area of the polygons are calculated using the Shoelace formula:

$$A = \frac{1}{2}\left| \sum_{n=1}^{N-1} x_n y_{n+1} + x_N y_1 - \sum_{n=1}^{N-1} x_{n+1} y_n - x_1 y_N \right| \ [\mathrm{m}^2] \tag{2.2}$$

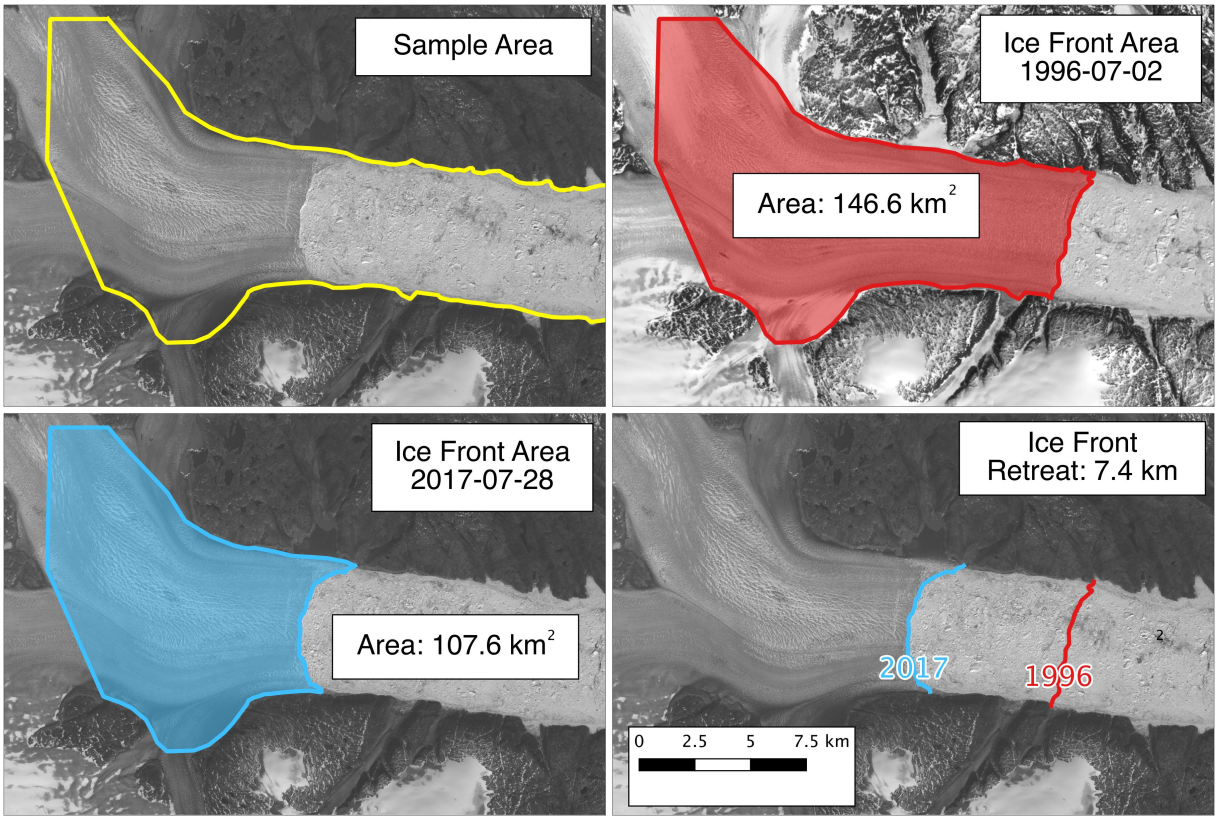

Figure 2.2: Ice Front Retreat Calculation Example

The total retreat distance is calculated as the area loss (39 km^2) divided by the width of the glacier fjord (5.3 km).

for the number of edges N of the polygon, and the verticies (x_n, y_n). The retreat/advance magnitude is the difference between the areas of these two regions. The area calculation is carried out in the coordinates of the UTM zone which pertains to the glacier's longitude (Table 2.1). This process results in the total change between the two fronts, and accounts for the circumstance where one end of the ice front advances and the other retreats. Figure 2.2 depicts the retreat calculation between two front observations at Helheim Glacier between July 2, 1996 and July 28, 2017.

2.2 Ice Velocity

The advection rate of ice – the ice velocity – is calculated using two main methods: feature tracking and interferometric synthetic aperature radar (InSAR).

Feature tracking is the strategy of determining the movement of patterns on the ice surface between two satellite image pairs. For optical sensor images, these patterns may pertain to crevasses, cracks, subaerial lakes, mineral residue from lateral moraines, and other discoloration patterns. For radar images, these patterns are derived from radar "speckle" – the variation in the phase and amplitude of the returned radar signal due to the texture of the glacier surface. Feature tracking is carried out using a sliding window which searches for the highest correlation between a "chip" in one scene and that in another. See, for example, Berthier et al. [2005] for an algorithmic description of this technique and Fahnestock et al. [2016] for a modern adaption of this process for large data sets. The vast quantity of overlapping Landsat data acquired over Greenland allows for sub-pixel precision, leading to errors less than 10 m/yr.

InSAR is the strategy of determining feature displacement within a pair of radar images. In this process, an interferogram is formed using the product of the first image and the complex conjugate of the other. The phase difference within the interferogram is then "unwrapped" to reveal the relative phase which, in turn, is the combination of topographic and displacement effects. By removing the topographic signature, the displacement (i.e. the ice velocity) is derived from the unwrapped interferogram. In terms of magnitude, errors associated with this method range from 1 m/d in regions of high coherence to 10-20 m/d where radar sampling is low and/or there is

Table 2.2: Summary of Ice Velocity Data Sources.

Source	Time Span	Sensor(s)	Method(s)
Mouginot et al. [2019]	1972-2018	Landsat 1, 2, 3, 4, 5, 7, 8	Feature Tracking
Mouginot et al. [2017]	2013-2016	Landsat 8 RADARSAT-2 Sentinel-1	Feature Tracking InSAR
Howat [2016]	2000-2010	Landsat 7	Feature Tracking
Rignot and Mouginot [2012]	2008-2009	ALOS, RADARSAT-1 Envisat	InSAR
Joughin et al. [2010] (MEaSURES)	2000 2005-2018	ALOS, RADARSAT-1 SENTINEL 1-A, TDX, TSX	InSAR
Rignot and Kanagaratnam [2006]	1996, 2000 2005	RADARSAT-1, ERS-1 ERS-2, Envisat	InSAR

significant ionospheric noise. For the flow direction, errors are highly constrained ($< 1°$) in fast flow areas, particularly near the coast, while errors may high ($> 20°$) in extremely low speed (< 10 m/yr) areas such as the interior of ice sheets [Rignot and Mouginot, 2012]. See Joughin et al. [1996] for a brief review of radar interferometry and an derivation of associated errors.

Data Sources There has been an international effort to map the velocity of Greenland's ice using both of the methods described above. See Table 2.2 for an outline of the major studies providing ice velocity data which have been sourced in this study.

Methods To formulate an annual record of ice front velocity from existing velocity products, velocity fields are averaged over one year from July 1 to June 30 onto a grid of 150 m resolution. The center time is chosen in winter when the acquisition of radar data has historically been most abundant. The velocity data is then converted to ice speed and sampled on a line parallel to the ice front position during a given year, 1 km upstream. The 1 km buffer between the actual ice front and the sampling location is induced to avoid spurious values associated with sea ice and decorrelation near the front. If the ice speed data is available for more than 75% of the 1 km sampling line, the mean values of the ice speed profile are taken as the mean ice speed of the glacier. If ice speed points are more sparse along the sampling line, an estimate is formed by scaling the averaged ice

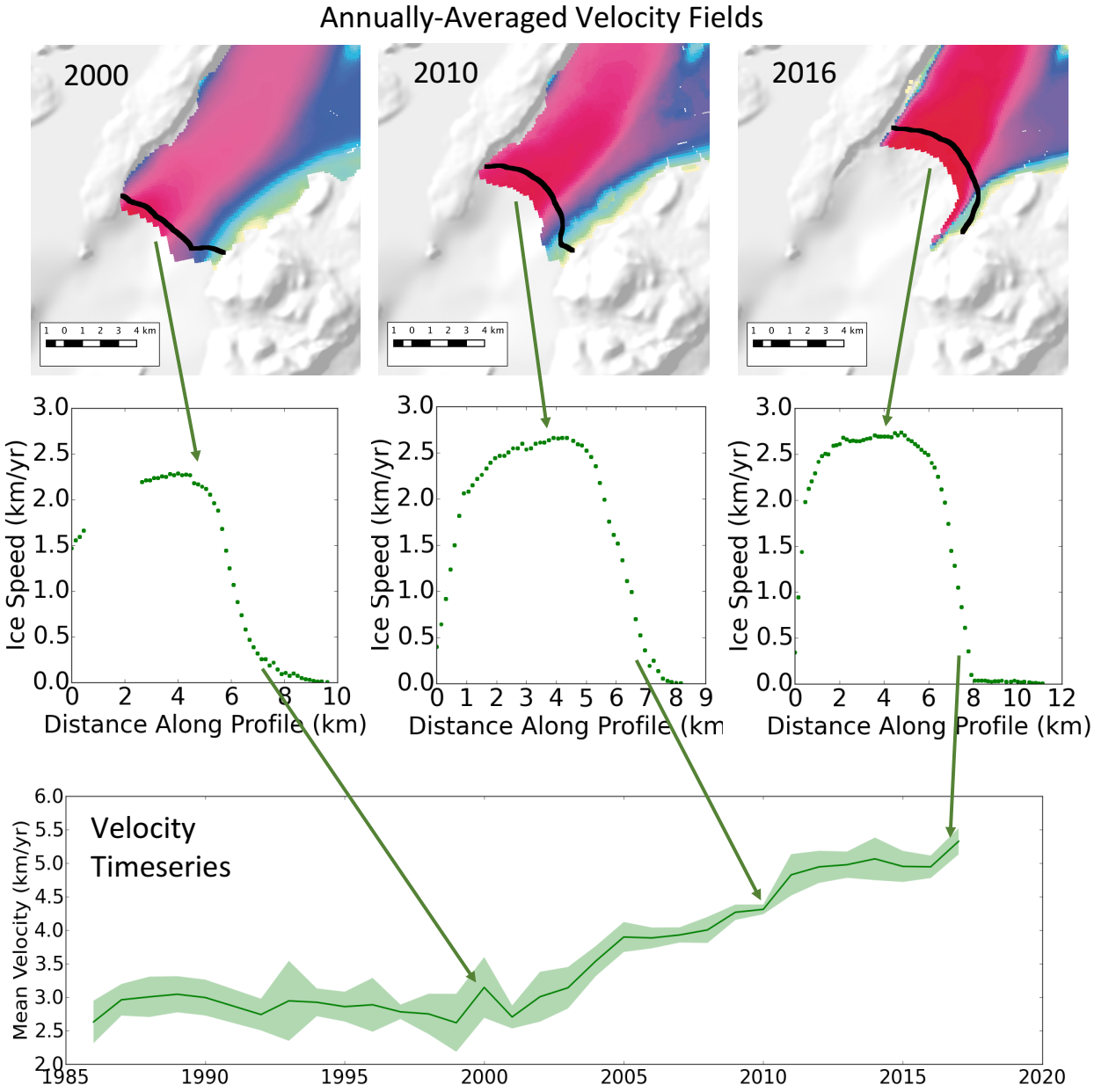

Figure 2.3: Velocity Sampling Calculation Example

Velocity timeseries are deduced from annual velocity fields sampled on lines parallel to and 1 km upstream of the ice front.

speed field 1985-2018 to the available velocity points during the given year. The 1 km line is then sampled along this scaled speed field.

Uncertainties in velocity are assessed from the sensor observations, the feature tracking and InSAR algorithms, and the averaging procedures utilized in this study. The uncertainties associated with the sensor observations and ice velocity algorithms are indicated collectively in the Data Sources section above. The errors in the scaled sampling method are typically several times larger than direct sampling due to the additional uncertainties associated with the scaling procedure.

Numerical Implementation The observed velocity field $V_{obs}(t, x, y)$ is converted to an observed ice speed field as

$$S_{obs}(t, x, y) = \sqrt{V_{obs,x}(t, x, y)^2 + V_{obs,y}(t, x, y)^2} \tag{2.3}$$

with errors computed from the observed error fields E_{obs} as

$$\Sigma_{obs}(t, x, y) = \sqrt{E_{obs,x}(t, x, y)^2 + E_{obs,y}(t, x, y)^2} \tag{2.4}$$

To derive the 1 km sampling line $\mathcal{L}$, a buffer is drawn around the closest-available terminus location so that for any point on the front, the closest buffer point is at least 1 km away. The portion of the buffer which coincides with the upstream ice area is then down-sampled to 200 points to define the sample line. The closest point in the ice speed field within 150 m is assigned to each sample line point. If there are no valid points within 150 m, the sample line point is not assigned an ice speed value.

For a given year T, if at least 75% of the sample line points are assigned ice speed values, the mean of these values is taken to estimate the mean ice speed $q_f(T)$, i.e.

$$q_f(T) = \overline{S_{obs}(T, x, y)} \text{ for } x, y \in \mathcal{L} \tag{2.5}$$

The errors associated with this sampling are taken as the mean absolute error:

$$\sigma(T) = \overline{\Sigma_{obs}(T, x, y)} \text{ for } x, y \in \mathcal{L} \tag{2.6}$$

If at least 75% of the sample line points do not have assigned ice speed values, the composite velocity field

$$C(x, y) = \overline{V(t, x, y)} \text{ for } t \in [1985, 2018] \tag{2.7}$$

is scaled to the observed ice speed. The scale factor $\alpha(x, y)$ is determined as the for each observed point as

$$\alpha(x, y) = \frac{V(T, x, y)}{C(x, y)} \tag{2.8}$$

and averaged to yield a single scale factor, α, for the sampling field. The error in this procedure is taken as the mean absolute difference between the available observed points and the scaled field:

$$\sigma(T) = \overline{|S_{obs}(T, x, y) - \alpha C(x, y)|} \tag{2.9}$$

Finally, the scaled field is sampled along the 1 km sampling line to yield an estimate of ice speed during the year:

$$q_f(T) = \overline{\alpha C(x, y)} \text{ for } x, y \in \mathcal{L} \tag{2.10}$$

See Figure 2.3 for an example calculation of an ice speed timeseries for Sverdrup Glacier in northwest Greenland.

2.3 Ice Front Undercutting

As described in section 1.3, melt within plumes of subglacial discharge water tend to undercut the ice front, causing grounding line retreat. Here, ablation processes are divided into melt at the base and any residual ice blocks which subsequently calve off as q_m and iceberg calving which occurs via other processes as q_c. Hence, the q_m term will hereafter be referred to as "ice front undercutting". In this study, a paramerization of q_m from Rignot et al. [2016] is utilized:

$$q_m = (Ahq_{sg}^{\alpha} + B)TF^{\beta} \text{ [m/d]} \tag{2.11}$$

where h is the mean water depth of the ice front, q_{sg} is the ice front area-averaged subglacial discharge and TF is the thermal forcing averaged on the glacier terminus. The constants in the parameterization are $A = 3 \times 10^{-4}$ d$^{\alpha-1}$ m$^{-\alpha}$ C$^{\circ-\beta}$, $\alpha = 0.3$, $B = 0.15$ m d^{-1} C$^{-\beta}$, and $\beta = 1.8$.

To quantify the uncertainty associated the q_m model, the uncertainties on h (σ_h), q_{sg} ($\sigma_{q_{sg}}$) and TF (σ_{TF}) are propagated through equation 2.11 assuming the uncertainty associated with each variable is independent. The partial derivatives with respect to each variable are

$$\begin{aligned}
\frac{\partial q_m}{\partial h} &= Aq_{sg}^{\alpha}TF^{\beta} \\
\frac{\partial q_m}{\partial q_{sg}} &= Ah\alpha q_{sg}^{\alpha-1}TF^{\beta} \\
\frac{\partial q_m}{\partial TF} &= \beta(Ahq_{sg}^{\alpha} + B)TF^{\beta-1}
\end{aligned}$$

With the general error propagation equation

$$\sigma_{q_m} = \sqrt{\left(\frac{\partial q_m}{\partial h}\sigma_h\right)^2 + \left(\frac{\partial q_m}{\partial q_{sg}}\sigma_{q_{sg}}\right)^2 + \left(\frac{\partial q_m}{\partial TF}\sigma_{TF}\right)^2}$$

the uncertainty on q_m (σ_{q_m}) is quantified as

$$\sigma_{q_m} = \sqrt{\left(Aq_{sg}^{\alpha}TF^{\beta}\sigma_h\right)^2 + \left(AhTF^{\beta}\sigma_{q_{sg}}\right)^2 + \left(\beta(Ahq_{sg}^{\alpha} + B)TF^{\beta-1}\sigma_{TF}\right)^2} \text{ [m/d]} \tag{2.12}$$

2.3.1 Ice Front Geometry

To estimate the mean water depth h at the terminus, it is assumed that the ice face is vertical from the ocean surface to the ice bed. Multi-beam echo sounding measurements of glacier front geometry indicate that ice fronts are approximately vertical [Fried et al., 2015, Rignot et al., 2015]. The mean water depth of the ice front is determined from the shape of the fjord bedrock in the vicinity of the ice front.

Data Sources Water depth in the terminus regions of marine terminating glaciers are sampled from the bed rock/bathymetry product BedMachine [Morlighem et al., 2017] which is currently released in Version 3. This data set has been updated to include all bathymetry measurements from NASA's Oceans Melting Greenland (OMG) campaign [OMG, 2016a] – an Earth Suborbital Venture 2 mission initiated in 2015 which encompasses a suite of measurements on fjord bathymetry, oceanographic properties, and ice geometry [Fenty et al., 2016]. See Table 2.3 for an overview of the measurement types and figure 2.7 for the spatial extent of the MBES- and airborne gravity-derived bathymetry measurements.

Bathymetry measurements from OMG were conducted by direct measurements using multi-beam echo sounders (MBES) mounted to the hulls of marine vessels, and indirect measurements from gravimeters flown over regions of interest. The MBES measurements were focused in the northwest and southeast regions of the ice sheet, and aimed at regions of the continental shelf and glacier fjords which had never been surveyed. The marine vessels used were the MV Cape Race, the RV Neptune, and the SY Ivilia during the 2015, 2016, and 2017-2018 seasons. In total, the multibeam survey covered approximately hundreds of square kilometers which had never been directly surveyed before, revealing bathymetry which was, in some locations, hundreds of meters deeper than the previous IBCAO maps indicated. While MBES measurements are highly accurate, the slow vessel speed ($\sim$ 4 nautical miles per hr) and impassable ice conditions within some fjords limit the spatial extent over which the measurements can be conducted. To broaden the regions in which bathymetry measurements can be made, OMG also collected airborne gravity measurements over the same regions. These fields can be "inverted" to retrieve an estimate of bathymetry as well as bed rock

Table 2.3: Overview of OMG Campaign Measurements

Component	Measurement Type	Sector(s)	Time Span
Bathymetry	Multibeam Echo Sounding	NW	2015, 2017
		SE	2016, 2018
	Gravity	NW, SE	2016
Temperature	CTDs	NW	2015, 2017
and Salinity	CTDs	SE	2016, 2018
	Airborne Expendable CTDs	All	2016-2021
Ice Geometry	Radar Interferometry	All	2016-2018

beneath the ice. The northwest gravity bathymetry measurements are detailed in An et al. [2019] while several subregions are detailed in Millan et al. [2018]. At the time of this writing, the study describing the full inversion of the southeast gravity fields are under review in the journal Geophysical Research Letters [An et al 2019b]. Uncertainties in the bed elevation are derived from their respective sources which are on the order of centimeters for direct single- or multi-beam sonar measurements, 10's of meters for airborne gravity measurements, and potentially more than 100 meters where measurements do not exist and synthetic/interpolated bathymetry is utilized to provide a complete map.

Methods To formulate records of mean water depth, the digitized ice front records described above are used to sample the BedMachine product. Within each profile, the submerged portions of the front are identified and averaged to yield records of the mean submerged depth as well as the submerged ice front area.

Numerical Implementation To find the mean water depth along the digitized ice front $(x, y) \in \mathcal{F}$, the front points are first sampled on BedMachine to yield a bed profile $B(x, y)$. Using these elevation points, an along-front profile $b(d)$ is constructed (e.g. see Figure 2.4 C(i-ii)). This profile is then limited to the region of the front below sea level, and the profile is integrated using the trapezoid rule to find the area A of the ice front:

$$A = \frac{1}{2} \sum_{i=1}^{N-1} (d_{i+1} - d_i)(B(d_{i+1}) + B(d_i)) \text{ [m}^2\text{]}$$

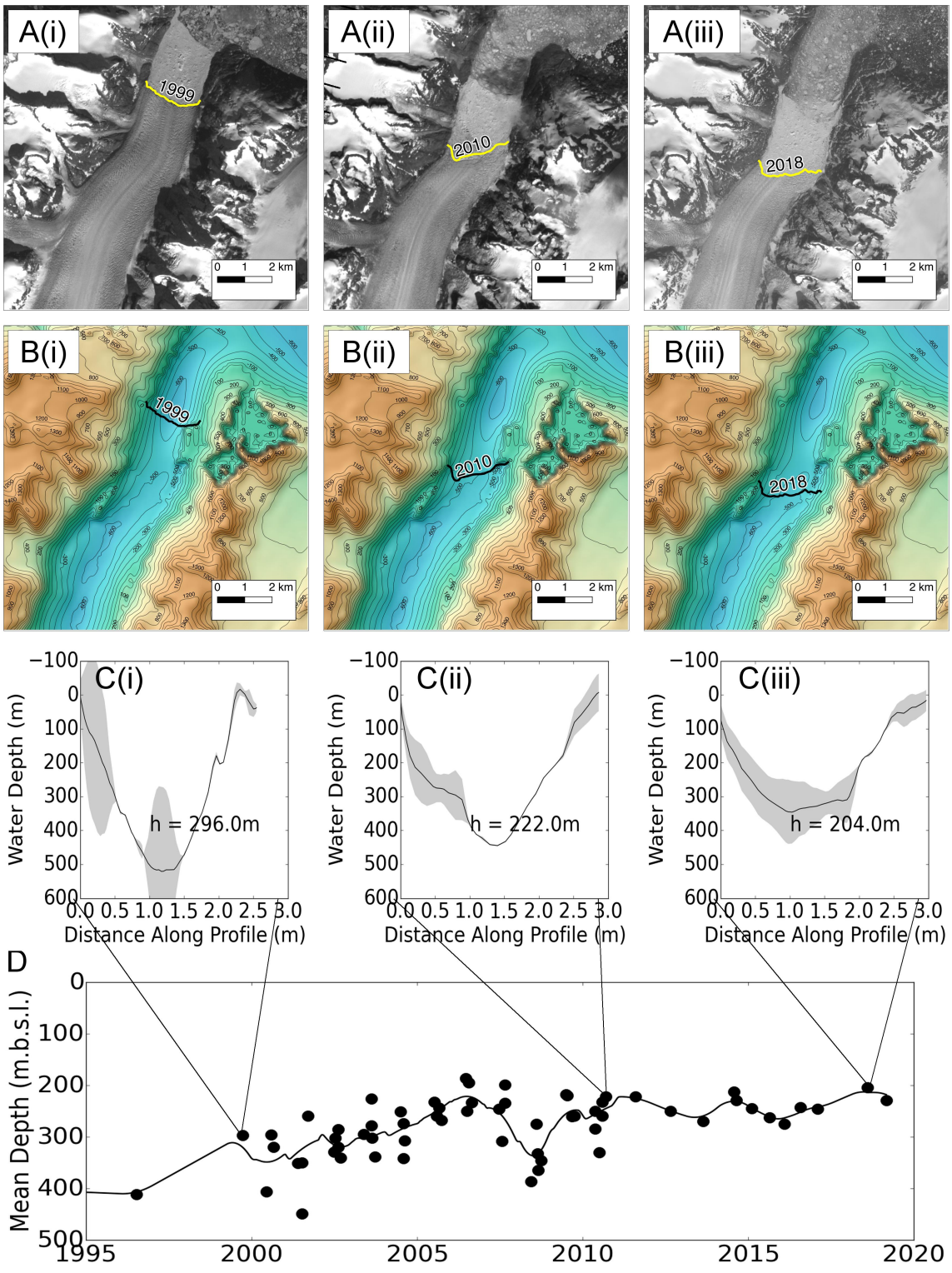

Figure 2.4: Ice Front Geometry Calculation Example

where the d_i's are the points in the along-front profile and $N = |\mathcal{F}|$. The mean water depth is deduced from the area divided by the length of the front L:

$$L = \sum_{i=1}^{N-1} (d_{i+1} - d_i)$$

i.e.

$$h = \frac{A}{L} = \frac{\frac{1}{2}\sum_{i=1}^{N-1}(d_{i+1} - d_i)(B(d_{i+1}) + B(d_i))}{\sum_{i=1}^{N-1}(d_{i+1} - d_i)} \text{ [m]} \tag{2.13}$$

2.3.2 Subglacial Discharge

Data Sources To calculate subglacial discharge, two datasets are used: one for ice sheet runoff and one for ice sheet basal melt. Ice sheet runoff is deduced from version 2.3 of the Regional Climate Model [RACMO, Noël et al. [2015]]. RACMO is developed and maintained by the Royal Netherlands Meteorological Institute (KNMI). As applied to Greenland, the model is forced using reanalysis data from the European Centre for Medium-Range Weather Forecasts to model surface mass balances process on the ice sheet at a resolution of approximately 11 km. Specifically, the study here utilizes the runoff fields from a 1 km downscaled version of RACMO2.3 (RACMO2.3p1, Noël et al. [2016]). Basal melt is the result of basal friction and geomthermal heat flux deduced using Ice Sheet System Model. The methods of this calculation are described in Seroussi et al. [2013] and initially utilized in Rignot et al. [2016] and Wood et al. [2018].

Methods To estimate subglacial discharge, basins are defined on the ice sheet which encapsulate the drainage of surface runoff from the interior of the ice sheet. Drainage basins are defined under the assumption that ice sheet runoff remains on the surface in the interior of the ice sheet, and flows through moulins and englacial hydrologic systems near the coast. This assumption is supported by the close comparison of discharge measurements and surface runoff near the town of Kangerlussuaq in West Greenland where it is possible to measure freshwater discharge on the periphery of the ice sheet [Mernild and Hasholt, 2009]. Accordingly, the boundary of the basins on the surface are defined by gradients of steepest descent in the GIMP DEM [Howat et al., 2014] for the areas on

the interior of the ice sheet. Near the coast, the basin boundaries are defined by velocity flow lines, assuming the net direction of subglacial hydrologic systems follows the ice flow directions.

The ice sheet runoff and basal melt fields are integrated over the defined basins which, in combination, make up the total freshwater flux. In the melt rate parameterization described above, subglacial discharge is utilized per unit area i.e. the total discharge volume is divided by the area of the ice front described in section 2.3.1.

Numerical Implementation The RACMO2.3p1 runoff R and ISSM-derived basal melt B are fluxes at field points on the ice sheet i.e.

$$R = R(t, x, y) \text{ and } B = B(x, y)$$

provided in mm of water equivalent per month over the glacier drainage basin $\mathcal{D}$. These fields are integrated for total monthly runoff as

$$Q_{sg}(t) = \int_{\mathcal{D}} [R(t, x, y) + B(x, y)] dxdy \text{ for } x, y \in \mathcal{D} \tag{2.14}$$

On the Greenland Ice Sheet, many basins extend from the coast to the continental divide, spanning several degrees of longitude. For example, the basin for Rink Isbrae spans 14.1 degrees from 51.7°W to 37.6°W. To get accurate measurements for the base area during the integration, the calculation must take place in an area preserving projection, just as for the retreat calculation in section 2.1. To achieve an accurate measurement, $\mathcal{D}$ is divided into several subareas ($\mathcal{D}_i$'s) pertaining to the area-preserving UTM projections which overlap the basin (See Table 2.1 for zone domains). The integration is then carried out by dividing each $\mathcal{D}_i$ into Delunay Triangles and integrating the fields over each triangle using the volume formula

$$V = \frac{1}{3}(h_1 + h_2 + h_3)A_{base}$$

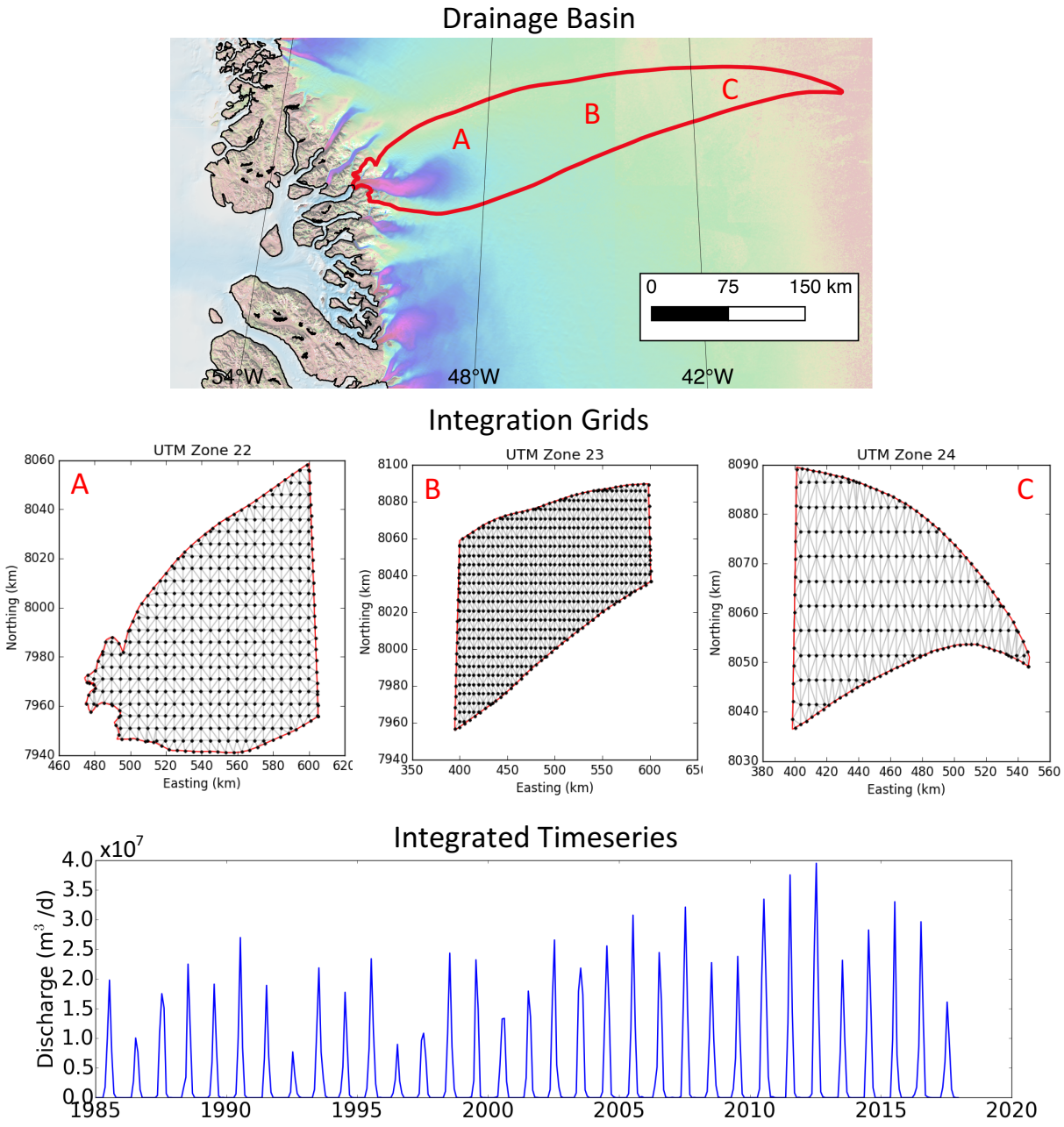

Figure 2.5: Subglacial Discharge Calculation Example

Example of the integration of subglacial discharge calculation for Rink Isbræ in central west Greenland. The drainage basin is divided into separate sections by UTM zone, the runoff is integrated on each subsection, and the combined result yields a record of runoff from 1985 to 2018.

where A_{base} is the area of the base. For efficiency, this area is calculated using the vertex formula

$$A = \left| \frac{v_{1,x}(v_{2,y} - v_{2,y}) + v_{2,x}(v_{3,y} - v_{1,y}) + v_{3,x}(v_{1,y} - v_{2,y})}{2} \right|$$

where the v_i's are the vertex coordinates of the triangular base. In terms of $S = R+B$ the numerical integration sum is

$$Q_{sg} = \sum_{\mathcal{D}_i} \sum_{N} \frac{1}{3}[S(x_1, y_1) + S(x_2, y_2) + S(x_3, y_3)] \tag{2.15}$$

where N is the number of Delunay triangles with vertices given by the field S. For points on the boundary of $\mathcal{D}$, S is interpolated linearly between nearby grid points. Finally, the area-average discharge is deduced by dividing Q_{sg} by the submerged area of the terminus determined in section 2.3.1. See Figure 2.5 for an example of this calculation for Rink Isbræ in West Greenland.

2.3.3 Thermal Forcing

Thermal Forcing – the difference between the *in situ* temperature of sea water and its freezing point – is used to quantify the heat available to melt glacial ice. Due to the lack of sufficient observations for the 1992-2019 time period investigated, it is necessary to use model simulations to examine thermal forcing over time. However, as described in section 1.2.2, presently-available simulations have two main draw backs: 1) they do not exist for the entire time period, and 2) the solutions do not extend into the glacier fjords. To remedy the first problem, two existing simulations are "merged" to create a product which spans the investigation period. To address the second problem, CTD measurements within the fjords are used to adjust the thermal forcing estimates on the continental shelf to estimates within the fjords. In the following section, the merging of model solutions on the continental shelf is addressed first, and the adjustment between shelf and fjord waters are addressed second.

Table 2.4: Comparison of ECCO Solutions.

	4 km Solution	LLC270 Solution
Time Span	1992-2011	2001-2017
Domain	Arctic	Global
Configuration	Forward	Data Assimilation
Resolution	4 km	13.5 km
Bathymetry	IBCAO V3	IBCAO V3

Thermal Forcing on the Continental Shelf

Data Sources The Estimating the Circulation and Climate of the Ocean (ECCO) consortium is a multi-intitutional framework which yields ocean state estimates on both regional and global scales. Two of these solutions – the "4 km Solution" [Rignot et al., 2012] and the "LLC270 Soluion" [Zhang et al., 2018] – were discussed in the introductory section 1.2.2. These solutions have important trade-offs as outlined in Table 2.4 leading to sometimes large differences in their solution. See, for example, the comparison of solutions in November 2005 (figure 2.6).

The historical CTDs were discussed previously in the introduction, in section 1.2.1. The available CTDs around Greenland include those in the World Ocean Database [Levitus et al., 2013] and the International Council for the Exploration of the Seas Database (http://ices.dk). More recently, CTDs are provided by the OMG campaign [OMG, 2016b] and other smaller research endeavors. CTD measurements taken during OMG were conducted both by ship and by air. The ship-based CTDs were taken from the ships used for the MBES bathymetry mapping. The MV Cape Race and RV Neptune were equipped with winches and specialized CTD probes designed to be used while the vessel was under way in relatively ice free conditions. On the SY Ivilia, and in icy conditions for all vessels, the CTDs were taken by hand. The ship based measurements were supplemented by airborne expendable CTDS (AXCTDs) deployed from DC-8 aircraft. The span of these measurements range from the interior regions of the fjords to the outer regions of the continental shelf, in all sectors of the ice sheet besides the southwest where ongoing surveys are conducted by DMI (Figure 2.7).

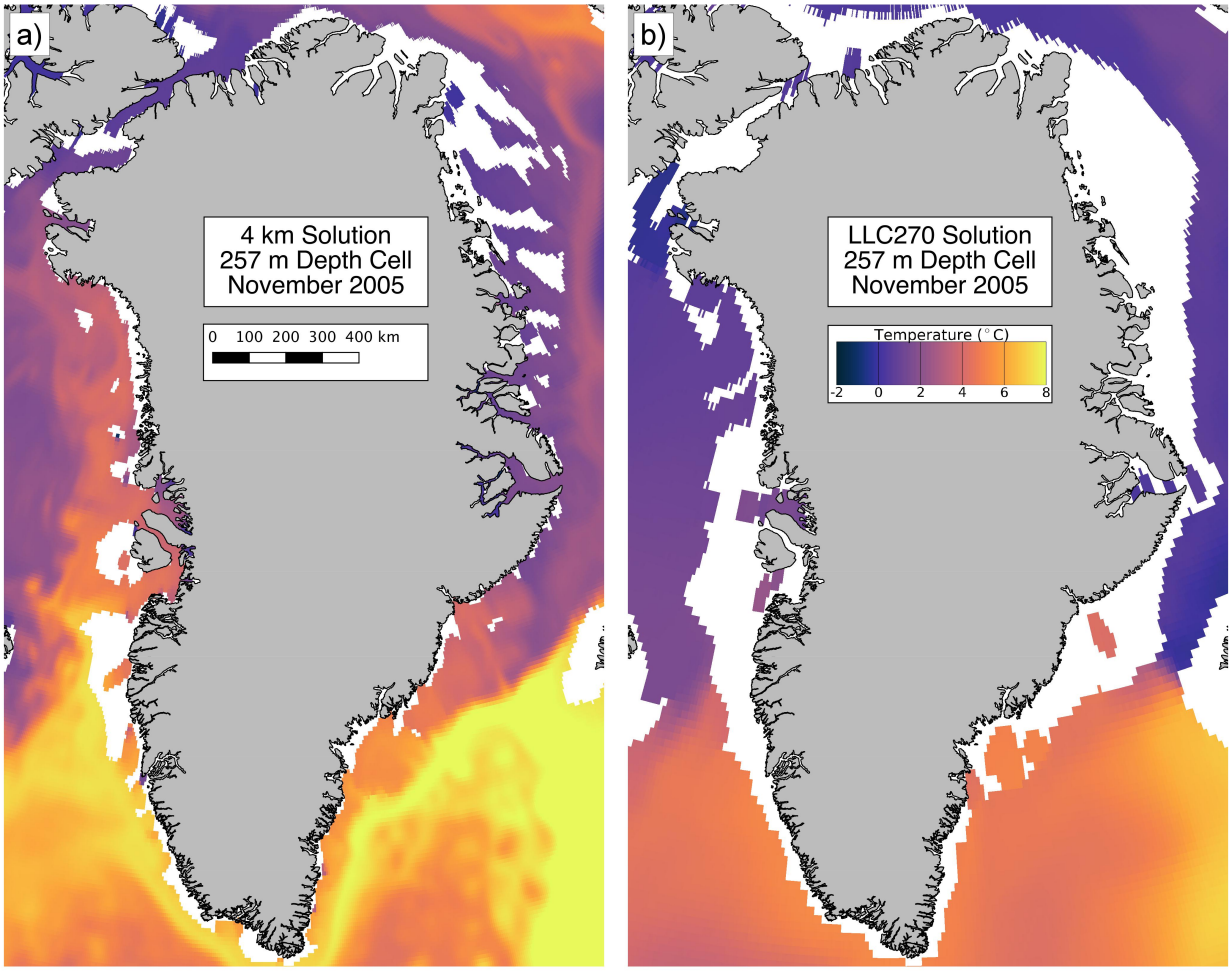

Figure 2.6: ECCO Solution Comparison.

The 4 km Solution in the left plot captures eddies and fine scale circulation such as the Irminger Current in southeast Greenland. The lower resolution LLC270 maintains the same general temperature structure but lacks many of the same details. Additionally, Baffin Bay and the Greenland Sea are much colder due to less efficient transfer of heat through defined currents.

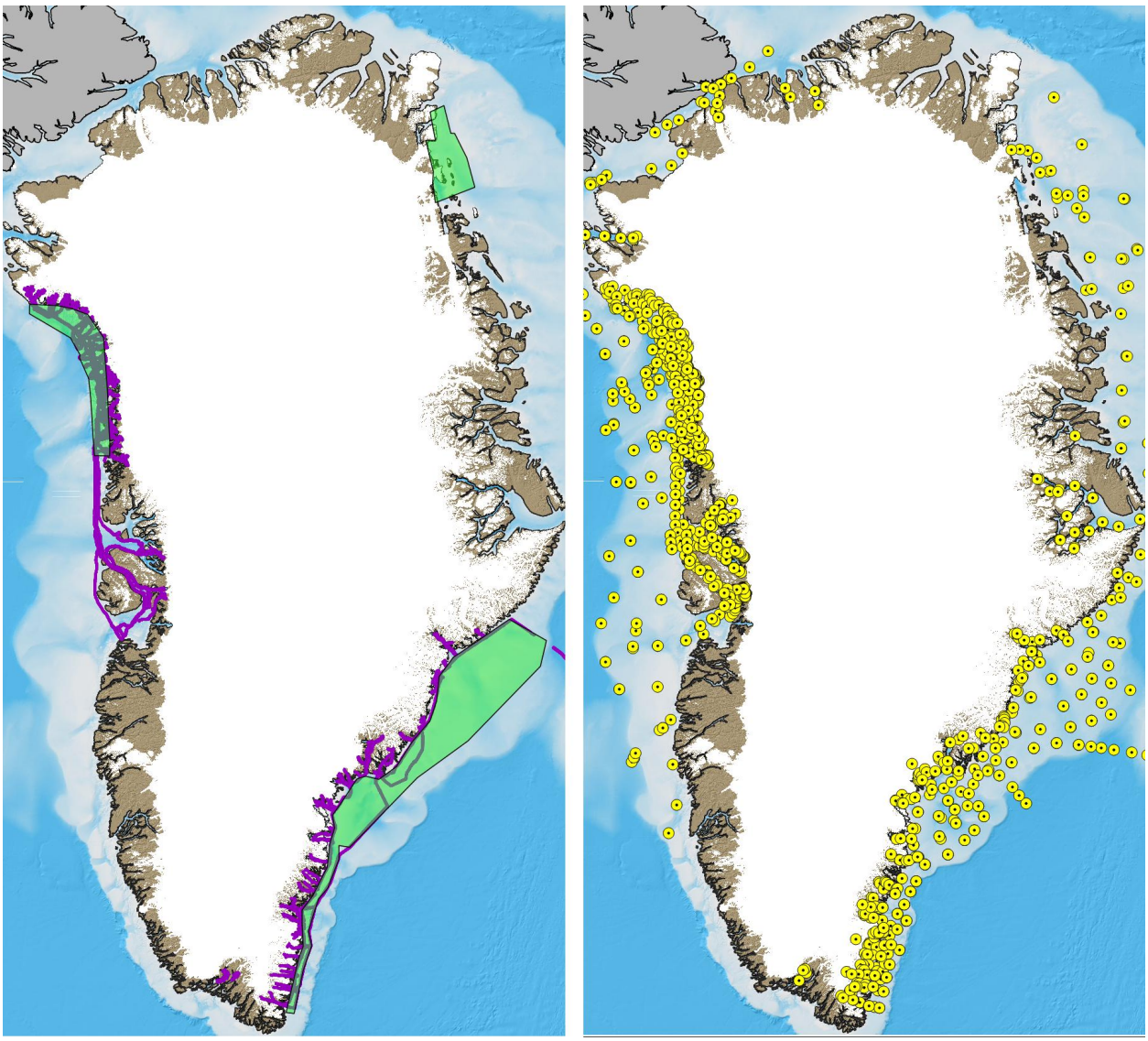

Figure 2.7: Overview of OMG Measurements

The left plot shows the extent of gravity measurements in green and MBES measurements in purple. The right plot shows the extent of AX/CTDs from the OMG campaign 2015-2018.

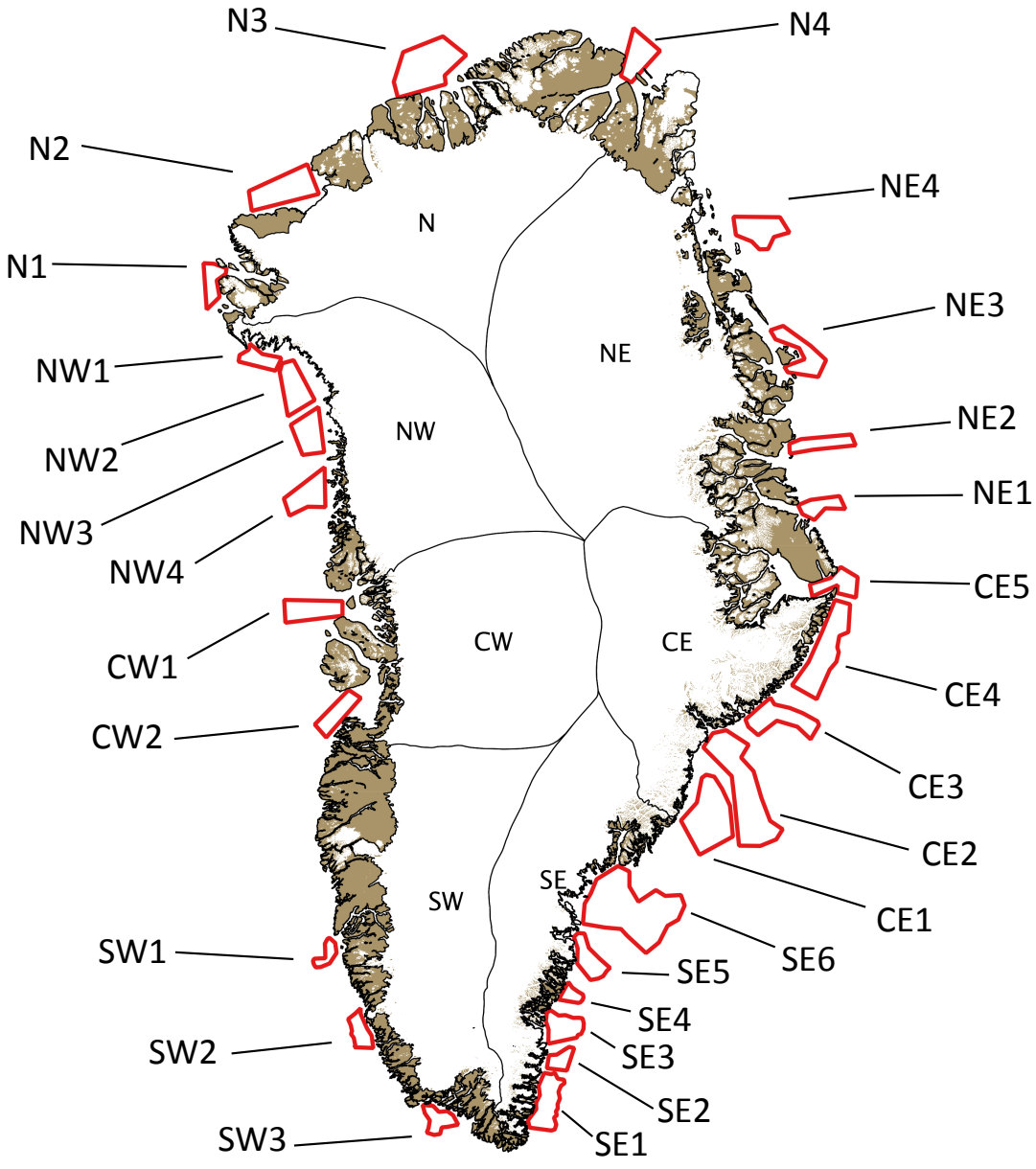

Figure 2.8: Sample Area Locations

The 28 sample regions defined around the Greenland Ice Sheet. The sample areas are chosen in deep areas of the continental shelf that represent pathways of deep, warm AW from the outer shelf area toward the glacier fjords.

Methods In the present ECCO model framework, the models have neither the resolution nor accurate bathymetry necessary to represent flow through troughs on the continental shelf and inside the glacier fjords. Therefore, to get an estimate of ocean properties within the fjords, it is necessary to first sample the ocean models in areas on the continental shelf which are nearby the individual glaciers and deep enough to capture deep, warm Atlantic water which has the potential to enter the fjords. There were 28 different areas chosen along the Greenland coastline which fit this criterion (Figure 2.8).

The ECCO solutions output three key variables required to deduce thermal forcing: potential temperature θ, salinity S and pressure P. With S and P, the in situ freezing point is deduced using the parameterization

$$T_{freeze} = -0.0575S \ \frac{^\circ\text{C}}{\text{PSU}} + 0.0901 - 0.000761P \ \frac{^\circ\text{C}}{\text{dbar}} \tag{2.16}$$

Thermal forcing, which provides a useful quantification of the heat available to melt glacial ice, is defined as

$$TF = T - T_{freeze} \tag{2.17}$$

where T is the in situ temperature of the sea water. To calculate TF from these variables, the potential temperature θ is converted to in situ temperature T using the Gibbs Seawater Oceanographic Toolbox software package (teos-10.org/software).

Figure 2.6 illustrates the need to reconcile the differences between the two solutions and form a merged ocean product in order to use them together for long-term solutions of ocean thermal forcing around Greenland. This merging procedure is conducted by first adjusting the vertical structure in the LLC270 solution to match that in the 4 km solution. The underlying assumption in this approach is that the higher resolution model will be able to better capture the heat transport processes that lead to the vertical water profile within the sample areas. Then, the adjusted solutions are merged by creating a linear smoothing between the the 4 km solution and the LLC270 solution over a common time period. Finally, the merged solution is adjusted with CTDs to provide

a best-match estimate to observations.

Numerical Implementation For each sample area S and for each model $M \in \{4\text{km, LLC}\}$, the thermal forcing is averaged horizontally, i.e.

$$TF_{M,S}(t,d) = \overline{TF_{M,S}(t,x,y,d)} \text{ for all } x,y \in S \tag{2.18}$$

See Figure 2.9 for an example of this sampling in the CW1 sample area.

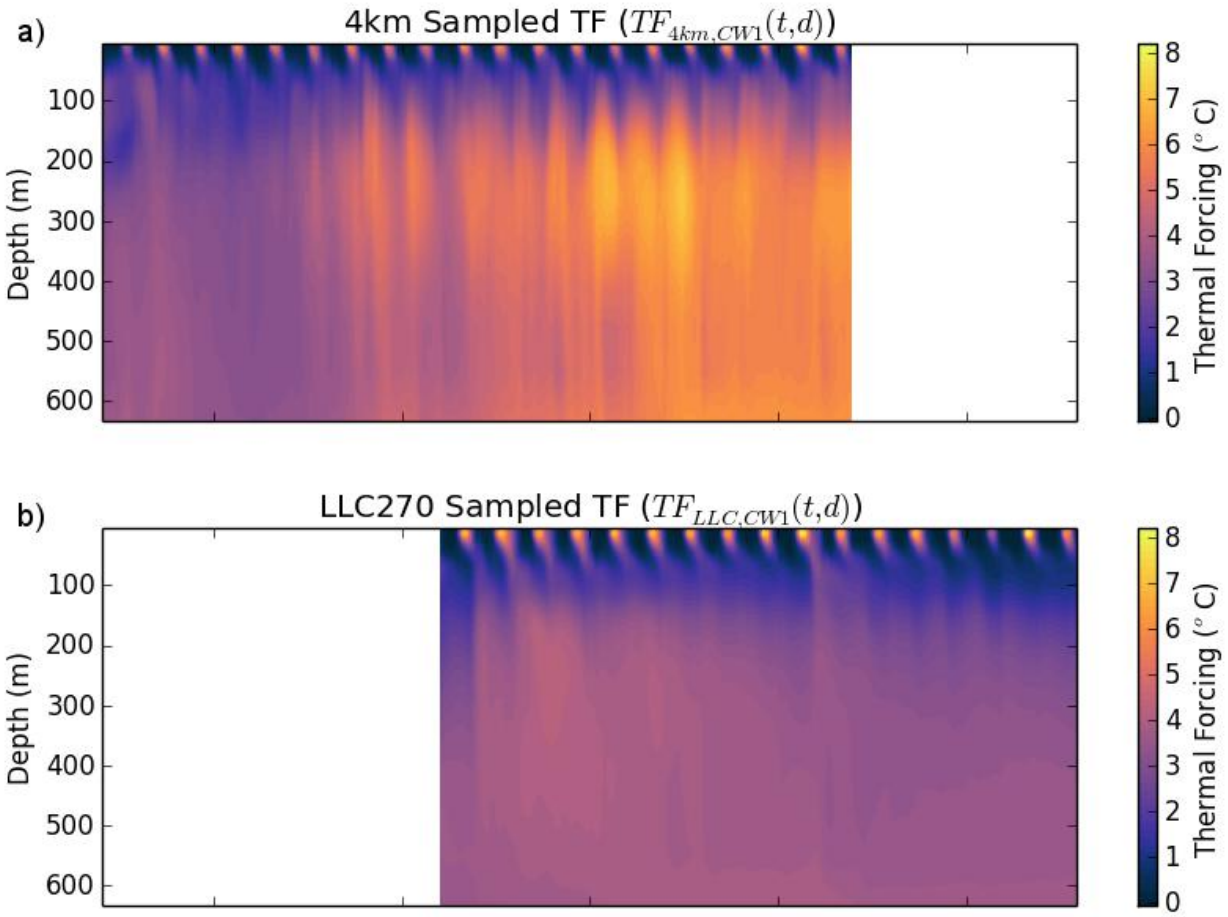

Figure 2.9: Thermal Forcing Comparison: Model Output

The differences in the vertical TF structure and temperature trend are clear in the horizontally averaged solutions.

Prior to merging the models, the 4 km Solution is adjusted to address the known biases: an overall $+0.4°$C bias and an initial $-1°$C bias in Baffin Bay. The $+0.4°$C bias is addressed by applying an

absolute adjustment $\mathcal{A}_1 = -0.4°\text{C}$ at all depths and times in the solution. The initial Baffin Bay bias is addressed by applying an additional, linearly-decreasing adjustment $\mathcal{A}_2(t)$ for the central west and northwest sample areas i.e.

$$\mathcal{A}_2(t) = \frac{2012 - t}{2012 - 1992} \, ^\circ C \tag{2.19}$$

With these adjustments, the adjusted thermal forcing for the 4 km Solution is

$$\widetilde{TF}_{4km,S}(t,d) = \begin{cases} TF_{4km,S}(t,d) + \mathcal{A}_1 & \text{if } S \notin \{\text{CW, NW}\} \\ TF_{4km,S}(t,d) + \mathcal{A}_1 + \mathcal{A}_2(t) & \text{if } S \in \{\text{CW, NW}\} \end{cases} \tag{2.20}$$

Once the biases have been removed from the 4 km Solution, the LLC270 is adjusted so that the depth-dependent mean difference from the 4 km Solution in the common 2001-2011 time period is 0. The depth-dependent adjustment $\mathcal{B}(d)$ is calculated as

$$\mathcal{B}(d) = \overline{\widetilde{TF}_{4km,S}(t,d) - TF_{LLC,S}(t,d)} \text{ for all } t \in (2001, 2012), d > \text{ depth threshold} \tag{2.21}$$

The depth threshold is 50 m to avoid spurious seasonal and interannual differences. An example adjustment profile for the CW1 area is shown in Figure 2.10.

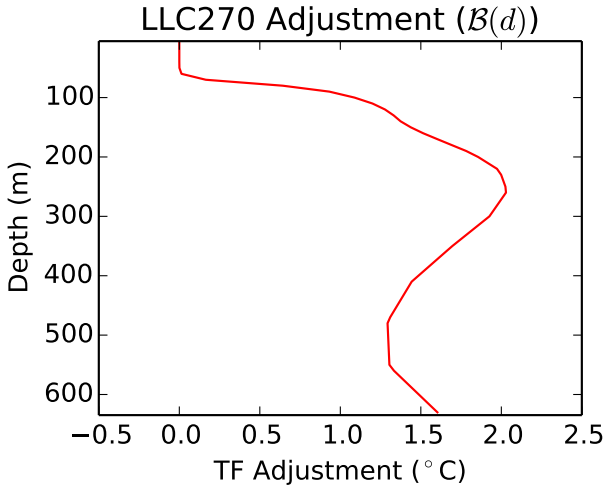

Figure 2.10: ECCO LLC270 Solution Adjustments Example

The adjustment profile added to the LLC270 solution to match the vertical structure of the 4 km solution.

Table 2.5: CTD Availability in Model Sample Areas.

Sample Area	NW1	NW2	NW3	NW4	NW5	
# of CTDs	2	17	40	40	23	
Sample Area	CW1	CW2				
# of CTDs	51	59				
Sample Area	SW1	SW2	SW3			
# of CTDs	75	52	24			
Sample Area	SE1	SE2	SE3	SE4	SE5	SE6
# of CTDs	71	6	76	19	44	245
Sample Area	CE1	CE2	CE3	CE4	CE5	
# of CTDs	34	203	22	54	31	
Sample Area	NE1	NE2	NE3	NE4		
# of CTDs	7	2	15	23		
Sample Area	N1	N2	N3			
# of CTDs	0	3	0			

After both solutions have been adjusted, they are merged over the 2009-2012 time period:

$$TF_S(t,d) = \begin{cases} \widetilde{TF}_{4km,S}(t,d) & \text{if } t < 2009 \\ \dfrac{\widetilde{TF}_{LLC,S}(t,d) - \widetilde{TF}_{4km,S}(t,d)}{2012-2009}(t-2009) + \widetilde{TF}_{4km,S}(t,d) & \text{if } 2009 \leq t \leq 2012 \\ \widetilde{TF}_{LLC,S}(t,d) & \text{if } t > 2012 \end{cases} \tag{2.22}$$

Preference is given to the 4 km Solution because it has a higher resolution which permits eddy heat transport onto the continental shelf.

After the solutions have been adjusted and merged, a final absolute adjustment is made to $TF_S(t,d)$ so that the mean model error from CTD observations is 0. Most of the sample areas have at least 2 CTD observations in the time period 1992-2018, as outlined in Table 2.5.

For the set of thermal forcing observations $\mathcal{O}_{TF,S}$ in the sample area, the mean model error is

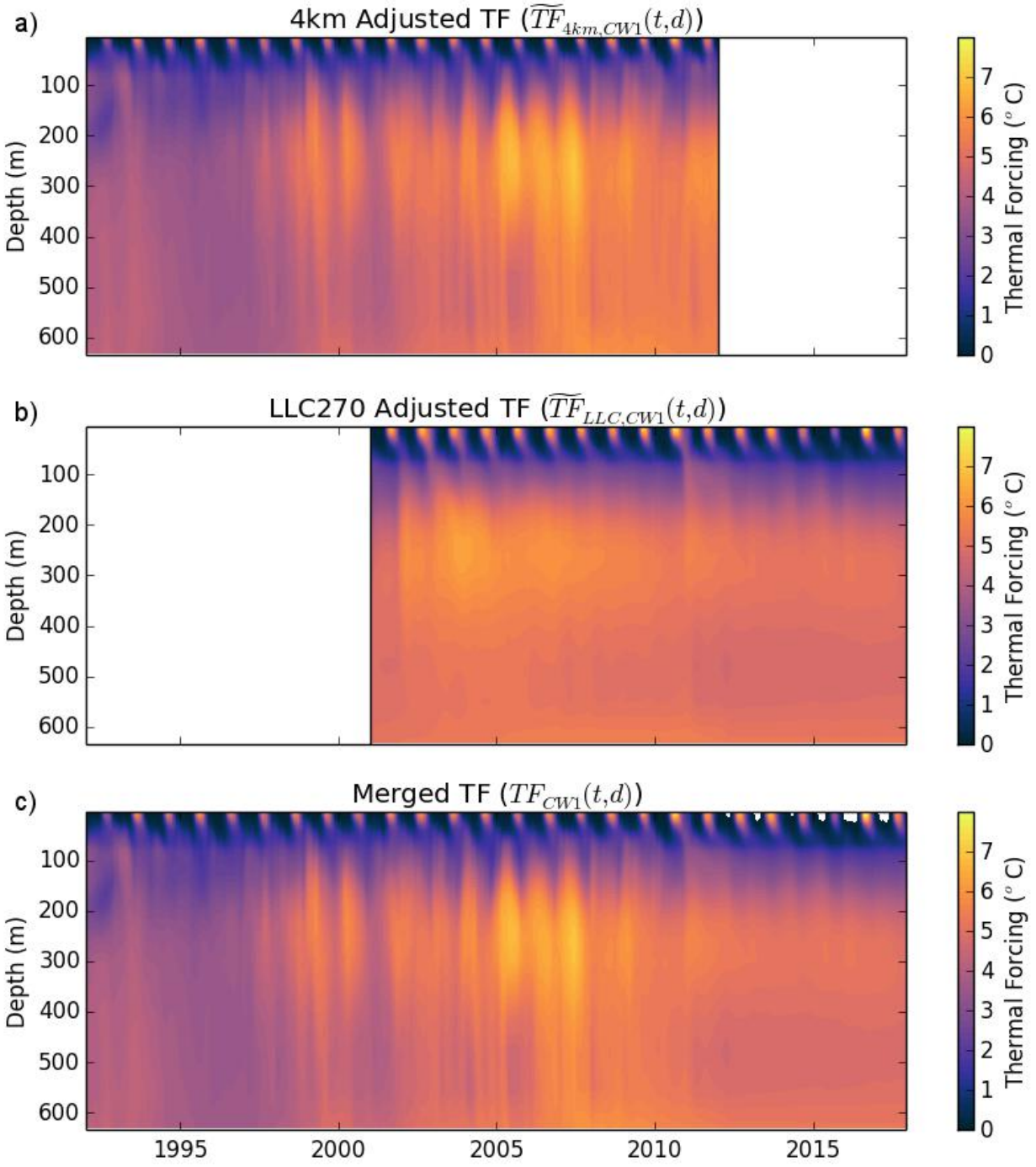

Figure 2.11: ECCO Solution Merging Example: CW1

a) The adjusted solution from the 4 km model. b) The adjusted solution from the LLC270 model. c) The combination of solutions merged over the 2009-2011 time period.

calculated as

$$\mathcal{E} = \overline{CTD_{TF}(d) - TF_S(t,d)} \text{ for all } d > 50\text{m and all } CTD_{TF} \in \mathcal{O}_{TF,S} \tag{2.23}$$

The depths above 50 meters are omitted because the mixed layer is more variable than the monthly time steps provided by the model. With this adjustment, the final merged and adjusted thermal forcing is

$$\widetilde{TF}_S(t,d) = TF_S(t,d) + \mathcal{E}_S \tag{2.24}$$

To test the differences from observations, the root mean square error σ is calculated below 50 m.

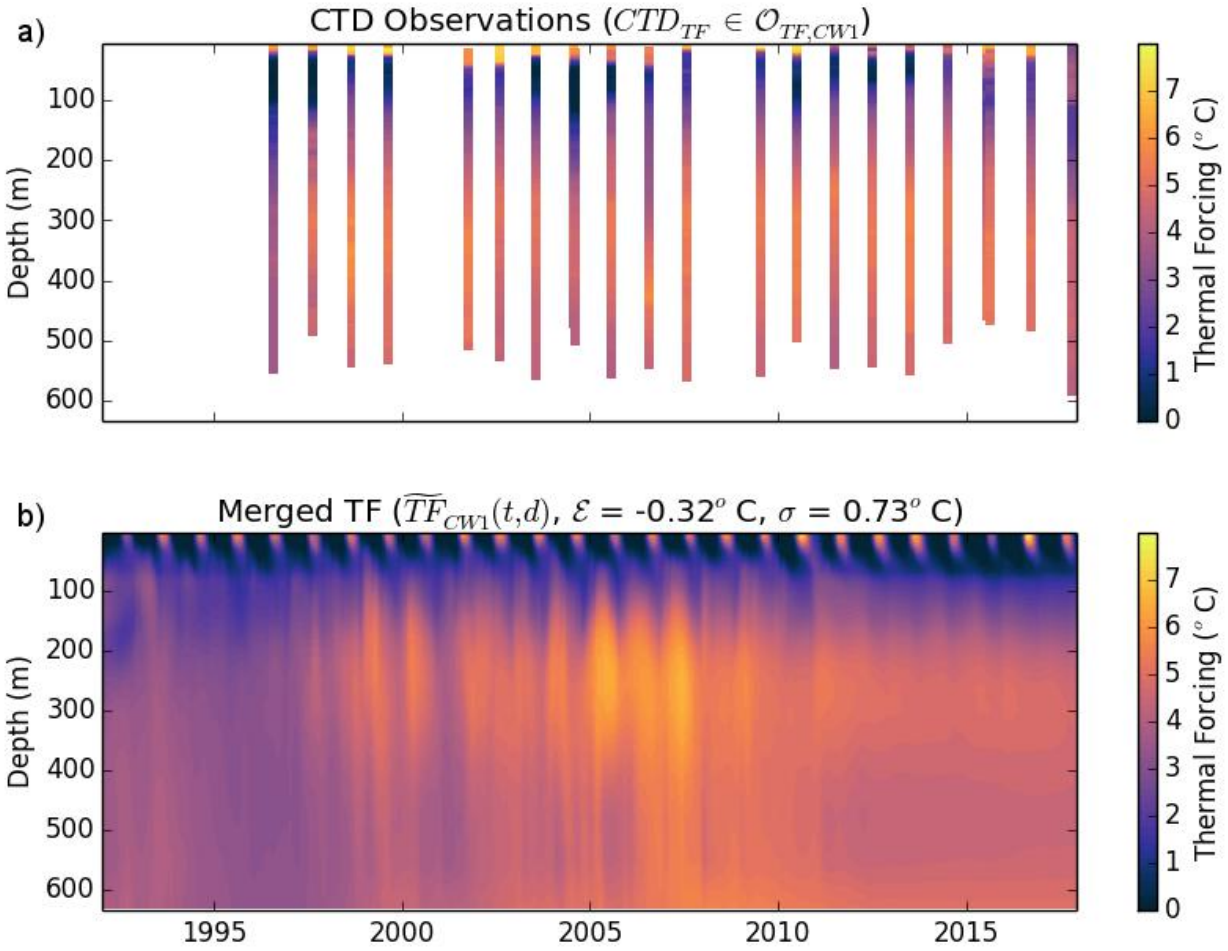

Figure 2.12: Merged Model and CTD Comparison

Thermal Forcing within Glacier Fjords

Methods The 4 km and LLC270 solutions used above are too coarse to resolve circulation and heat transport within the glacier fjords, so an additional adjustment must be generated to modulate the simulated thermal forcing on the shelf for use within the fjords. This adjustment is conducted by applying an absolute shift to the thermal forcing profile to match the collection of CTDs which are available within the fjord. If no CTDs are available, then the shelf solution is taken as-is. After the fjord TF has been derived within the fjord, the TF record is integrated over the geometry of the glacier ice front to derive an average TF value for use in the q_m parameterization.

Numerical Implementation First, the set of CTD thermal forcing profiles $\mathcal{O}_{TF,G}$ within 20 km of a glacier G are collected and averaged in monthly bins. Then, similar to the mean error between the merged model and CTDs on the shelf, the mean error between $\widetilde{TF}_S(t,d)$ and the CTDs within the fjord is calculated as

$$\mathcal{E}_G = \overline{CTD_{TF}(d) - \widetilde{TF}_S(t,d)} \text{ for all } d \text{ and all } CTD_{TF} \in \mathcal{O}_{TF,G} \tag{2.25}$$

for the glacier G. With this adjustment, the adjusted thermal forcing within the fjord is

$$TF_G(t,d) = \widetilde{TF}_S(t,d) + \mathcal{E}_G \tag{2.26}$$

and σ_G as the root mean square error between $TF_G(t,d)$ and the CTDs in $\mathcal{O}_{TF,G}$.

The numerical implementation for average thermal forcing is based on the results from Xu et al 2013 which found that the entrainment plume is in contact with the ice face for the deeper 60% of the maximum ice front depth. Here, we average thermal forcing below this depth threshold in the following steps:

Step 1: Obtain the ice front position F and the maximum ice front depth D_M.

Step 2: For the bathymetry/bed $B(x,y)$, create a depth-averaged thermal forcing field defined as

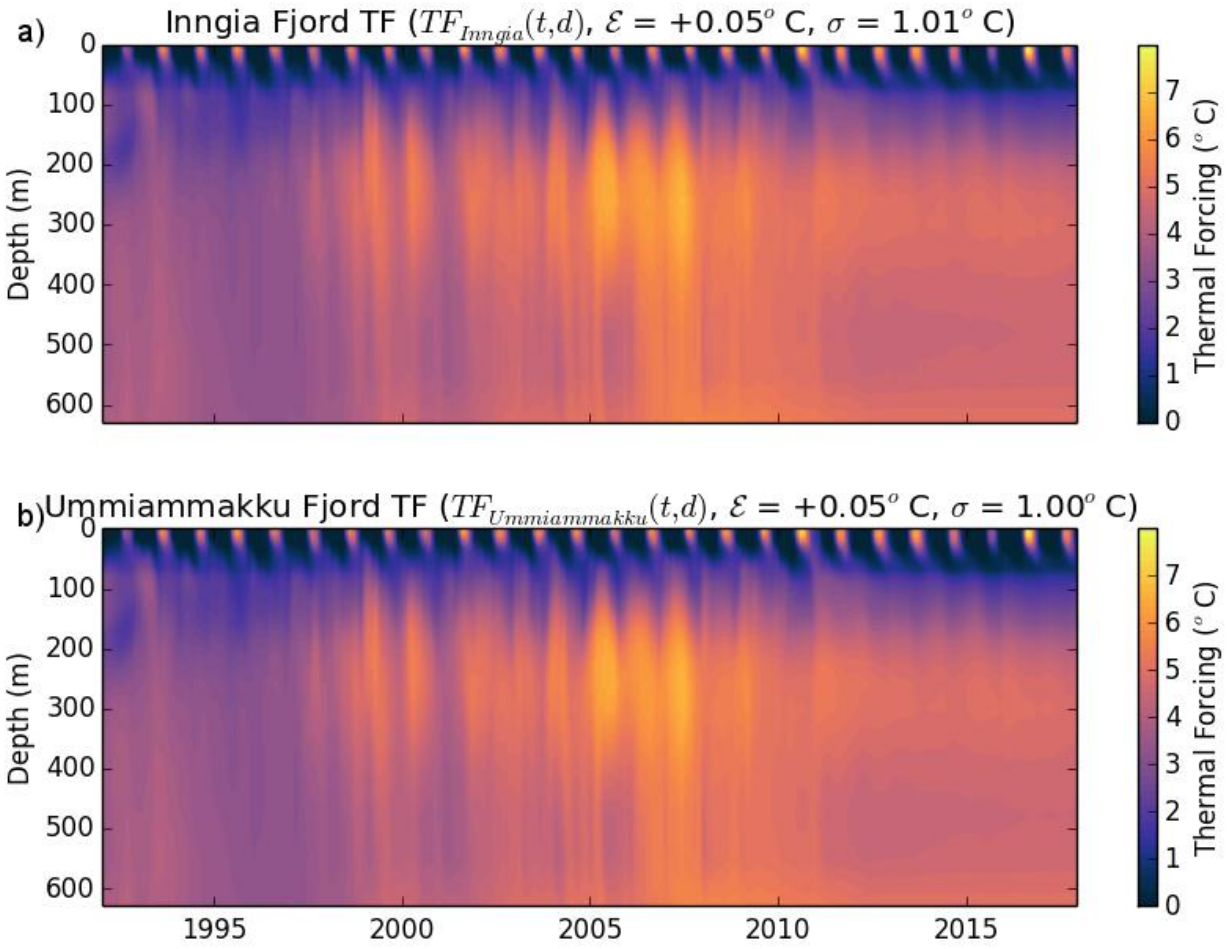

Figure 2.13: Fjord Thermal Forcing Example

Two adjacently-located glaciers will have similar fjord TF profiles.

follows:

$$TF_G(t,x,y) = \begin{cases} \overline{TF_G(t,d)} \text{ for } d \in (0.4D_M, D_M) & \text{if } B(x,y) > 0.4D_M \\ \\ \text{undefined} & \text{otherwise} \end{cases} \tag{2.27}$$

for all (x, y) in the bed domain. This field represents the average thermal forcing that the ice front would be exposed to, if it occupies the location (x, y).

Step 3: Average the thermal forcing field points which are defined for locations of the ice front, i.e.

$$\overline{TF}_G(t) = \overline{TF_G(t,x,y)} \text{ for } (x,y) \in F \tag{2.28}$$

Figure 2.14 provides two examples of this calculation for Inngia Isbræ and Ummiammakku Isbræ which are sourced by the CW1 waters.

Concluding Comments on Thermal Forcing

Although glaciers which terminate in adjacent fjords may have similar thermal forcing profiles ($TF_G(t,d)$), the averaged thermal forcing across the ice front may differ significantly if the glacier geometry is different. For example, consider the two examples for Inngia Isbræ and Ummiammakku Isbræ shown in figure 2.14, which have very similar profiles. Although $TF_{Inngia} \approx TF_{Ummiammakku}$, $\overline{TF}_{Inngia}(t_m) = 4.07°\text{C}$ while $\overline{TF}_{Ummiammakku}(t_m) = 4.73°\text{C}$ for $t_m =$ August 2002. This is largely due to differences in the front depth: the front of Inngia has a maximum depth of 280 m while that of Ummiammakku is 409 m i.e. Ummiammakku is exposed to a greater amount of the deep, warm water than Inngia. Hence $\overline{TF}_{Ummiammakku}(t_m) > \overline{TF}_{Inngia}(t_m)$.

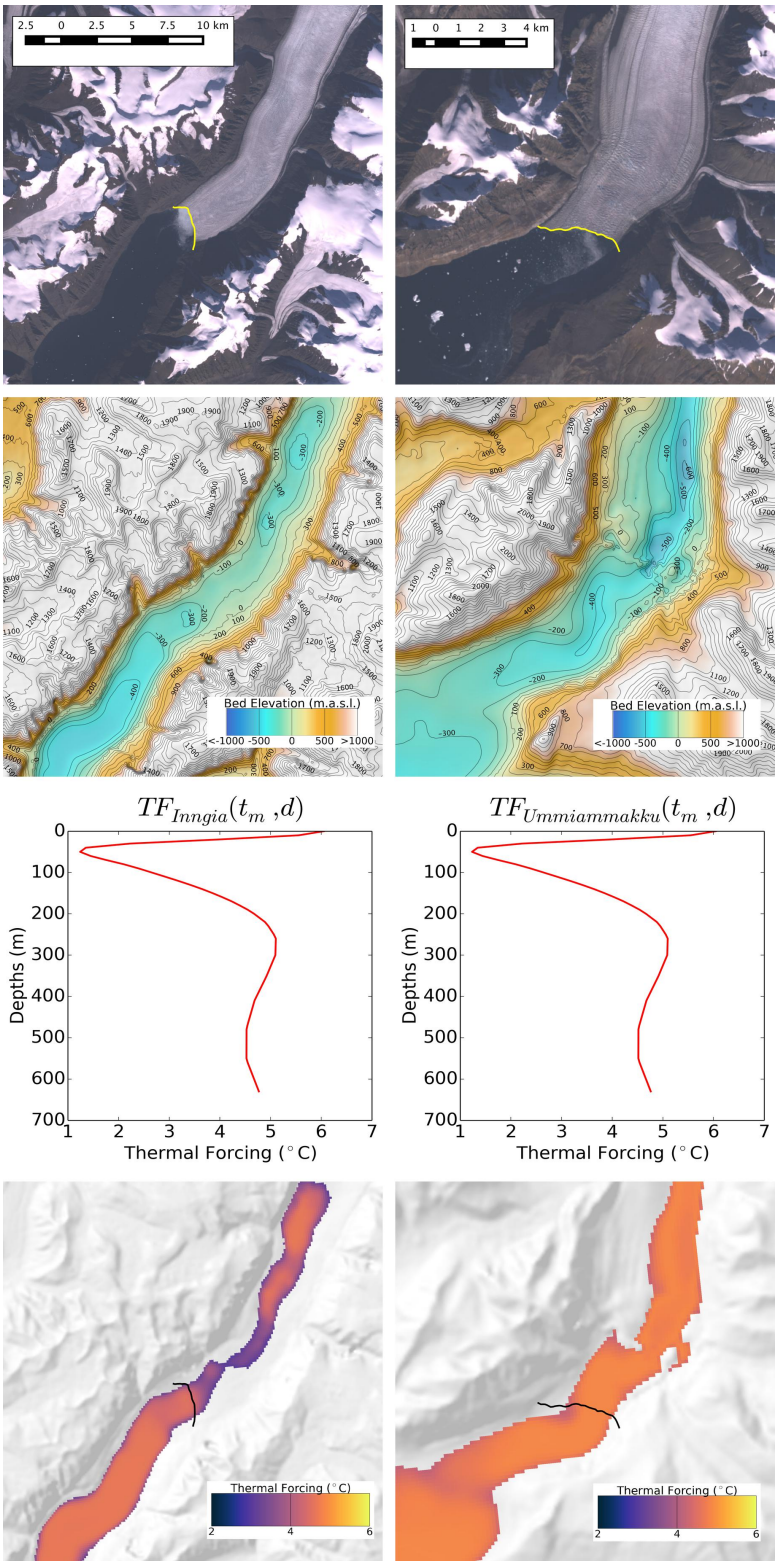

Figure 2.14: Integrated Thermal Forcing Example: Inngia Isbræ and Ummiammakku Isbræ

2.4 Cumulative Mass Balance

Equation 2.1 represents the balance of fluxes at the glacier terminus region during a specific time. Yet, to compare the relative magnitudes over several years, it is helpful to provide integrated values over time which tend to smooth out spurious seasonal and inter-annual variability.

The synthesis section in Chapter 4 will provide a comparative assessment of total advection and accumulation processes through time. For this analysis, the total integrated values of retreat, ice velocity, ice front undercutting, and iceberg calving are observed through time, i.e.:

$$R := \int_{t_0}^{t_1} q_r \; dt = \int_{t_0}^{t_1} q_f - q_m - q_c \; dt := F - M - C \text{ [m]} \tag{2.29}$$

where, if not otherwise noted, $t_0 = 1992$ and $t_1 = 2018$.

As mentioned in Section 1.4, one of the main hypotheses of this research is that ocean heat *anomalies* in the past several decades has induced the retreat of Greenland's glaciers. To calculate the subsequent anomalies in ice front undercutting, a baseline undercutting rate is defined as

$$q_m^{ref} := \overline{q_m(t)} \tag{2.30}$$

where the averaging is calculated over the 1992-1998 time period. This period is chosen as the baseline because the majority of glaciers were stable during this time i.e. ice fronts remained stationary and discharge rates were consistent through this period. In this equilibrium state, the average melting during this time is assumed to balance calving processes and advection to keep the ice front in a consistent position. With this baseline melt, the *cumulative undercutting anomaly* at a time t is defined as

$$M^{anom}(t) = \int_{1992}^{t} \left(q_m - q_m^{ref} \right) \; dt \tag{2.31}$$

This value represents the additional ice which was melted by the ocean to induce a retreat of the ice front.

Chapter 3

Regional Assessments

The Greenland Ice Sheet can be split into 7 broad sectors: the northwest (NW), central west (CW), southwest (SW), southeast (SE), central east (CE), northeast (NE) and northern (N) sectors. The approximate longitudinal and latitudinal extents of the glacier terminus regions within these sectors is outlined in Figure 3.1. The following sections break down each sector of the ice sheet into several smaller regions, and discuss the recent evolution of the glaciers. Special focus is given to the role of ocean thermal forcing and increased melt rates in modulating the position of glacier margins. The sectors, regions, and glaciers are presented in counter-clockwise order around the continent beginning with the far western branch of Savissuaq Gl. in Melville Bay, NW Greenland, and ending with Harald Moltke Bræ outside of Inglefeld Gulf. Summary statistics for each glacier are provided in the Appendix, and the locations of Greenland towns and other landmarks described here are shown in Figure 1.2.

Greenland glaciers are often referred to by names from a mix of Greenlandic, Danish, English and other foreign languages. In this study, glaciers are indicated by the names which are most common in the scientific literature. A comprehensive guide to these names is provided by Bjørk et al. [2015] although many glaciers have not been assigned a name. In such cases, glaciers are identified according to the closest nearby glacier with identifiers based on their relative location (e.g. “N” for north, ”E” for east, etc). For example, in the CE, there is Kista Dan Glacier and

Table 3.1: Overview of Greenland Ice Sheet Regions

Sector	Mean Ice Discharge (Gt/yr)	Tidewater Glaciers (#)	Ice Sheet Area (10^5 km^2)	Areal Ice Loss Grounded (km^2)	Areal Ice Loss Total (km^2)
NW	100	58	2.8	749	749
CW	79	19	2.4	200	288
SW	30	15	2.2	41	41
SE	154	49	1.7	336	336
CE	84	45	2.2	240	240
NE	32	12	4.3	336	859
N	22	28	2.6	558	1109
Total	**498**	**226**	**18.1**	**2460**	**3622**

The mean ice discharge estimates are from Mouginot et al. [2019] averaged over 1992-2018. The areal ice loss estimates are from this study, and calculated over 1992-2019.

Kista Dan Glacier W, and in the SE there is Danell Glacier, Danell Glacier S, Danell Glacier SS, and Danell Glacier SSS, which represent glaciers successively further south from the main branch of Danell Glacier. Moreover, several names have historically been used for more than one glacier in different areas of the ice sheet including Sermeq Avannarleq, Nordenskiöld Glacier, Sermilik, and Sermeq. Every effort has been made to distinguish these cases when appropriate.

3.1 Northwest Greenland

NW Greenland is the second-most productive region of the ice sheet with a mean discharge of approximately ∼100 Gt/yr between 1992-2018 [Mouginot et al., 2019]. The recent retreat of the 58 glaciers in this region represents the largest loss of grounded ice from the ice sheet margin between 1992 and 2018 (749 km^2 or 30% of grounded ice loss). Correspondingly, ice discharge increased 41% over the same time from 88 Gt/yr in 1992 to 124 Gt/yr in 2018 – the largest increase in discharge from any sector. The NW can be spatially divided into 3 broad subregions: Melville Bay (26 glaciers), the area surrounding the island and town of Kullorsuaq (16 glaciers), and the area surrounding the archipelago and town of Upernavik (16 glaciers). The largest glacier in this region is Kong Oscar which discharges an average 8.8 Gt/yr.

The northwest sector was surveyed extensively during the OMG campaign, providing two years

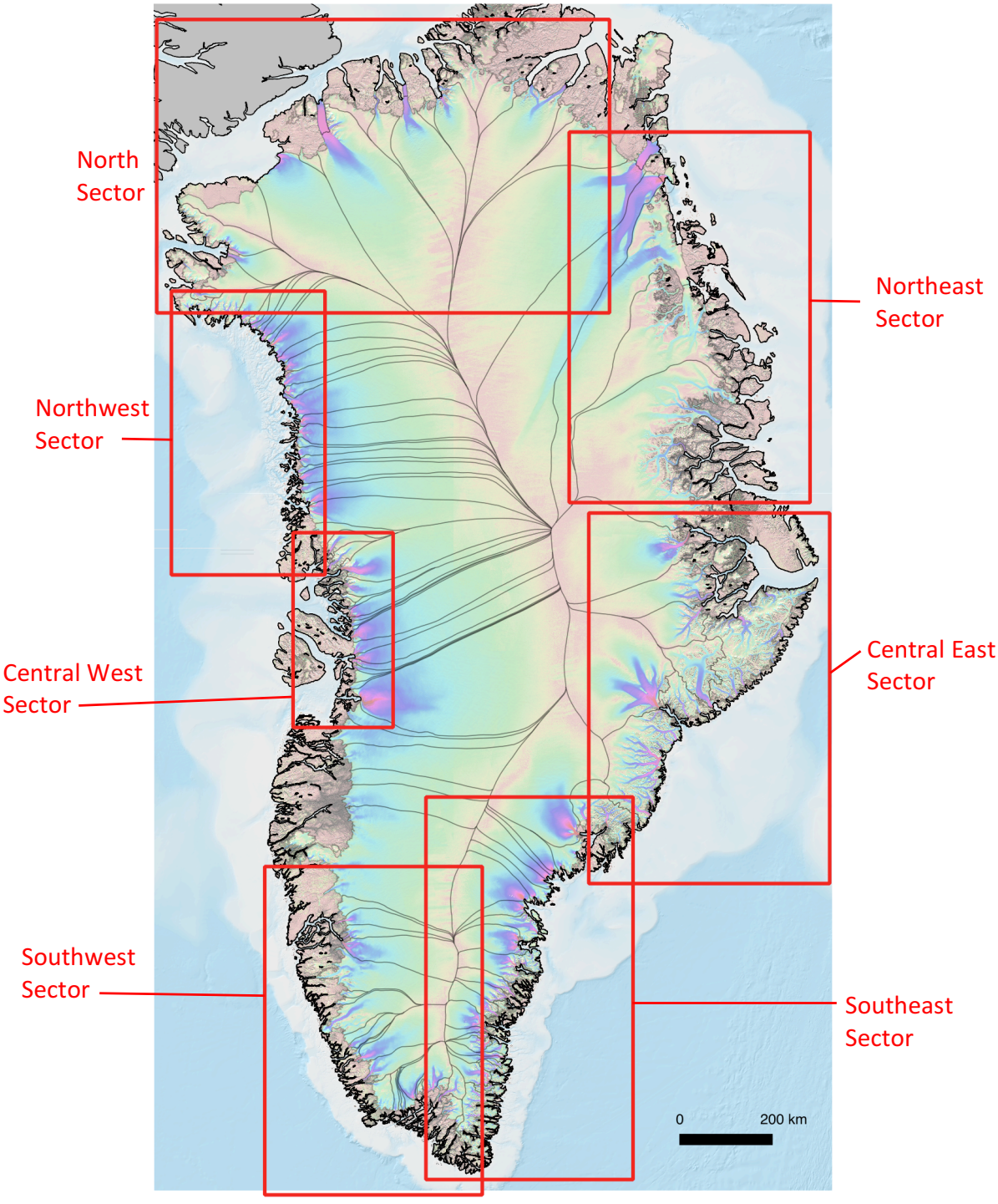

Figure 3.1: Map of Greenland Sectors

Break down of the 7 sectors of the Greenland Ice Sheet. The coastline between the central west and southwest is not represented because the glaciers in this region are land-teminating.

of MBES-derived bathymetry and a complete mapping with airborne gravity. The inversion of airborne gravity [An et al., 2019] and the mutibeam data has been incorporated into the latest BedMachine product [Morlighem et al., 2017]. The OMG campaign has also provided hundreds of CTDs along the northwest coast, providing an abundant constraint on ocean thermal forcing records in the years since 2015.

The following results for the NW sector of Greenland have been previously published as part of this research track in the journal *Geophysical Research Letters* in the year 2018. See Wood et al. [2018].

3.1.1 Melville Bay

Melville Bay encompasses the northeast area of Baffin Bay comprising 26 glaciers. Glaciers in this area are grouped according to a local source glacier, as several are not associated with official names. The glaciers in this sector include 5 branches of Savissuaq Glacier, 3 branches of Helland Glacier, Yngvar Nielsen Glacier and its western branch, Mohn Glacier, Carlos Glacier and its western branch, Gade Glacier, Morell Glacier and its western branch, 3 branches of Døcker Smith Glacier, 3 branches of Rink Glacier, Issuusarsuit Sermia, and 3 branches of Kong Oscar Gl.

Glacier Evolution The glaciers in Melville Bay underwent substantial retreat between 1992-2019 totaling 252 km^2, yet, in the majority of cases, ice margins remained stable until approximately the year 2000 when widespread retreat initiated. The only glaciers which remained stable were Gade and Issuusarsuit, which remain within 1 km of their pre-2000 position, and the northern branch of Kong Oscar, which did not retreat until a large collapse of the ice front in 2010. The most substantial retreat is observed at Døcker Smith and Savissuaq, but nearly all glaciers in this region underwent substantial retreat of several km.

The Role of Ocean Melt In Melville Bay, TF rose substantially after 1997 and correspondingly, the melt rate increased significantly on the ice fronts of the glaciers within this region. The timing of this increase in melt corresponded closely with the retreat of glacier ice margins. For the first

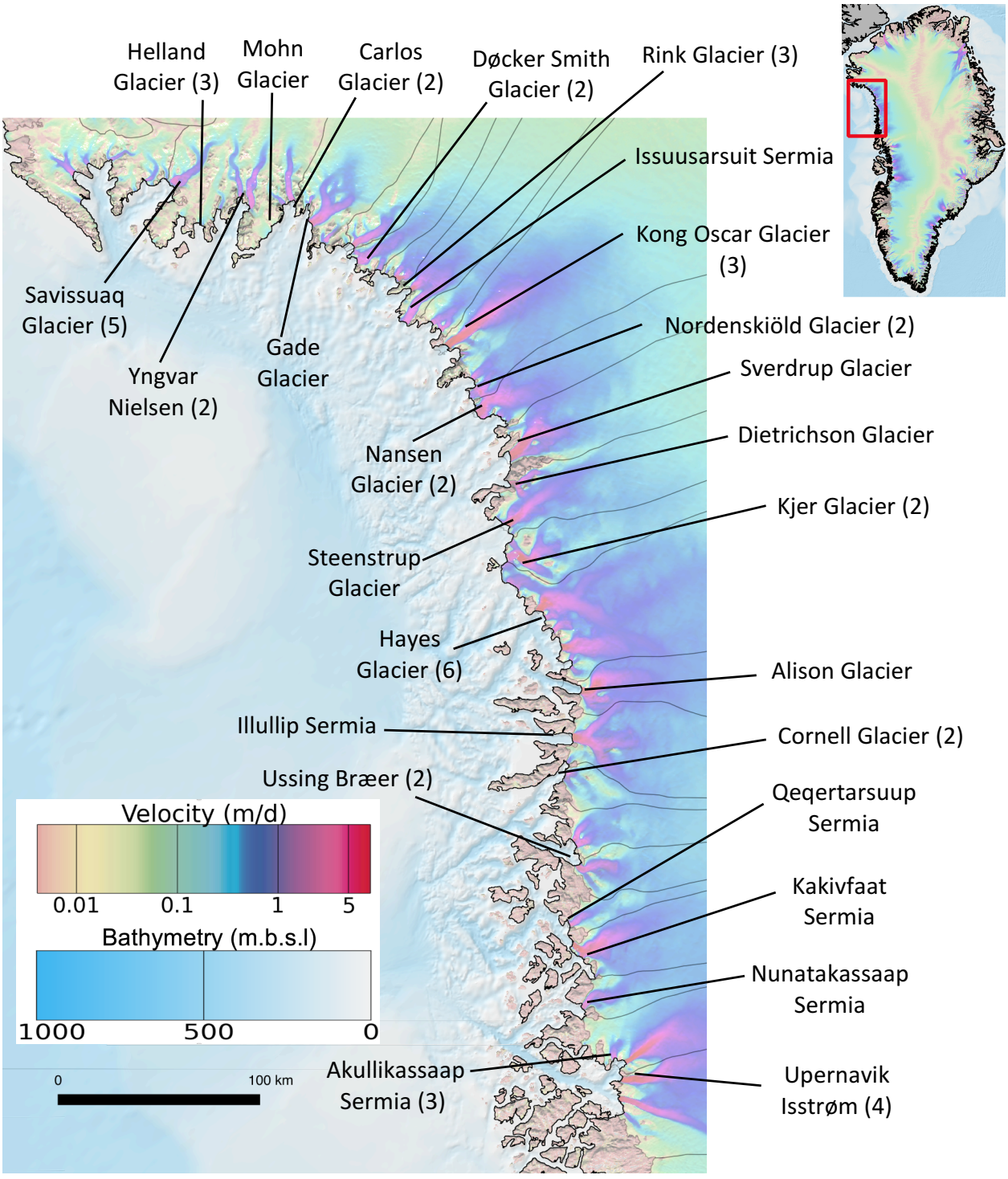

Figure 3.2: Map of Northwest Greenland Glaciers

Overview of glacier in northwest Greenland. Numbers in parenthesis represent the number of glacier branches encompassed by the name indicate. If no numbers are given, the name refers to a single glacier.

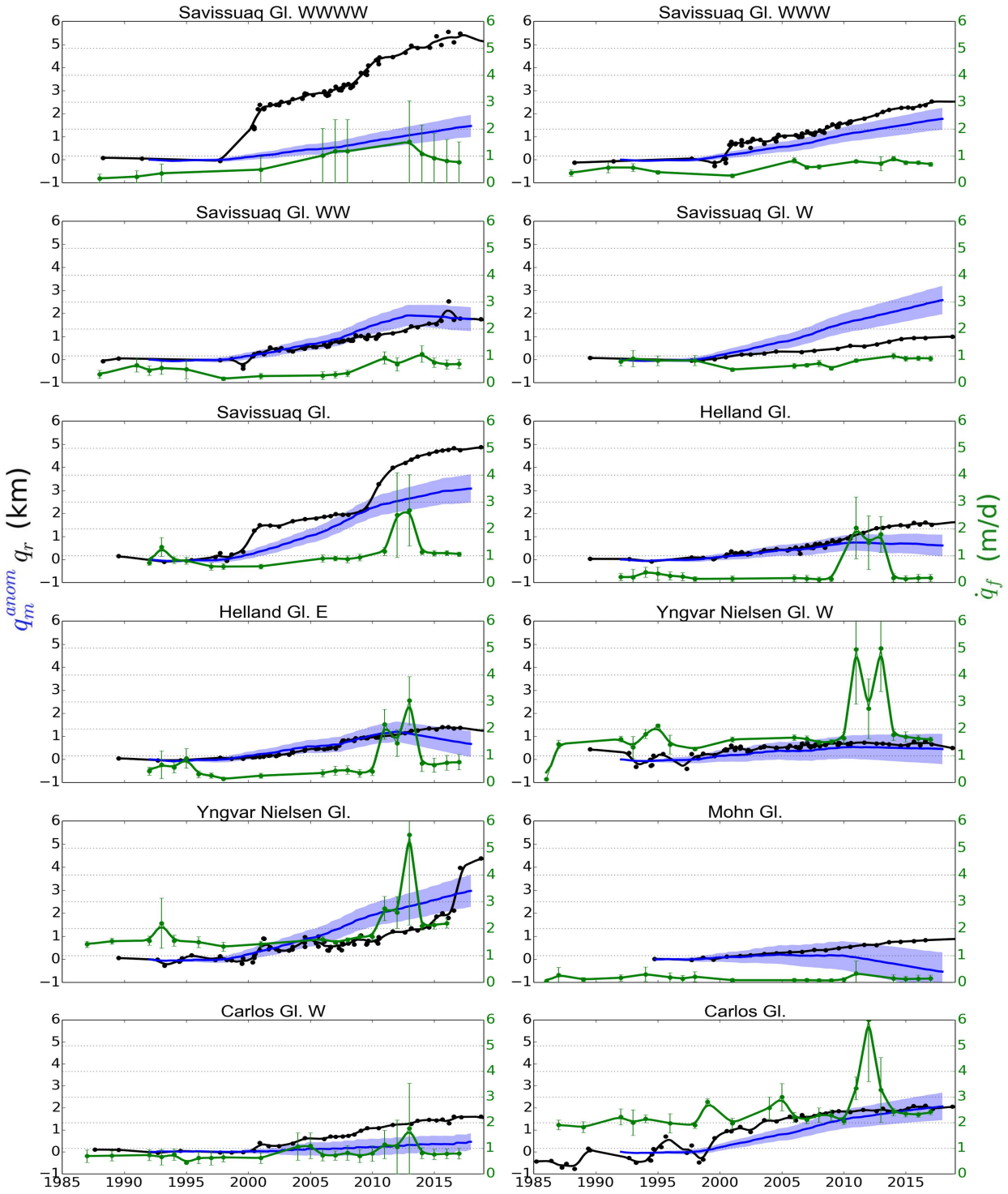

Figure 3.3: West Melville Bay Glacier Results

Summary of the ice front retreat (q_r), cumulative melt anomaly (q_m^{anom}), and ice velocity (q_f) for 12 glaciers in NW Greenland.

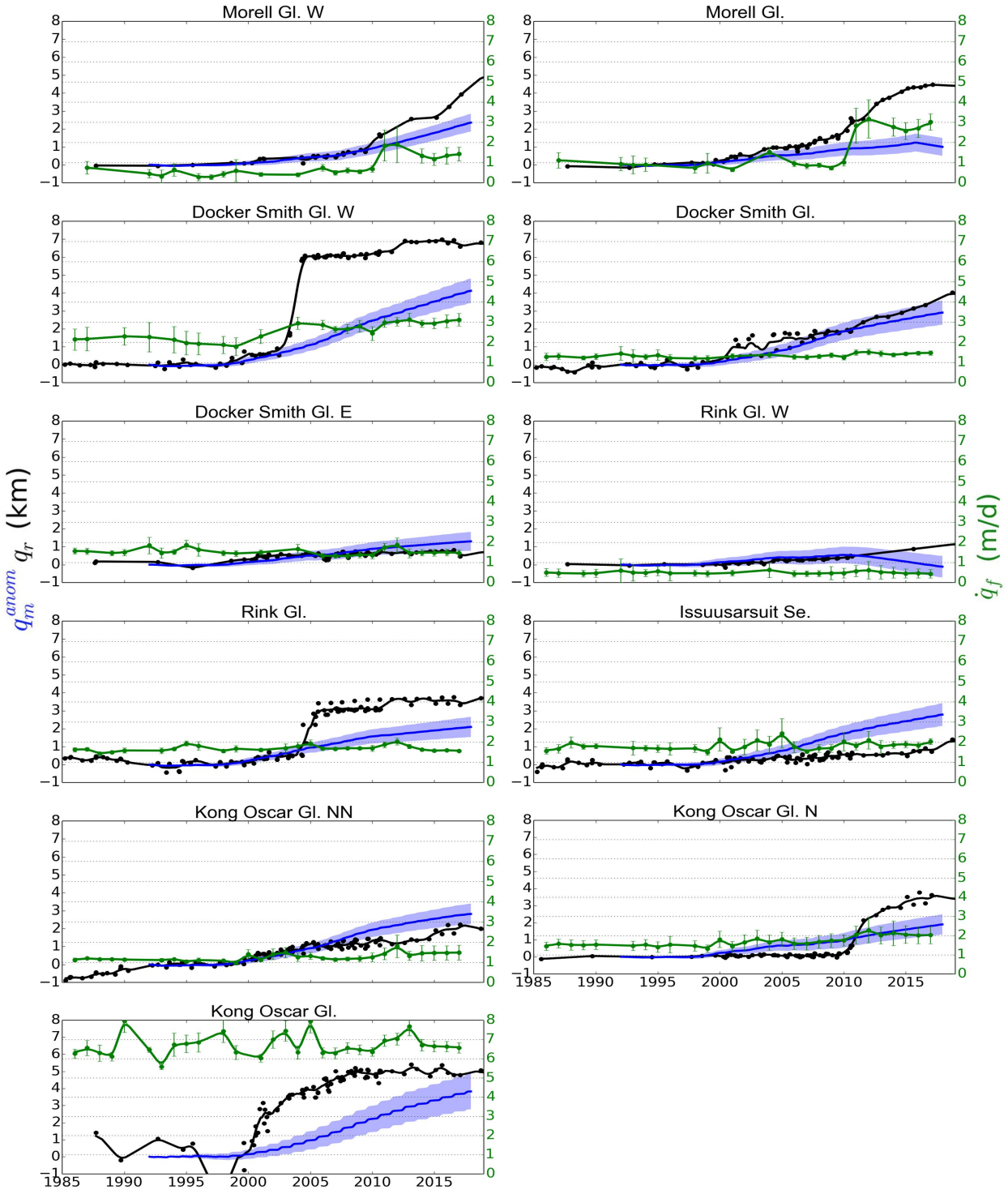

Figure 3.4: East Melville Bay Glacier Results

Summary of the ice front retreat (q_r), cumulative melt anomaly (q_m^{anom}), and ice velocity (q_f) for 11 glaciers in NW Greenland.

several years of glacier retreat, the ice front records matched closely with cumulative anomalies in ice front undercutting. As retreat continued, several glaciers retreated into deeper portions of their bed, and retreat accelerated significantly. In particular, Savissuaq WWWW, Savissuaq, Morell, Docker Smith W, and Kong Oscar underwent rapid retreat associated with a change in their fjord shape along the progression of ice front retreat. In these cases, the stress and strain balance in the ice terminus region changes in response to the new glacier-fjord geometry, and retreat ensued until the glacier front re-adjusted to a new, stable region of the bed. The retreat of these glaciers subsequently subsided in new fjord locations upstream of their previous locations. For the other glaciers in this region, the retreat history matches closely with the calculated undercutting anomalies, indicating the retreat was largely controlled by undercutting directly, with little change in the stress/strain relationship, and in turn, the calving rate. In total, for glaciers that showed a response to enhanced melt, the total melt anomaly accounted for 67% of the magnitude of retreat on average.

The only glaciers which did not show a distinguishable response to enhanced undercutting were Gade and Issuusarsuit, which remained stable. For these glaciers, the presence of fjord constrictions dampens the effect of undercutting on the terminus, and the ice front positions are inferred to be controlled by calving processes instead of melt processes. The final glacier to note in this region is the western branch of Helland which has a very shallow fjord – only 4 m deep – in the BedMachine dataset. With this purported depth, the ice front would only be influenced by heat in its fjord surface waters which was derived from the atmosphere, instead of the circulation of warm AW around Greenland. However, this fjord was not surveyed in the OMG campaign (or any other survey) and this geometry is likely inaccurate as the branch showed the same timing of retreat as those adjacent to its terminus.

3.1.2 Kullorsuaq Area

The town of Kullorsuaq (74.58°N, 57.23°W), located south of Melville Bay, is positioned near 16 marine-terminating glaciers: Nordenskiöld Glacier and its northern branch, Nansen Glacier and its southern branch, Sverdrup Glacier, Dietrichson Glacier, Steenstrup Glacier, Kjer Glaciers and its

northern branch, six branches of Hayes Glacier, and Alison Glacier.

Glacier Evolution The progression of retreat in the Kullorsuaq area is very similar to that of the Melville Bay area discussed in the previous section – that is, glaciers in this region began to retreat around the year 2000 after a long period of ice front stability. The only glaciers which remained approximately stable were the northern branch of Nordenskiöld and the southern branch of Nansen. The largest changes observed were a 5 km retreat at Nordenskiöld which detached from two pinning points on local islands, a 6 km linear retreat at Sverdrup, and a 6 km retreat at the southern branch of Hayes. These glaciers experienced the same triggering of retreat observed at some glaciers in Melville Bay associated with changes in their fjord shape. At Kjer glacier, retreat continued unabated from 1985 to present, and eventually led to the collapse of an ice bridge between the main branch and the northern branch in 2016 for a total 8 km retreat at Kjer and a 6 km retreat at Kjer N. Finally, Alison Glacier on the southern end of Kullorsuaq experienced a substantial 16 km retreat which was associated with the break-up of its floating ice extension that began in 2004.

The Role of Ocean Melt As for the Melville Bay region, the glaciers near Kullorsuaq follow a varied response to enhanced melt. At the northern branch of Nordenskiöld, the increase in melt was minimal, and the melt anomaly accumulated to approximately 1 km, matching well with the retreat distance. The same progression was observed at the northern branch of Kjer (until the break up of the ice bridge referenced above), and several branches of Hayes. In other cases, such as Nordenskiöld, Sverdrup, and Steenstrup, the retreat exceed the melt anomaly, which is consistent with the glacier terminus retreating into deeper waters. It is impossible to determine the impact of ocean melt on the retreat of Kjer because the baseline anomaly is taken to be in the 1992-1998 period – since Kjer was not stable during this time period, the anomaly would not reflect a deviation in the environmental conditions from those which promote stability. At Alison, the break-up of the ice tongue occurs at the same time that simulated melt increases, but the unique geometry of this glaciers is likely misrepresented by the parameterization for q_m, which was derived for a vertical ice face. This glacier, and others which previously maintained extensive floating section, will be

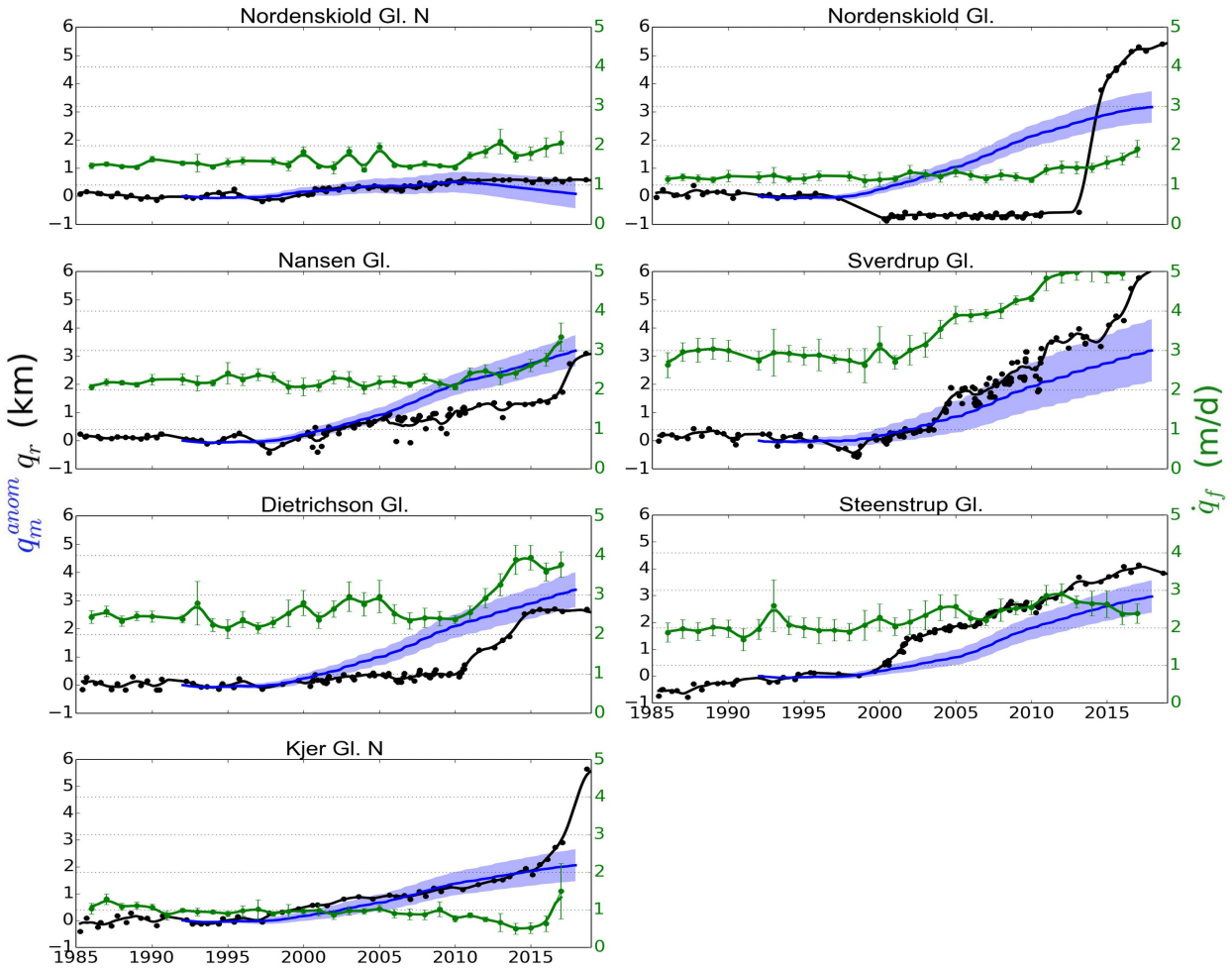

Figure 3.5: Kullorsuaq Area Glacier Results Part 1

Summary of the ice front retreat (q_r), cumulative melt anomaly (q_m^{anom}), and ice velocity (q_f) for 7 glaciers in NW Greenland.

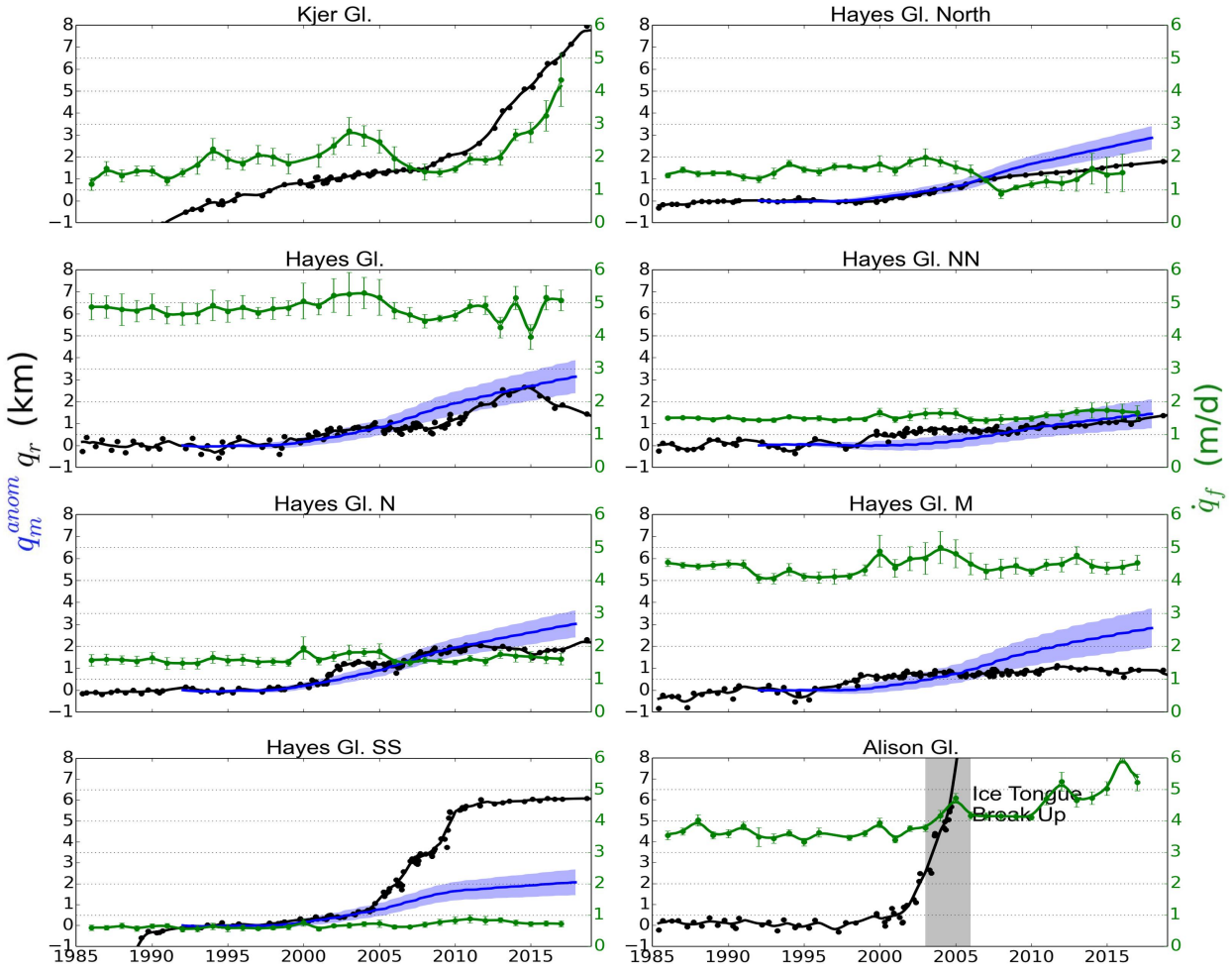

Figure 3.6: Kullorsuaq Area Glacier Results Part 2

Summary of the ice front retreat (q_r), cumulative melt anomaly (q_m^{anom}), and ice velocity (q_f) for 8 glaciers in NW Greenland. Note that q_m^{anom} is not plotted for Kjer Gl. or Alison Gl. due to unique retreat circumstances described in the text.

discussed in depth in Section 4.2.2.

3.1.3 Upernavik Area

The town of Upernavik (72.78°N, 56.14°W) in NW Greenland is located near the mouth of the Upernavik Isfjord. The 16 glaciers which terminate near this area include Illullip Sermia, Cornell Glacier and its northern branch, Ussing Bræer and its northern branch, Qeqertarsuup Sermia, Kakivfaat Sermia, Nunatakassaap Sermia, three branches of Akullikassaap Sermia, and 5 branches of Upernavik Isstrøm.

Glacier Evolution Glacier retreat has been variable in the Upernavik Area, ranging from stability at Nunatakassaap and Ussing Bræer to substantial retreat at Upernavik Isstrøm. Several glaciers underwent small, step-wise retreat associated with the detachment of the ice front from shallow protrusions near the grounding line. For example, Illullip Sermia, Ussing Bræer N, and Qeqertarsuup Sermia all experienced an approximately 1 km retreat through narrow overdeepenings on their northern flank, but otherwise remained stable. Ussing Braær has maintained an approximately constant position within the fjord constriction where it terminates. Kakivfaat Sermia is relatively well protected behind a shallow sill on its southern flank, but in recent years, the ice front has undergone rapid retreat. The most substantial changes are observed in the Upernavik Isfjord where the previously-conjoined N and NW branches began a prolonged retreat beginning around the year 2000. The retreat of the NW branch was gradual until the ice front restablized on a shallower section of the fjord inland, and the northern branch underwent rapid retreat around the year 2007. The retreat at the C branch was largely initiated around 2010 while the S branch has seen only small changes in its ice front position in the last 25 years.

The Role of Ocean Melt The response of glaciers to ocean melt in the Upernavik area is more subdued than their more northern counterparts, likely due to their location within long fjords which tend to modulate the profile of thermal forcing toward a lower state as compared to glaciers terminating closer to the open continental shelf. Still, evidence for a melt-dominated

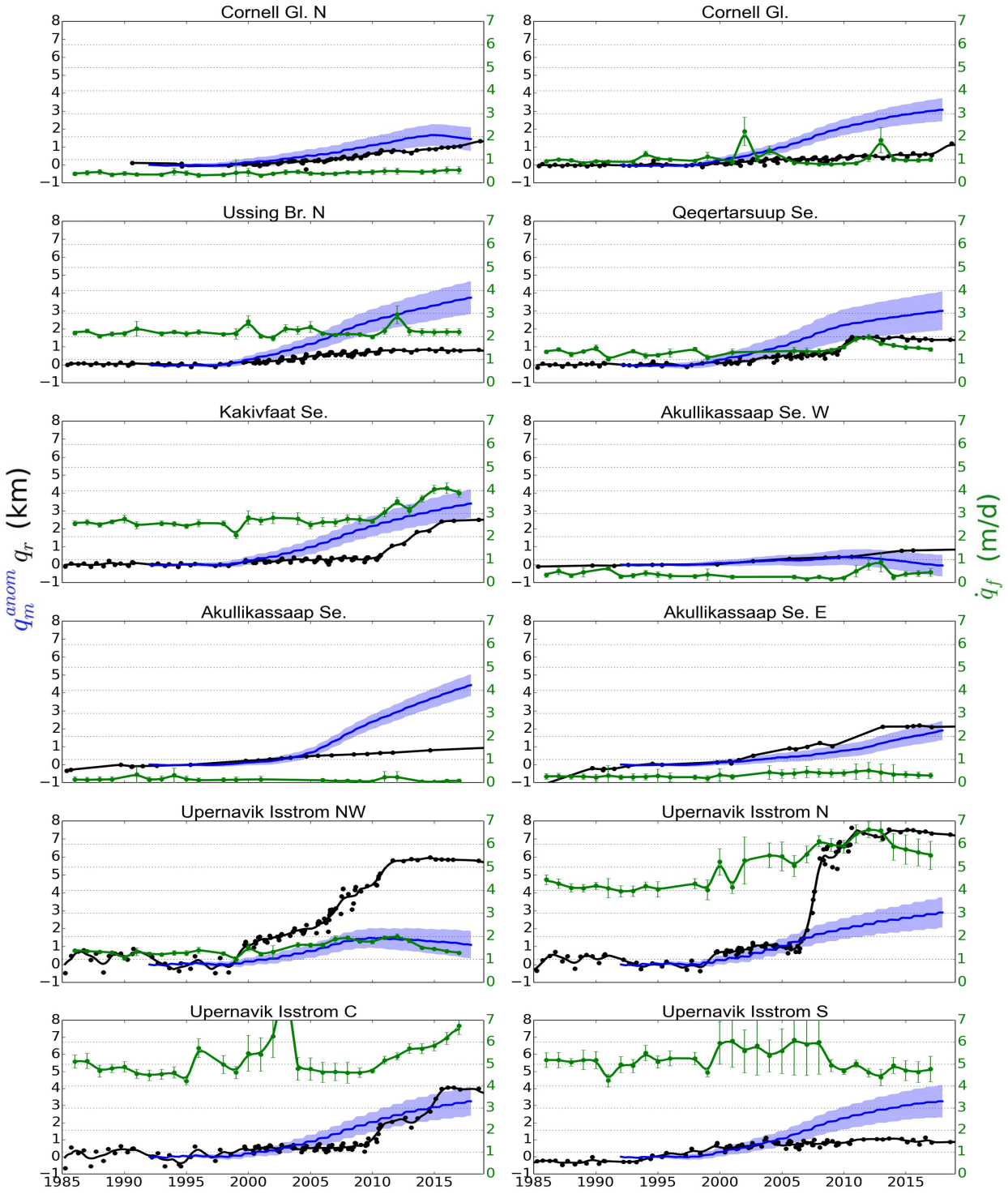

Figure 3.7: Upernavik Region Glacier Results

Summary of the ice front retreat (q_r), cumulative melt anomaly (q_m^{anom}), and ice velocity (q_f) for 12 glaciers in NW Greenland.

retreat is observed at the northern branch of Cornell and Akullikassaap which had retreats that mirror anomalies in ice front undercutting. At the main branches of Cornell and Ussing Bræer, undercutting anomalies far exceed the retreat distance, which is likely due to an overestimation of melt associated with the geometry of their fjords: as these glacier terminate in fjord constrictions, ice front undercutting does not likely remove grounded ice from the terminus region, but instead acts on small floating sections that develop as ice is advected from upstream. Finally, at Upernavik, the response of the glacier ice front matches well with the anomalies in undercutting until the glaciers reach over-deepenings in locations upsteam of the ice front. These follow the same triggering progression observed at similar glaciers further north in Baffin Bay.

3.2 Central West

Despite having only 19 glaciers, the central west sector of the ice sheet discharges a substantial 79 Gt/yr with approximately 46% from the prominent Jakobshavn Isbræ (JI) [Mouginot et al., 2019]. The break-up of JI's floating extention in 2003 [Podlech and Weidick, 2004] comprised a >100 km^2 areal loss, contributing a total 171 km^2 by 2018 to the total 288 km^2 areal loss from the CW sector. The loss of grounded ice in the CW led to a substantial acceleration in discharge, reaching 79 Gt/yr in 2018 compared to 64 Gt/yr in 1992.

The central west glaciers are split between the Ummannaq Region (11 glaciers) and Disko Bay (8 glaciers), which are divided by the Nuussuaq Peninsula. The central west region is one of the most completely surveyed sectors in Greenland due to its relatively easy access from several medium-sized towns and harbors, and the early melting of its seasonally-formed sea ice layer. Bathymetry measurements in this area are largely provided by OMG but other campaigns, including the Ph.D. work of Nolwenn Chauché have contributed substantially to the maps in this area [Chauche, 2016]. CTDs are also available within the majority of fjords in this area.

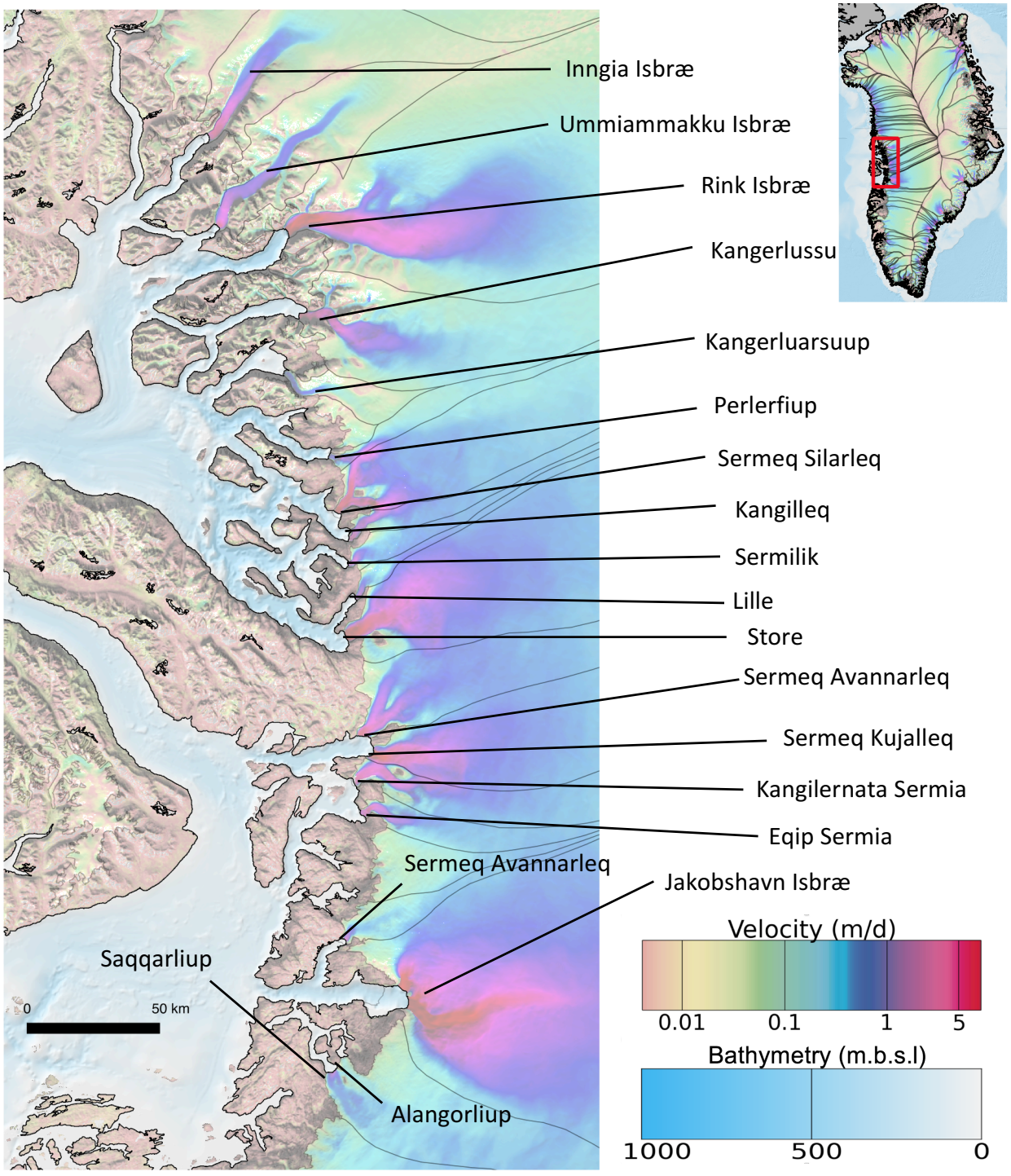

Figure 3.8: Map of Central West Greenland Glaciers

Overview of CW Greenland glaciers. Note that there are two glaciers named Sermeq Avannarleq – one which terminates in the more southern Illulisat Isfjord and another which terminates in Torssukataq Fjord.

3.2.1 Uummannaq Region

Near the town of Uummannaq (70.68°N, 52.13°W), the 11 glaciers include Inngia Isbræ, Ummiammakku Isbræ, Rink Isbræ, Kangerlussup Sermia, Kangerluarsuup Sermia, Perlerfiup Sermia, Sermeq Silarleq, Kangilleq, Sermilik Isbræ, Lille Glacier, and Store Glacier.

Glacier Evolution From 1985 until the end of the 1990's, the ice margins of Uummannaq glaciers maintained approximately constant positions. The turn of the millennium brought widespread changes to the glacier ice fronts, with a uniform retreat initiated at Inngia Isbræ (10 km), Ummiammakku Isbræ (4 km), Kangerluarsuup Sermia (1 km), Perlerfiup (3 km), Sermeq Silarleq (5 km), and Lille Glacier (1.5 km). The retreats of Inngia Isbræ, Sermeq Silarleq, and Lille Glacier occurred at a nearly constant rate while the other three experienced a step-wise retreat which restabilized at inland fjord constrictions. The impact of fjord geometry on inland retreat has previously been emphasized for these glaciers by Felikson et al. [2017]. While these 6 glaciers have retreated, the other 5 adjacently-located glaciers have maintained approximately constant front positions over the same time period.

The Role of Ocean Melt Ice front undercutting rates cover a wide range from an average of 0.41 m/d at Kangerluarsuup Sermia to 1.58 m/d at Rink Isbræ. Variations in undercutting largely account for inter-glacier variations in retreat experienced following increased thermal forcing. At Inngia Isbræ, q_m increased from 0.8 m/d 1992-1997 to nearly 1.2 m/d 1999-2003, yielding a positive q_m^{anom} which was sufficient to trigger a retreat that continued through 2019. The decline in fjord depth with retreat reduced q_m back to 0.8 m/d as a smaller portion of the ice front was in contact with deep, warm, AW. This style of retreat differs from that of Kangerluarsuup which was controlled completely by undercutting where $R \approx q_m^{anom}$.

At Sermilik, the stable ice front is well-explained by variations in TF and q_m: the glacier terminus rests in shallow water (<100 m) and the ice front is in contact with colder surface waters which did not experience the same increase in TF as the deeper glaciers. The other three glaciers in Uummannaq – Rink Isbræ, Kangerlussuup Sermia, and Store Glacier – did experience substantial

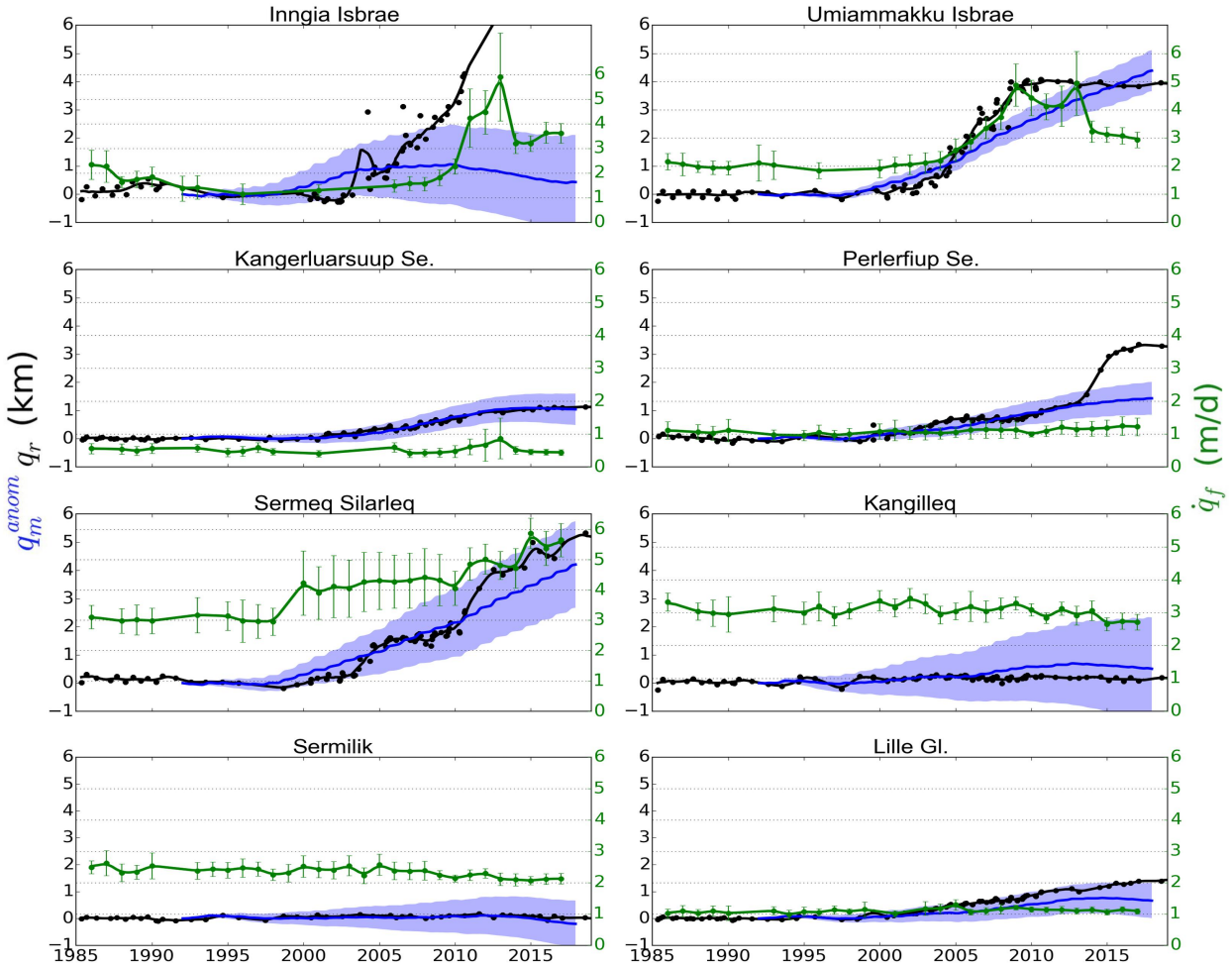

Figure 3.9: Uummannaq Region Glacier Results

Summary of the ice front retreat (q_r), cumulative melt anomaly (q_m^{anom}), and ice velocity (q_f) for 8 glaciers in Uummannaq Bay.

melt increases but did not experience ice front retreat. The contrasting stability of these glaciers is explained by their fjord geometry and ablation mechanisms: all three terminate in fjord constrictions and have documented calving via large tabular ice bergs [e.g. Medrzycka et al. [2016]]. In effect, these glaciers are calving dominated.

3.2.2 Disko Bay

There are 8 glaciers which terminate in Disko Bay: Sermeq Avannarleq, Sermeq Kujalleq, Kangilernata Sermia, and Eqip Sermia in or around Torssukataq fjord, and Sermeq Avannarleq, Jakobshavn Isbræ, Alangorliup, and Saqqarliup in Illullisat Isfjord.

Glacier Evolution Ice front retreat has been minimal in Torssukataq fjord with a short-lived 1 km retreat observed at Sermeq Kujalleq in 1997-2998 and little change observed at Sermeq Avannarleq. In fact, the ice front of Sermeq Avannarleq has been stable for more than a century [An et al., 2018]. At the adjacent Kangilernata Sermia and Eqip Sermia, ice front retreat is observed to start around the year 2000, and continued to 2015.

In Illullisat Isfjord, the retreat of Jakobshavn Isbræ associated with the break-up of its floating ice extension is well-documented (e.g. [Holland et al., 2008, Podlech and Weidick, 2004]), but the other three peripheral glaciers in the area have also undergoing ice front retreat: Sermeq Avannarleq began a 3 km retreat around the year 2000 while Alangorliup Sermia and Saqqarliup Sermia have reatreated by 0.5 km and 1 km, respectively, over the same time period.

The Role of Ocean Melt Similar to the changes observed in Uummannaq, Disko Bay warmed by more than 2°C between 1992-1997 and the 1997-2008 periods. The mean undercutting rates range from 0.39 m/d at the shallow Sermeq Avannarleq terminating in Illullisat Isjord to 1.01 m/d at Eqip Sermia. At Kangilernata and Saqqarliup, melt anomalies are observed to control glacier retreat, with the magnitude of the melt anomaly approximately equivalent to the retreat distance. The parameterized melt at Jakobshavn Isbræ yields an estimated mean undercutting rate of 1.92 m/d, and a peak around 5 m/d but this rate may likely be estimated poorly due to the presence

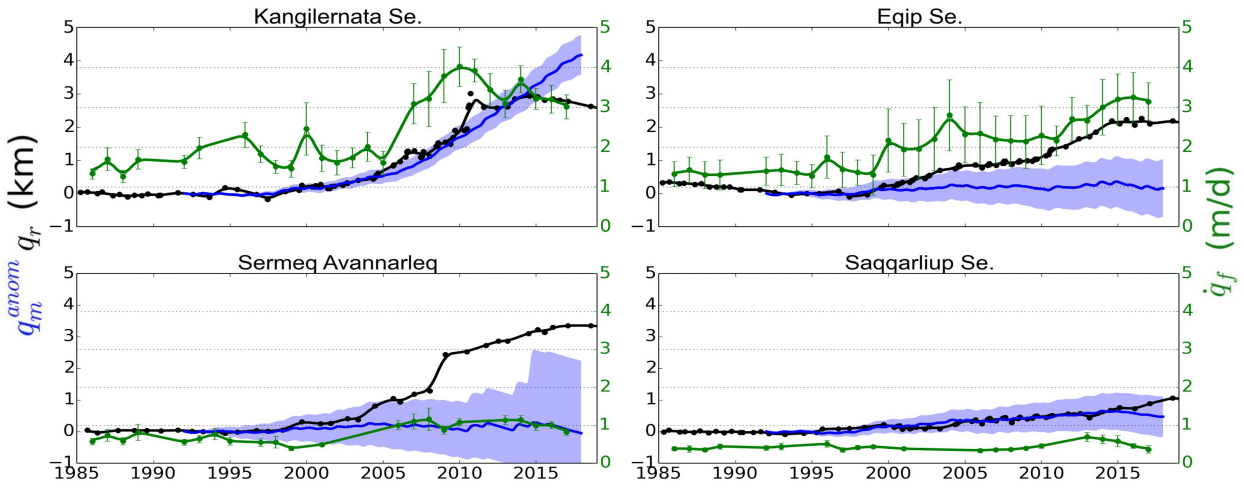

Figure 3.10: Disko Bay Region Glacier Results

Summary of the ice front retreat (q_r), cumulative melt anomaly (q_m^{anom}), and ice velocity (q_f) for 4 glaciers in Disko Bay.

of a floating extension and unique fjord geometry. In fact, Khazendar et al. [2019] estimate peak melt rates which are twofold higher than these estimates.

3.3 Southwest Greenland

The southwest sector of the ice sheet has the fewest number of marine-terminating glaciers (15) and accordingly, constitutes the second-lowest lowest flux (30 Gt/yr or 6%) from the ice sheet. The SW sector has seen the smallest ice area loss with only 41 km^2 of retreat between 1992 and 2019. More than half of this area loss is observed at Narsap Sermia which retreated by 21 km^2, or 5 km on average. By flux, the most significant glacier in the region is Ukaasorsuaq which discharged an average 6.1 Gt/yr between 1992 and 2018 [Mouginot et al., 2019], equivalent to 20% of the sector total. In all, the glaciers terminating in this sector can be divided into three broad regions: 3 glaciers which terminate in Godthåbsfjord near the capital city of Nuuk, 5 glaciers which terminate near the town of Paamiut, and 7 glaciers which terminate near the town of Narsarsuaq.

Despite being surveyed nearly every year, brash ice conditions have prevented the measurement of bathymetry near the terminus of any glacier in SW Greenland, although the majority of Godthåbsfjord

has been surveyed. CTDs are abundantly available from annual cruises conducted by the Danish Meteorological Institute on the continental shelf and within Godthåbsfjord, although measurements near the glacier terminus positions are non-existent.

3.3.1 Godthåbsfjord

Due to its proximity to the capital city of Nuuk (64.18°N, 51.69°W), Godthåbsfjord represents one of the best-studied areas in all of Greenland. Yet, while oceanographic measurements are abundant within the fjord, thick brash ice has prevented direct measurements of the bathymetry near the terminus regions. The three glaciers in this region include Narsap Sermia, Akullersuup Sermia, and Kangiata Nunaata.

Glacier Evolution Prior to the late 1990's, glacier ice margins were approximately constant in this region. Kangiata Nunaata has routinely grown an approximately 2 km floating extension in the winter time which subsequently breaks up during the summer months [Motyka et al., 2017]. Near the turn of the century, the ice margin of Kangiata Nunaata began to retreat, sustaining a 2 km retreat between 2000 and 2010. During this time, the ice fronts of the neighboring glaciers remained approximately constant. After 2010, as Kangiata Nunaata began to restabilize, the ice front of Narsap Sermia began a 5 km retreat from a moraine where it had terminated since the Little Ice Age [Motyka et al., 2017]. The ice front of Akullersuup Serma has remained in approximately the same condition since 1985.

The Role of Ocean Melt As observations within Godthåbsfjord are abundant since 2006, it is possible to assess the history of ocean state within the fjords directly from observations. This fjord is known to have two main sources of heat: one from the west Greenland current and one internal to the fjord [Mortensen et al., 2011]. Observations since 2006 show a warming trend within the fjord occurring around 2010, around the same time Narsap Sermia underwent a 4 km retreat. The undercutting rates at these three glaciers are similar at 0.8 m/d on average, but the shallow bathymetry of Akullersuup (< 50 m) did not allow for a substantial increase in melt. On the other

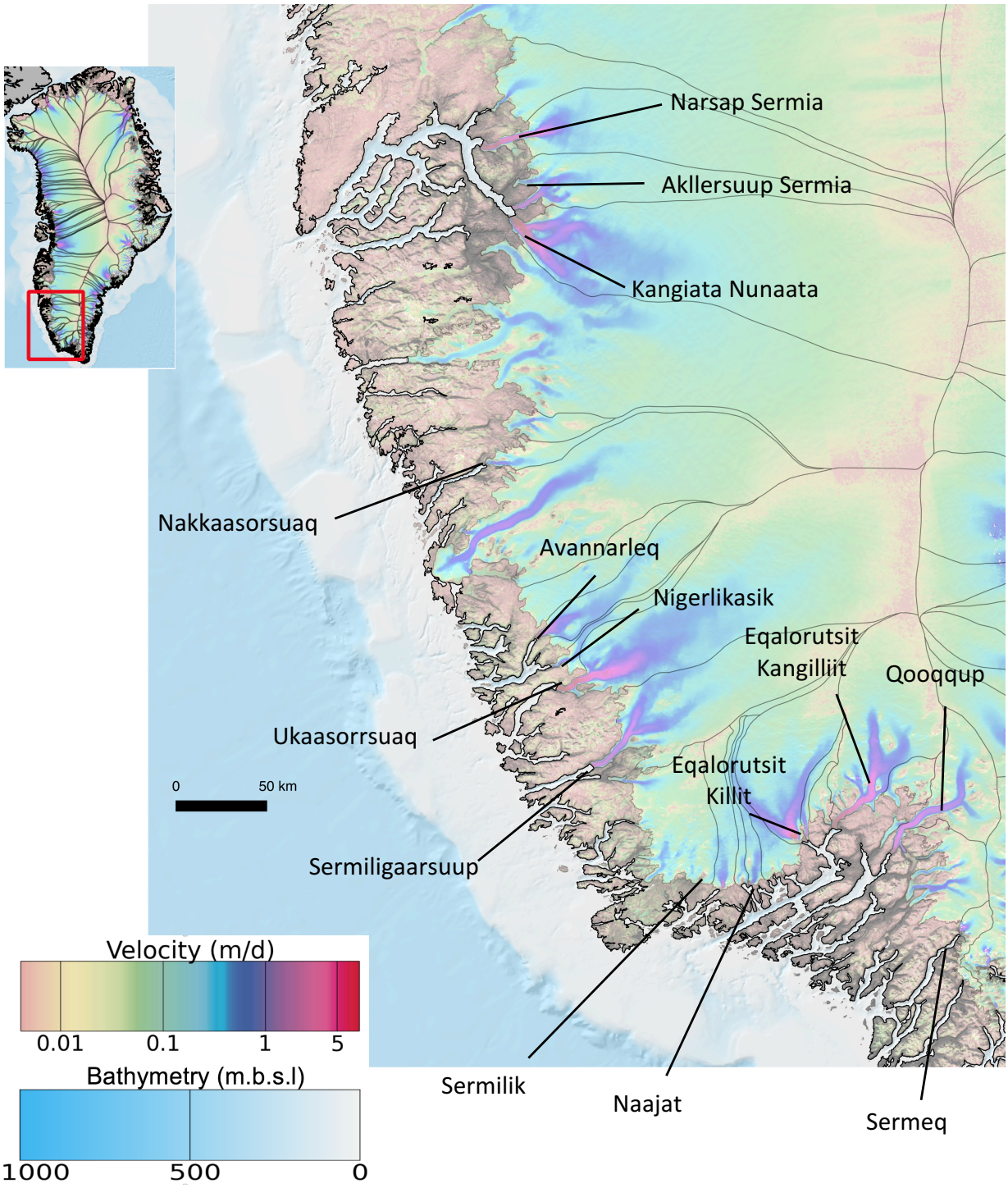

Figure 3.11: Map of Southwest Greenland Glaciers

Overview of CE Greenland glaciers. Note that Eqalorutsit Killiit encompasses two branches - the main branch and the eastern or "E" branch.

hand, melt increased nearly two fold on Narsap Sermia and Kangiata Nunaata, coincident with the retreat of their ice fronts. At both of these glaciers, the retreat distance of the front exceeds the cumulative melt anomaly by 1-2 km, indicating enhanced calving processes associated with retreat contribute substantially to their retreat.

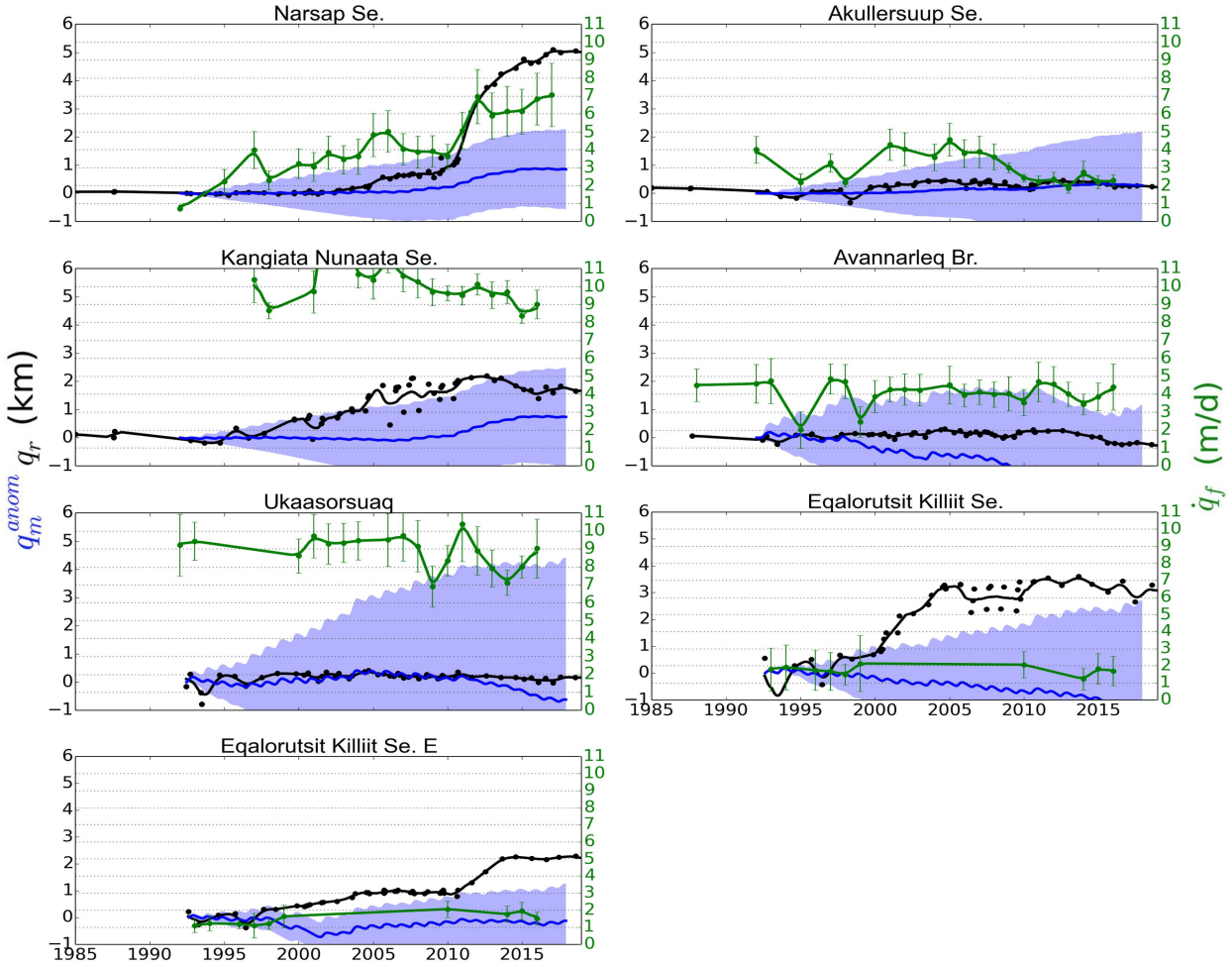

Figure 3.12: SW Region Glacier Results

Summary of the ice front retreat (q_r), cumulative melt anomaly (q_m^{anom}), and ice velocity (q_f) for 7 glaciers in southwest Greenland.

3.3.2 Paamiut Region

Near the town of Paamiut (61.99°N, 49.67°W), there are 5 marine-terminating glaciers: Nakkaasorsuaq, Avannarleq Bræ, Nigerlikasik, Ukaasorsuaq, and Sermiligaarsuup Bræ. In contrast to

Godthåbsfjord to its north, the glaciers in this region have been poorly surveyed – only Ukaasorsuaq and Avannarleq Bræ have ice fronts which, in the BedMachine dataset, terminate in fjords deeper than 50 m mean water depth. For the other three glaciers, the mean water depth is below 5 m.

Glacier Evolution The five glaciers in this region underwent only small perturbations in their front position: the largest retreat was 1.09 km at Nigerlikasik which occurred between 2000 and 2010 while the ice front positions at other glaciers remained within 500 m between 1992 and present.

Role of Ocean Melt Due to the shallow bathymetry and lack of oceanogrpahic measurements in this region, it is only feasible to assess the retreat of Ukaasorsuaq and Avannarleq Bræ in the context of oceanic change. Both glaciers in this region are relatively shallow – 91 m and 57 m mean depth, respectively – and are largely in contact with near-surface waters influenced heavily by seasonal air-sea heat exchange. Neither glacier shows a substantial melt anomaly and the ice fronts of these two glaciers are accordingly stable.

3.3.3 Narsarsuaq Region

Near the town of Narsarsuaq (61.16°N, 45.43°W) on the southern shores of Greenland, there are 4 large marine-terminating glaciers – Eqalorutsit Killiit Sermia and its eastern branch, Eqalorutsit Kangilliit Semia, and Qooqqup Sermia – along with 3 smaller glaciers including Sermilik Bræ, Naajat Sermia, and Sermeq. Bathymetry measurements are not available at at majority of these glaciers but inverted gravity fields are provided at inland locations for Eqalorutsit Killiit and Eqalorutsit Kangilliit [Millan et al., 2018] providing some constraint on the shape of the bed near the terminus..

Glacier Evolution The glaciers around Narsarsuaq have shown a varied evolution since 1992 with Eqalorutsit Kangillit Sermia remaining stable while the adjacent glaciers retreated. The largest retreats are observed at Sermilik Bræ (4.9 km) and Eqalorutsit Killiit Sermia (3.1 km). Sermilik underwent a near continuous retreat between 1992 and 2011, while Naajat retreated 1 km in a

step-wise fashion between 2000 and 2005. The main branch of Eqalorutsit Killiit mirrored the step wise retreat of Naajat, losing 3 km of its terminus between 2000 and 2005, while the eastern branch of Eqalorutsit Killiit experienced the most substantial component of its retreat (1.5 km of 2.5 km in total) between 2010 and 2014. In contrast to the other glaciers near Narsarsuaq, Eqalorutsit Kangillit has maintained a constant front position since 1992. Finally, Qooqqup retreated 1 km between 1995 and 2005 before stabilizing at an inland location, and Sermeq has undergone a slow but continuous retreat since 2000, totaling approximately 1 km of ice loss.

The Role of Ocean Melt Due to sparsely surveyed bathymetry in the region and a lack of CTD measurements, it is difficult to ascertain the role of ocean melt in driving the retreat of glaciers in this region. The ice front depths at Sermilik, Naajat, and Sermeq all terminate in waters less than 2 m in depth on average in the BedMachine dataset. At Eqalorusit Kangillit, the ice front terminates in deep ($\sim$ 400 m) water which would be in contact with the warm AW later at depth. Accordingly, the estimate of melt anomalies suggest this glacier should have retreated. However, the BedMachine dataset reveals a shallow sill present in the outer-fjord area. Measurements in this region of the fjord are necessary to verify the presence of this sill, but if it indeed exists, it would be sufficient to block the access of warm water to the glacier and help support the stability of the ice front. At Qooqqup, the retreat of the ice front follows a progression from shallow ($<$ 100 m) water to deep water ($>$ 300 m) which yields a greater contact with warm waters in the interior of the fjord. However, the deep section of the fjord is deduced from mass conservation while the exterior of the fjord is interpolated. Thus, the increase in melt from 1 m/d on average to 3 m/d likely does not reflect the change in melt on the glacier. There is an increase in TF associated with the retreat timing, but it is impossible to discern the impact of melt on the retreat of this ice front.

3.4 Southeast Greenland

SE Greenland, with a mean discharge of 154 Gt/yr between 1992 and 2018, discharges more ice than any other region on the ice sheet despite only making up 9.4% of the ice sheet by area [Mouginot et al., 2019]. The glaciers in this region underwent substantial retreat between 2000 and 2006

[Howat et al., 2008] with several continuing to retreat to the present day [Bunce et al., 2018]. In total, the retreat of SE glaciers accounted for the loss of 336 km^2 of grounded ice between 1992 and 2019 (14% of grounded ice loss). Over this same time, ice discharge increased 30 Gt/yr (or 18%) over the same time with the majority of ice acceleration occuring between 2000 and 2005 in the regime of fast grounded ice loss. The SE can be spatially divided into 4 broad subregions: the southern and northern area of the Kong Christian IV Coast (21 and 13 glaciers, respectively), Køge Bay and Ikertivaq Bay (10 glaciers), and the well-studied Sermilik fjord (5 glaciers). The most significant glaciers in this region by flux are Helheim Glacier and the central branch of Køge Bugt with ice discharges of 28 Gt/yr and 19 Gt/yr, respectively – two of the most productive glaciers in Greenland. The sector also contains Midgård Glacier which underwent one of the most significant retreats of any glacier on the Greenland Ice Sheet.

This region was surveyed extensively during the OMG campaign, providing bathymetric measurements and CTDs in very close proximity to the glacier calving fronts. Most fjords have near-complete measurements from the fjord mouth to the glacier terminus, with notable exception including Gyldenløve Fjord and A.P. Bernstorff Fjord. In addition, gravity measurements are provided near the terminus regions of several glaciers, as detailed inMillan et al. [2018].

3.4.1 Southern King Christian IV Coast

The southern section of the King Christian IV coastline contains several regions that encompass 21 different glaciers. From south to north, there are 4 branches of Danell Glacier, Kangerluluk Glacier, two branches of Herluf Trolle Glacier, two branches of Anorituup Kangerlua Glacier, four branches of Napasorsuaq Glacier, 3 branches of Puisortoq Glacier, and 5 branches of Mogens Heinesen Glacier.

Glacier Evolution In the southern section of the King Christian IV coastline, the reconstructed glacier front history reveals little change before the year 2000, widespread retreat between 2000 and 2008, and a varied evolution thereafter with some glaciers continuing to retreat while others restabilized in upstream fjord constictions. For the Danell Glaciers, the two middle branches (S

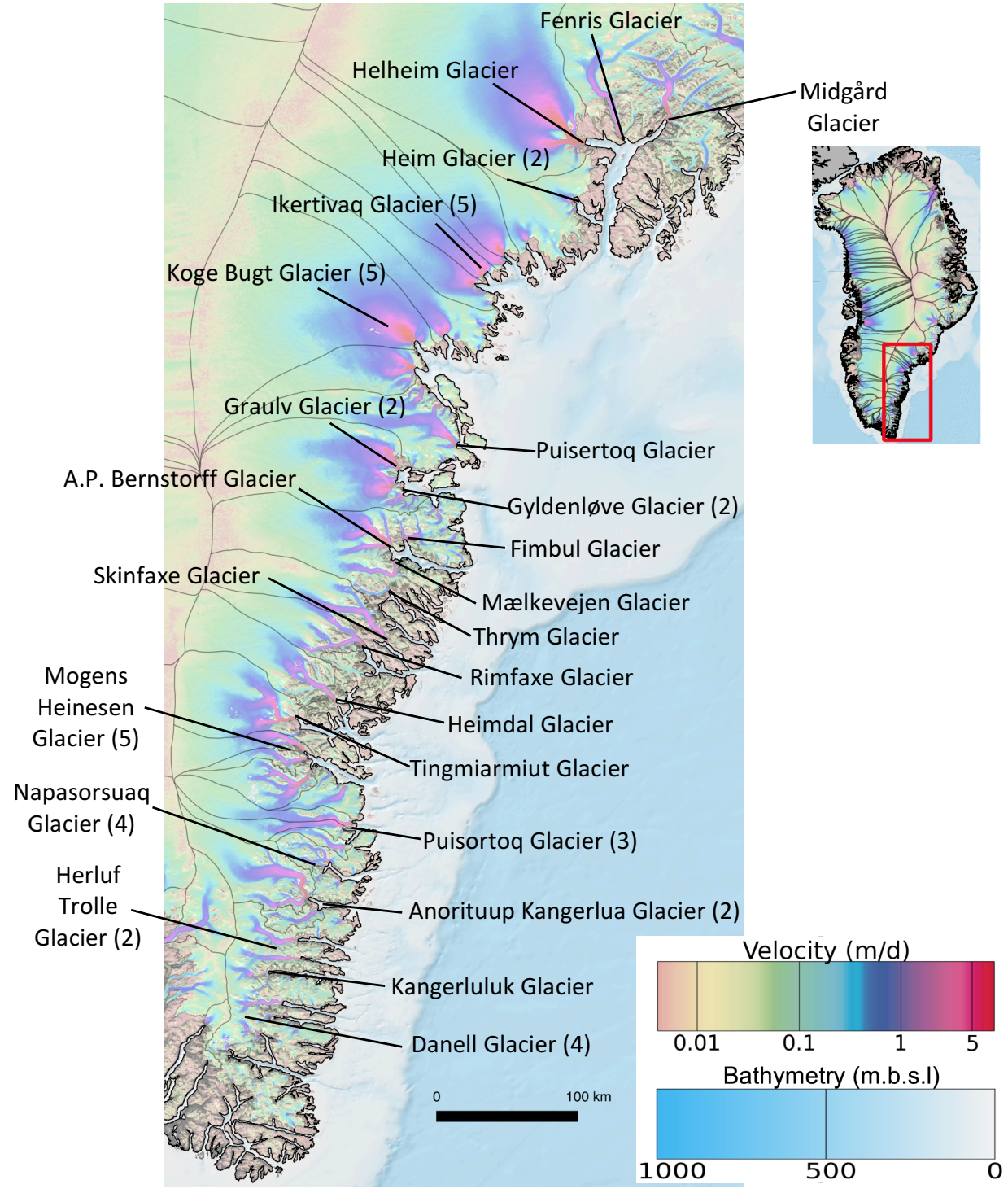

Figure 3.13: Map of Southeast Greenland Glaciers

Overview of SE Greenland glaciers. Numbers in parenthesis represent the number of glaciers encompassed by the name indicated. Names without numbers provided refer to a single glacier.

and SS) which terminate in the same fjord retreated most substantially at 1.5 km each. The most southern branch (SSS) retreated a minimal 0.5 km while the main Danell Glacier has maintained an approximately constant front position despite a brief retreat and re-advance between 2000 and 2008. Kangerluluk Glacier retreated substantially with a 2 km retreat 1997 - 2005, an abrupt 6 km retreat in 2005 through a wider portion of the fjord, and a subsequent 2 km retreat between 2006 and 2011 before the ice front re-stabilized in a narrow upstream location. The S and N branches of Herluf Trolle Glacier retreated by 2.5 km and 1 km respectively, with each showing a step-wise retreat beginning around 2000 and ending around 2005. The S branch of Anorituup Kangerlua shows a similar 1 km retreat in a step-wise fashion, while the N branch has experienced continued retreat totaling 5 km despite a brief re-advance between 2005 and 2015. The Napasorsuaq glaciers experienced similar trends, with the SS and N branches experiencing a step-wise retreat (1 km and 1.5 respectively), the S branch continuing a 2.5 km retreat, and the C branch remaining stable over the past 30 years. The Puisortoq glaciers have retreated continuously since the year 2000 after a period of stability over at least 15 years. The majority of the Mogens Heinesen glaciers have experienced substantial retreat of 4-8 km, with only the small SS branch experiencing relative stability.

The Role of Ocean Melt At Danell Glacier SSS and SS, the BedMachine dataset reveals a fjord which remains deep until the glacier terminus where it rises above sea level immediately upstream of the glacier front. In this fjord geometry, enhanced undercutting associated with increased temperature of deep AW within their fjords would not play a significant role in causing the glaciers to retreat, and accordingly, the retreats have been small and the parameterized melt is vastly overestimated. In other words, the evolution observed at these glaciers is largely dominated by calving processes associated with their flow off of shallow plateaus into the ocean. At Danell S, the depth of the fjord remains consistent with a mean water depth 100-200 m below sea level, and ice front undercutting is observed to play a dominant role in the retreat of the ice front: the cumulative undercutting anomaly at this glacier is consistent with the 1.5 km retreat which ensued following an increase in melt around the year 2000. At Danell Glacier, on the other hand, melt anomalies do not accrue over the entire time period, and the ice front is observed to remain stable.

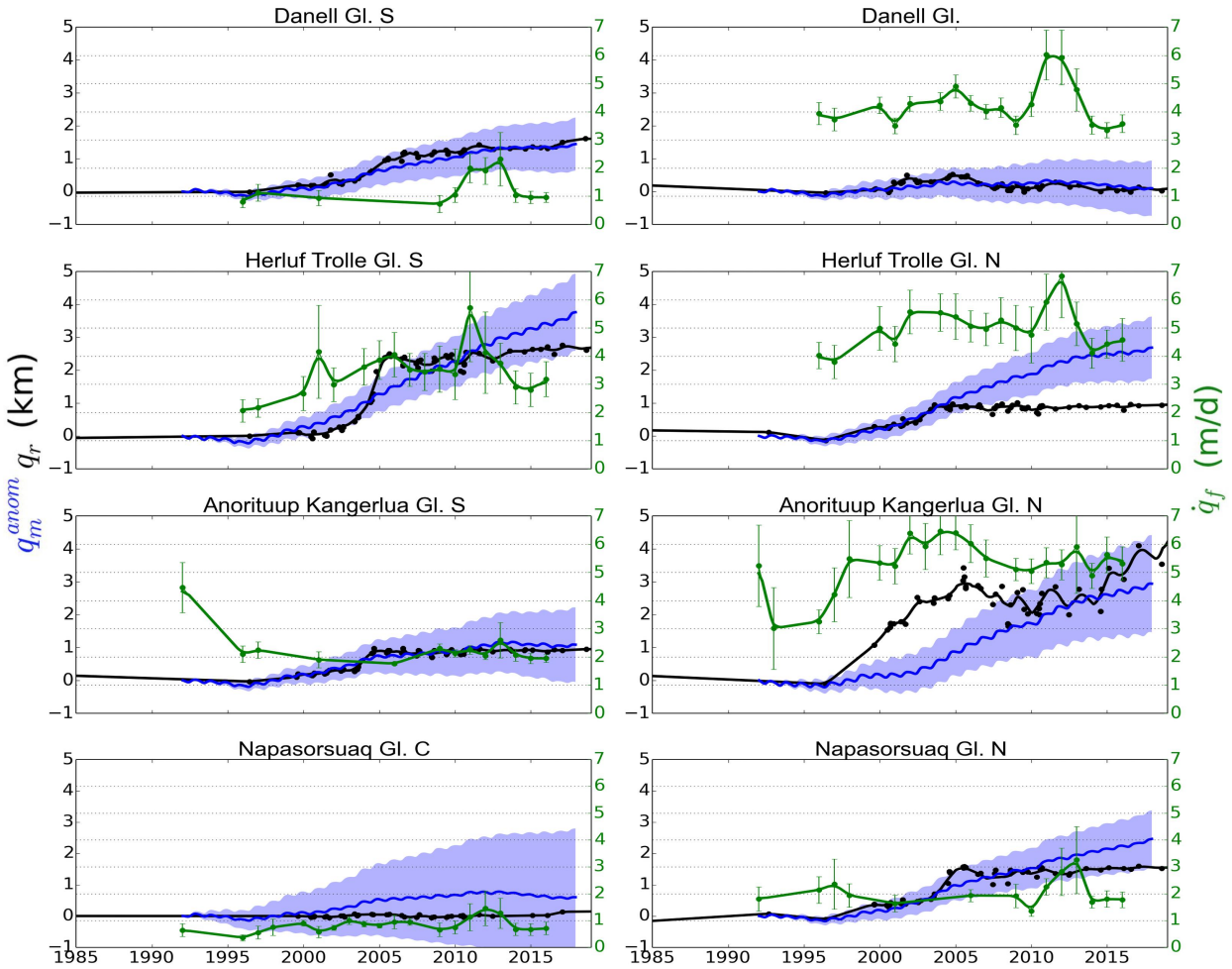

Figure 3.14: Southern King Christian VI Coast Glacier Results: Part 1

Summary of the ice front retreat (q_r), cumulative melt anomaly (q_m^{anom}), and ice velocity (q_f) for 6 glaciers in southwest Greenland.

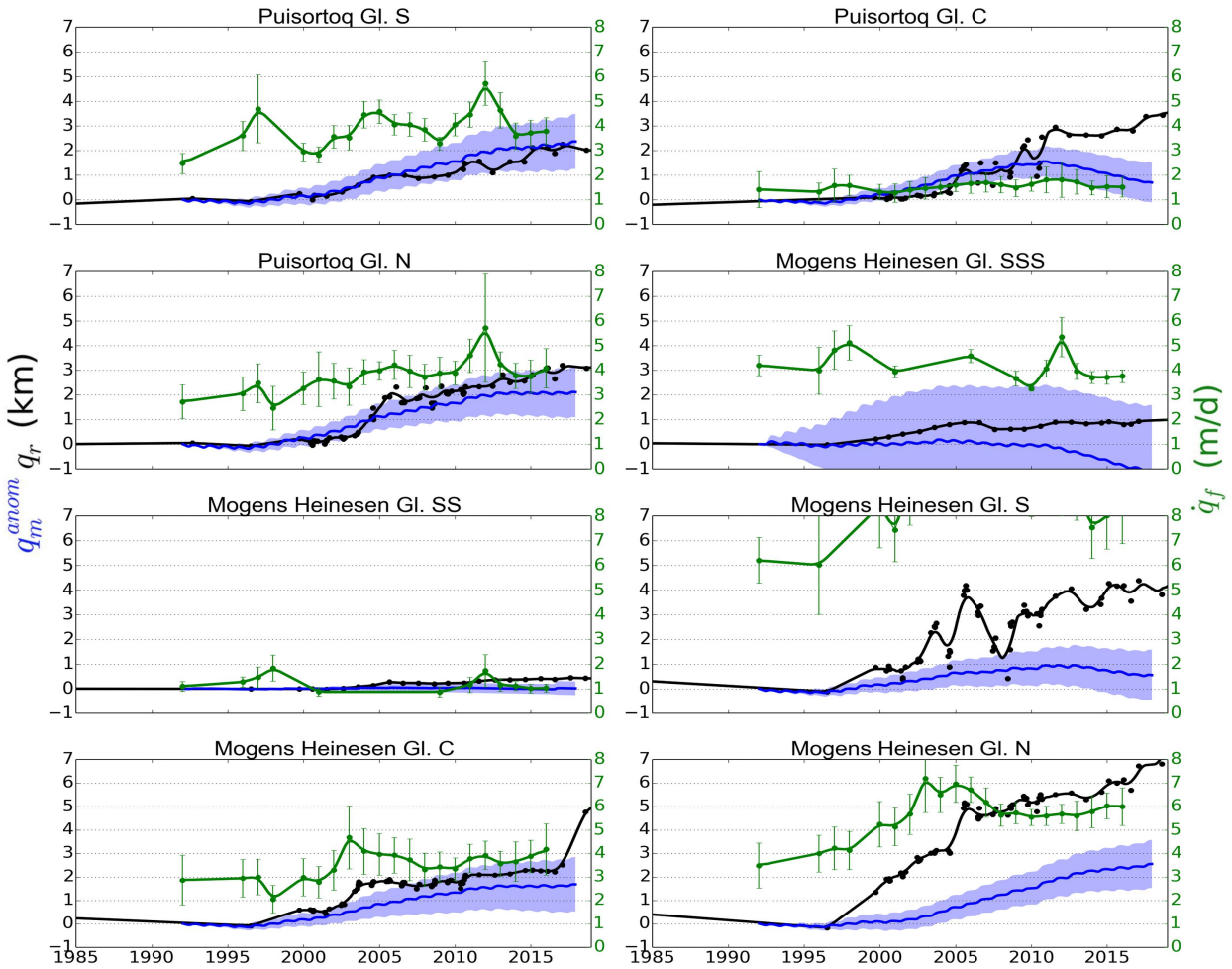

Figure 3.15: Southern King Christian VI Coast Glacier Results: Part 2

Summary of the ice front retreat (q_r), cumulative melt anomaly (q_m^{anom}), and ice velocity (q_f) for 6 glaciers in southwest Greenland. Note that the velocity scale bar for Mogens Heinesen S is greater than for the other examples.

In the continuously-deep fjord where Herluf Trolle S terminates, increased TF after 1997 led to an increase in q_m from 1.5 m/d to 2 m/d, at the same time that the ice front began to retreat. The total retreat distance for this glacier is within the bounds of uncertainty for M^{anom}, indicating that the retreat of this glacier is largely dominated by melt processes. While TF at Herluf Trolle N is similar to its southern counterpart, the bed elevation upstream of the calving front quickly becomes shallow. Thus, the increase in TF after 1997 initial raises melt to induce a retreat, but the ice front quickly re-stabilized in an upstream constriction on a shallow bed, and calving processes are the substantial form of ablation in this region of the fjord. At Anorituup Kangerlua S, the progression of melt anomalies is consistent with the progression of retreat.

3.4.2 Northern King Christian IV Coast

There are 13 glaciers in the northern section of the King Christian IV coastline including Tingmiarmiut Glacier, Heimdal Glacier, Rimfaxe Glacier, Skinfaxe Glacier, Thrym Glacier, Mælkevejen Glacier, A.P. Bernstorff Glacier, Fimbul Glacier, two branches of Gyldenløve Glacier, two branches of Graulv Glacier, and Puisertoq Glacier.

Glacier Evolution In the northern section of the King Christian VI coastline, the majority of glaciers began multi-kilometer retreats initiated around the year 2000, while others have remained stable. For example, Tingmiarmut underwent a 4 km retreat between 2000 and 2019 with substantial inter-annual oscillations in its front position. Yet, the three glaciers to the north of Tingmiarmiut – Heimdal, Rimfaxe, and Skinfaxe – have remained approximately stable during this same time period. The glaciers in Bernstorff fjord – Mælkevejen, A.P. Berstorff, and Fimbul – have undergone substantial retreat which were initiated at the end of the 1990's. The retreats of Mælkevejen (6 km) and Fimbul (4 km) have been nearly continuous until 2019 while A.P. Berstorff underwent a step-wise retreat, restabilizing in 2005. The glacier evolution in Gyldenløve fjord is similar with ice front retreat starting at the turn of the millennium. Gyldenløve S began a slow, 1 km retreat between 2000 and 2010, and then retreated 2 km between 2010 and 2012 before stabilizing in an upstream position. Gyldenløve N, on the other hand, has retreated nearly continuously

since 2000, with a total retreat distance of 2 km. The main branch of Graulv underwent an abrupt 1.5 km retreat between 2002 and 2004 while the eastern branch had only a 0.5 km retreat over the same time. Finally, Puisertoq began retreating in 1997 and has continued this retreat until present day.

The Role of Ocean Melt For the 13 glaciers in this region of the southeastern coastline, there is clear evidence for ocean-induced retreat at 7 glaciers. For Tingmiarmiut, Gyldenlove N, Puisertoq, and Graulv, the cumulative melt anomaly matches closely with both the magnitude and timing of glacier retreat, indicating that increased undercutting is the primary driver of the multi-kilometer retreats observed at these ice fronts. For the other 3 glaciers – Maelkevejen, A.P. Bernstorff, and Gyldenlove S – melt anomalies increased at the time the glacier began to advance but the cumulative anomaly is smaller than the total retreat, reflecting a triggering of retreat. In these cases, the rate of iceberg calving increased as the ice front retreated into a different bed geometry regime. For Maelkevejen and A.P. Bernstorff, ice velocity more than doubled once retreat was initiated while Gyldenlove S maintained consistent flow speeds. The three stable glaciers – Heimdal, Rimfaxe, and Skinfaxe – are positioned on clearly defined glacial sills. As mentioned for glaciers in the previous sections, these sills maintain stability by naturally undercutting the glacier terminus as it advances, causing calving with little influence from enhanced ocean melt. Hence, these glaciers represent additional cases where the ocean has played a negligible role over the past several decades. Finally, for the eastern branch of Graulv, Fimbul, and Thrym, the currently available data for fjord geometry indicates extremely shallow bathymetry in the vicinity of their ice fronts. For these cases, it is impossible to conclude on the ocean's role in modulating their ice front positions.

3.4.3 Køge Bugt and Ikertivaq

Between the King Christian IV Coast and Sermilik Fjord, there are two large bays where several glaciers terminate: Køge Bugt and Ikertivaq, each with 5 separate glaciers.

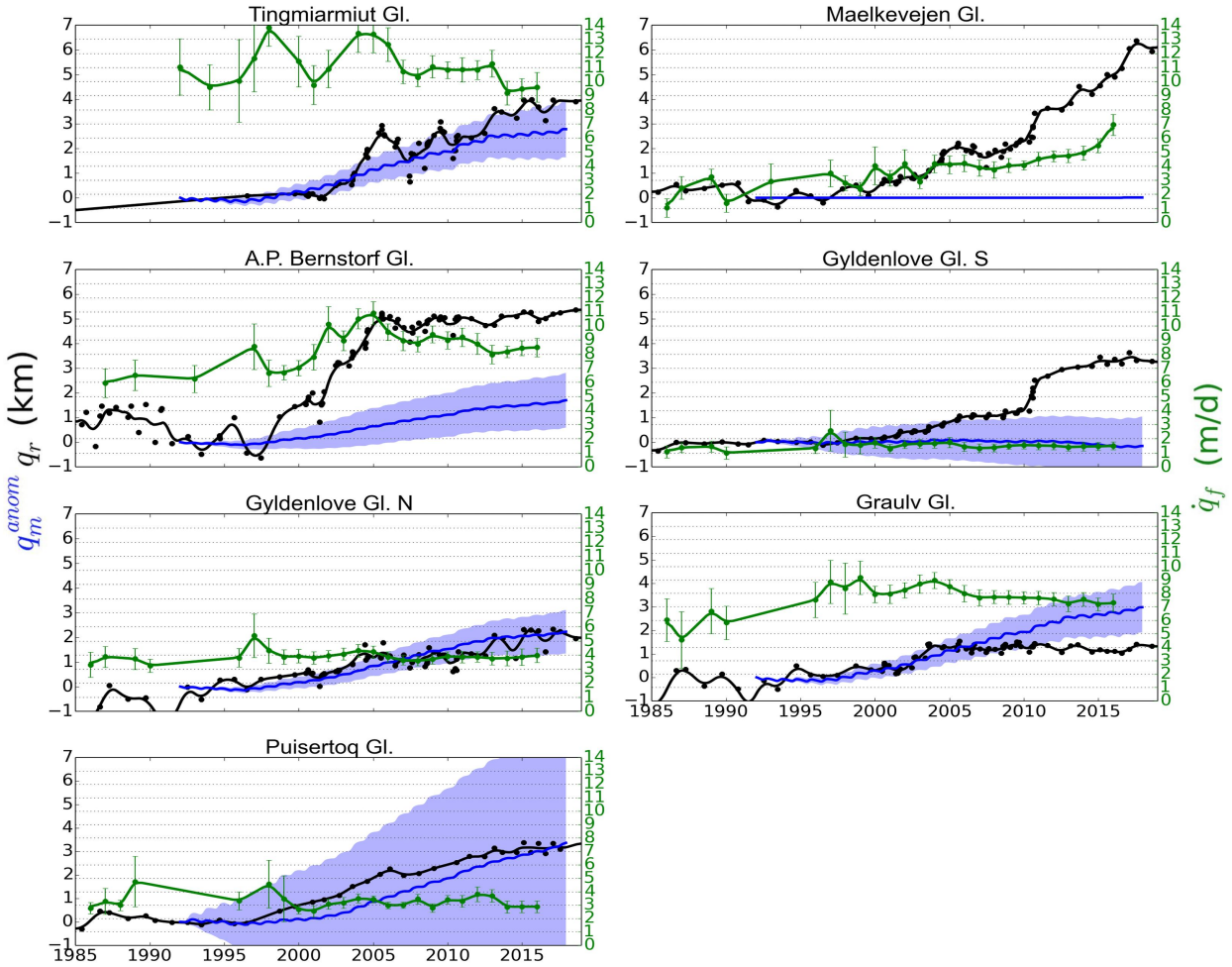

Figure 3.16: Northern King Christian VI Coast Glacier Results

Summary of the ice front retreat (q_r), cumulative melt anomaly (q_m^{anom}), and ice velocity (q_f) for 6 glaciers in southwest Greenland.

Glacier Evolution Køge Bugt SSS and SS terminate on the outer periphery of Køge Bugt, separate from the main center of the fjord. On this periphery, the SSS branch remained stable since 1985, while the SS branch underwent a step-wise, 1 km retreat between 2000 and 2005. Similar small changes are seen in the main interior the the bay, with Køge Bugt S, C, and N undergoing retreats of 0.5 km, 1 km, and 1 km, respectively. The glacier evolution in Ikertivaq bay follows a nearly identical progression, with small retreats observed to initiate around the year 2000. The southern branch underwent a step-wise, 1 km retreat between 2003 and 2007, while the 1.5 km, 1 km, 4 km, and 2 km retreats of the M, N, NN, and NNN branches have taken place approximately continuously since their start around the year 2000.

The Role of Ocean Melt Consistent with the trends in melt rates for other areas in the southeast, ice front undercutting increased in the Køge and Ikertivaq Bays at the end of the 1990's. Despite the relatively high discharge rates from this collection of 10 glaciers, the small increases in melt have had a clear impact on retreat of calving margins. In Køge Bugt, the cumulative melt anomalies match well with the retreat progression at the C and N branches, with magnitudes equivalent to the 1 km retreats observed since the year 2000. The S branch within this bay, on the other hand, flows from a relatively shallow bed into the deeper bay i.e. the glacier terminates on a steep prograde slope. Similar to the geometry of glaciers with shallow sills, Køge Bugt S naturally forms small floating extensions which calve off from the face, naturally undercutting the ice front. In this geometry, increases in ocean melt do not play a substantial role in retreating the ice front margin. The SS and SSS branches both terminate in unsurveyed waters which are less than a 5 meters below sea level in the BedMachine dataset.

The situation is similar in Ikertivaq Bay - the S, M, N and NNN branches are well-explained by the progression of melt where the retreat distance is approximately equivalent to that of the cumulative melt anomaly. In contrast to these glaciers where melt has controlled the retreat of the ice fronts over a few kilometers, the front of Ikertivaq NN was experienced a triggered retreat where, after an increase in melt, calving rates increased and the total retreat distance exceeded that of melt alone.

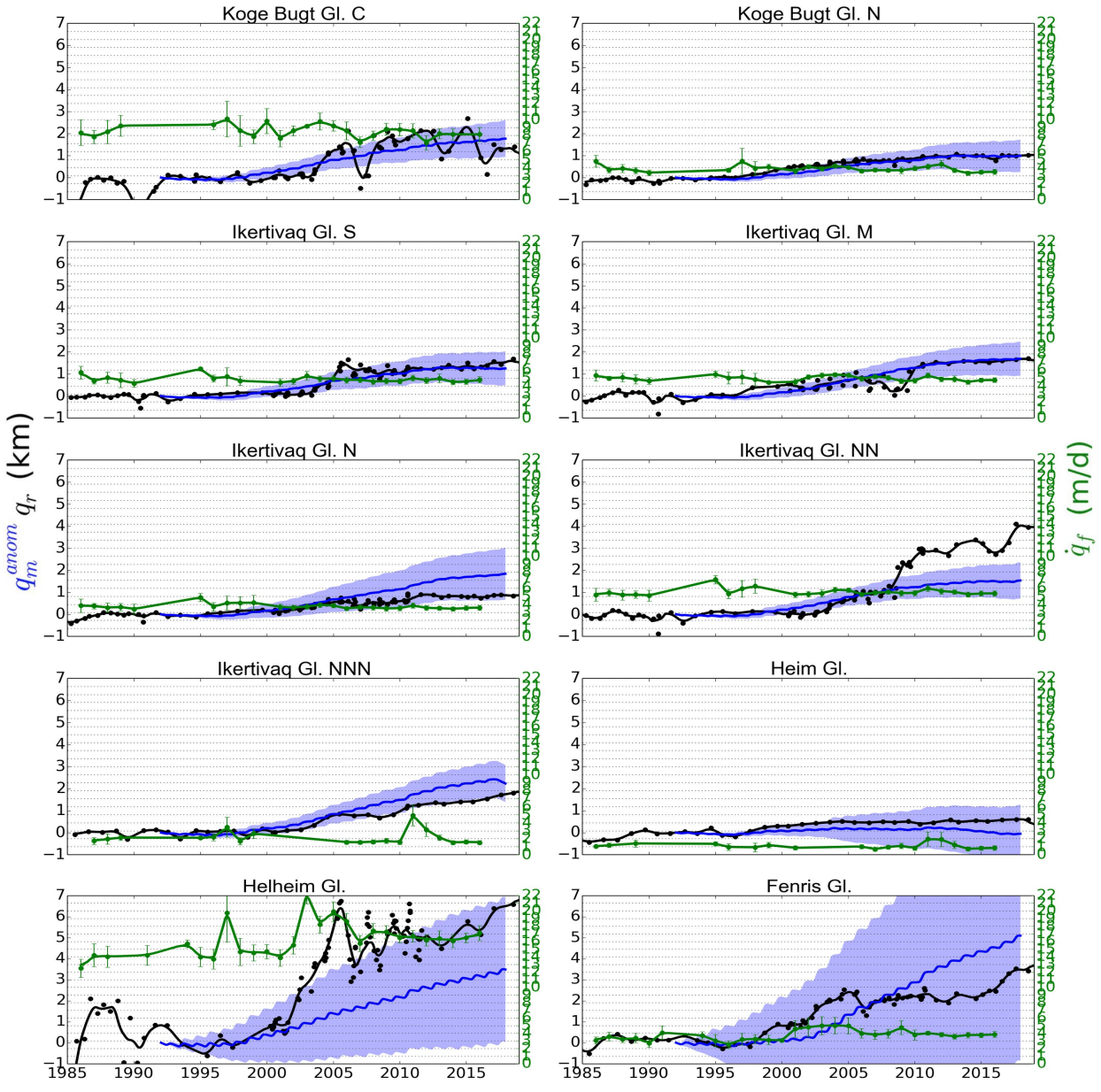

Figure 3.17: Køge Bugt, Ikertivaq, and Sermilik Fjord Glacier Results

Summary of the ice front retreat (q_r), cumulative melt anomaly (q_m^{anom}), and ice velocity (q_f) for 6 glaciers in southwest Greenland.

3.4.4 Sermilik Fjord

Sermilik fjord is one of the best studied fjords on the east coast of Greenland. There are 5 glaciers which terminate here including Heim Glacier and its southern branch, Helheim Glacier, Fenris Glacier, and Midgård Glacier.

Glacier Evolution Heim Glacier is the smallest glacier in Sermilik and terminates in two branches near the mouth of the fjord. Ice front change has been relatively small at these two glaciers, with variations in the front position totaling no more than 0.5 km over the past 30 years. This glacier behavior contrasts greatly with the three large glaciers upstream where large changes have been observed. At Helheim, the ice front position underwent only small seasonal and inter-annual perturbations until 2002 when a large retreat event occurred, retreating the calving front a maximum of 8 km from its previous position. The front rebounded nearly 4 km in the subsequent two years, before undergoing a continued retreat that has lasted until 2019. Fenris Glacier has seen a similar evolution with an initial 2 km retreat between 1998 and 2005, a small re-advance after 2005, and a continued retreat thereafter, totaling 4 km of ice loss by 2019. Finally, Midgård has retreated 15 km since 1985 with the majority of retreat occurring between 2002 and 2011. The ice front has retreat far enough inland to reach a dividing rocky outcrop, which has recently split the terminus into two separate calving fronts.

The Role of Ocean Melt The two branches of Heim Glacier have a similar geometry in which the glaciers flows from an above-sea level position into the fjord. Similar to other glacier further south (e.g. Køge Bugt S), these glaciers are naturally undercut, and their front position is dominated by calving processes rather than those which are related to ocean melt. At Helheim Glacier, the substantial 8 km retreat event observed around 2002 was preceded by an increase in melt. Hence, the retreat at Helheim was initiated by warmer ocean conditions but the large retreat distance relative to the cumulative melt anomaly indicates that calving processes also played an important role in the total retreat of Helheim's ice front. At the nearby Fenris glacier, a similar but smaller progression of retreat is observed to start along with the increased melt anomaly. However, the

large uncertainties in the bed shape near the terminus (due to a lack of bathymetric measurements) leads to large uncertainties in the quantification of the melt rate at this glacier. Last but not least, the ongoing retreat of Midgård is observed to be most substantial when fjord conditions triggered retreat at other glaciers in the region, but uncertainties in the bed shape prevent a full quantification of the ocean's impact on the retreat. While the glacier is observed to be in contact with the ocean in successive satellite images, the latest bathymetric dataset indicates extremely shallow bathymetry of less than a few meters at some points during the glacier's retreat. Because of the extreme retreat of Midgård's ice front, this fjord represent a key area where more bathymetry mapping should be focused.

3.5 Central East Greenland

The central east sector of the ice sheet discharged an average 84 Gt/yr through 45 tidewater glaciers between 1992 and 2018. Over this same time, the CE lost an approximate 240 km^2 or nearly 10% of the total loss from the ice sheet as a whole. The most significant glacier in the region is Kangerlussuaq Glacier which discharges 25.3 Gt/yr or about 30% of the ice from the CE sector.

There are 3 distinct regions of this sector including the coastline between Sermilik Fjord and Kangerlussuaq Fjord (15 gaciers), the outer arc on the Geikie Plateau (16 glaciers), and Scoresby Sound (13 glaciers). The southern portion (below Kong Christian IV Glacier) of this coastline was surveyed during the OMG campaign. CTDs are available for all glaciers except the northern branch of Laube and the southern branch of Deception Ø.

3.5.1 Sermiligaaq Fjord to Kangerlussuaq Fjord

To the best of my knowledge, there is no specific name designated for the region between Sermiligaaq Fjord and Kangerlussuaq Fjord. From south to north, the glaciers along this region of coastline include Kaarale Glacier, Knud Rasmussen Glacier and its western branch, K.I.V. Steenstrup Nordre Bræ, Laube Glaciers and its northern and southern branches, Kruuse Glacier, Uunartit Glacier,

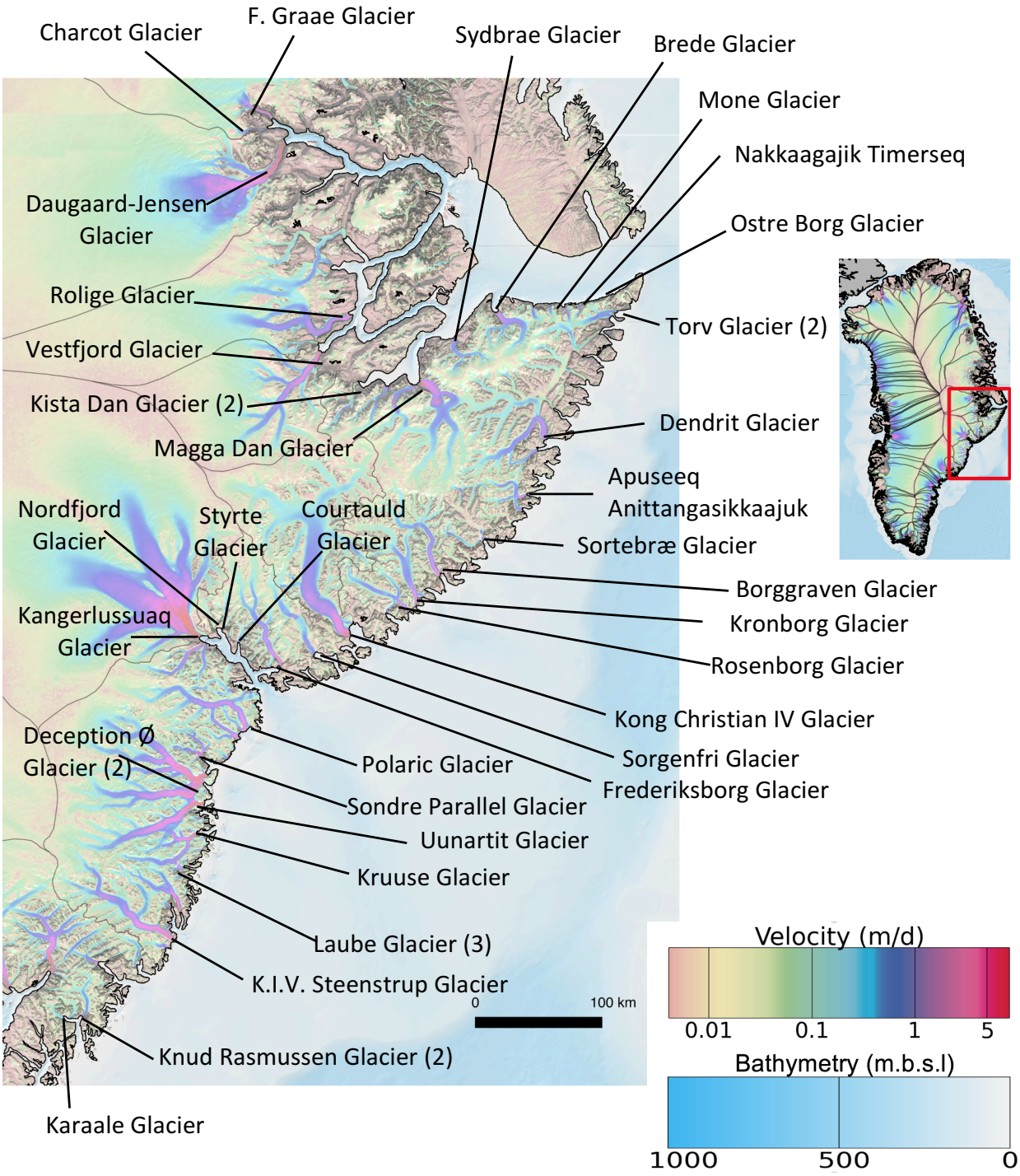

Figure 3.18: Map of Central East Greenland Glaciers

Overview of CE Greenland glaciers. Numbers in parenthesis represent the number of glaciers encompassed by the name indicated. Names without numbers provided refer to a single glacier.

two branches of Deception Ø Glacier, Sondre Parallel Glacier, Polaric Glacier and its southern branch, and Kangerlussuaq Glacier.

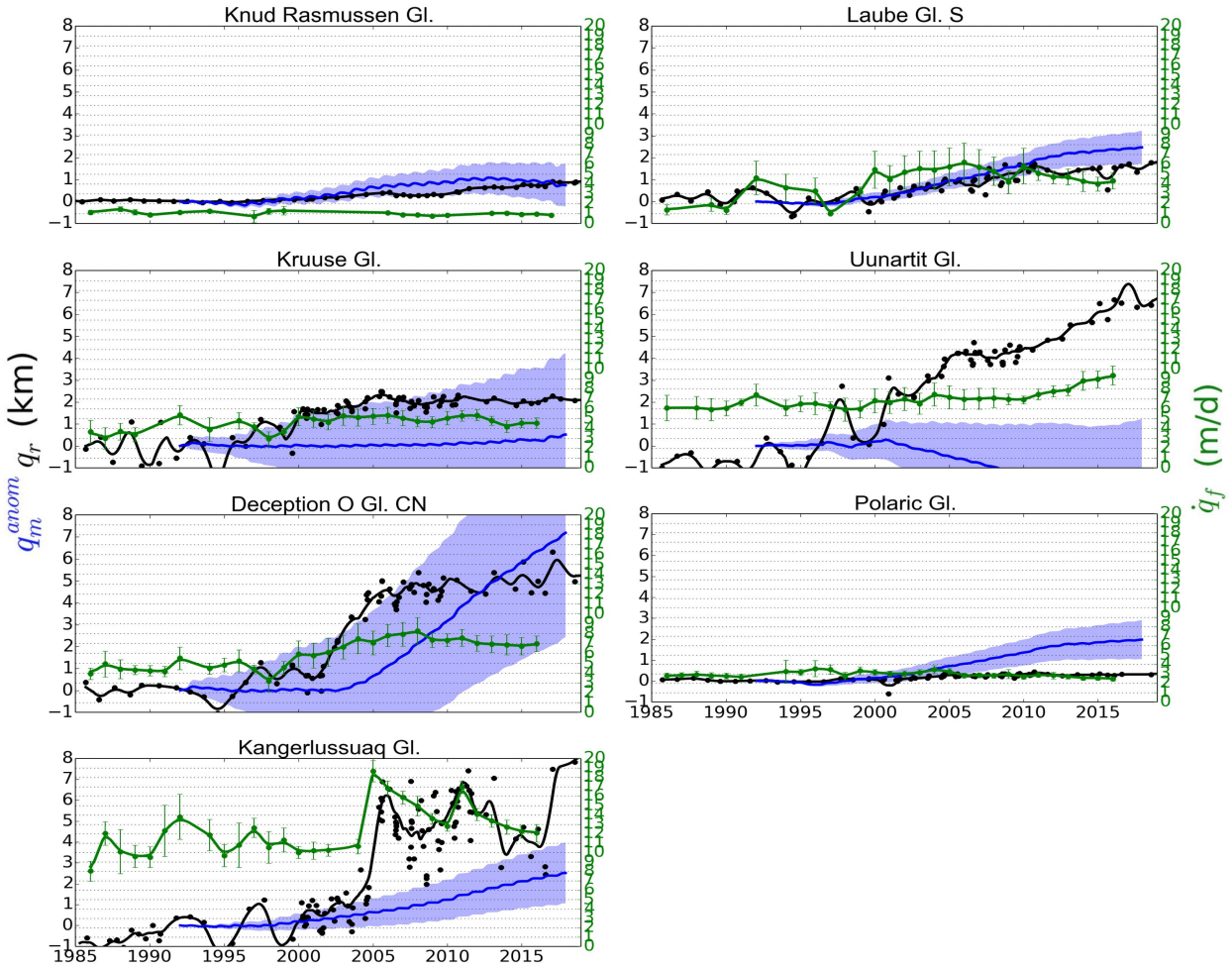

Figure 3.19: Sermiligaaq to Kangerlussuaq Fjord Glacier Results

Summary of the ice front retreat (q_r), cumulative melt anomaly (q_m^{anom}), and ice velocity (q_f) for 6 glaciers in southwest Greenland.

Glacier Evolution In Sermiligaaq Fjord, Kaarale has retreated approximately 2 km since 1985, with a near-continuous retreat rate over this time period. The western branch of Knud Rasmussen, in the same fjord, has been stable for the past 30 years, while the main branch of Knud Rasmussen underwent a 1 km retreat which started around 2005. North of Sermiligaaq Fjord, K.I.V. Steenstrup maintained a stable from position on a narrow sill from 1985 to 2016 when an abrupt 2 km retreat ensued over the past 2 years. At Laube Glacier S, the ice front retreated 1.5 km between

2000 and 2010, with large seasonal variations taking place thereafter. Laube Glacier has steadily retreated a total of 2 km, which started in 1997 while Laube Glacier N has been in a stable position since 1985. At Kruuse Glacier between 1985 and 1997, the ice front underwent large seasonal fluctuations possibly associated with the extension of a 1-2 km floating portion of the glacier, but these oscillations subsided as the glacier retreated 1997-2000 over a total distance of approximately 2 km. A similar progression is observed at Uunartit Glacier with ice front oscillations prior to retreat which initiated around 1997. The retreat of Uunartit was nearly 4-fold that of Kruuse, however, reaching an inland location approximately 8 km upstream. Deception Ø has two branches which are partitioned around a large nunatak, with both branches showing a similar retreat trend that started around 1995 and progressed until 2005. The northern branch retreated approximately 1.5 km while the southern branch retreated by nearly 6 km. At Polaric glacier, the majority of change is observed on the southern branch which retreated 2 km 2000-2019, while the main, wide branch has remained in approximately the same position. Within Kangerlussuaq Fjord, the fast-flowing Kangerlussuaq Glacier has undergone large changes since an initial 6 km retreat that occurred in 2006, triggering a near-doubling of ice advection from 10 m/d to 20 m/d. Since this initial retreat, the ice front has seen substantial seasonal and inter-annual fluctuations, contributing to a total 8 km retreat by 2019.

The Role of Ocean Melt In Sermiligaaq Fjord, the main branch of Knud Rasmussen has experience a retreat which mirrors the cumulative melt anomaly of its terminus, indicating that this glacier is largely controlled by changes in ocean conditions. The western branch of this glacier, on the other hand, terminates in a very shallow region of the fjord which leaves it impervious to changes in oceanic conditions at depth. Accordingly, the western branch of Knud Rasmussen has been quite stable over the past several decades. This stability is in direct contrast to the evolution at Kaarale which has experience ongoing retreat over the past several decades. This retreat progression is concurrent with cumulative melt anomalies but, as for glaciers like Kjer in the northwest sector, the baseline melt used to define the melt anomaly is likely not representative of that which would maintain stability at the ice front.

Further north, the stability of K.I.V. Steenstrup until recent years despite warming ocean condi-

tions near its terminus is explained by a prominent moraine/sill that has developed at its terminus location, yielding another case where iceberg calving rather than ocean melt dominates its progression of retreat. At Laube glacier, the retreat of the southern branch shows a high influence of ocean melt while the other two branches that show differing behavior both terminate in fjords which are less than 5 meters below sea level. North of Laube, both Kruuse and Uunartit have experienced several kilometers of retreat yet there is little change in melt over this time. However, large uncertainties persist in the melt rates due to a lack of bathymetric measurements in their ice-choked fjords. The timing of their terminus retreat in comparison to oceanic warming in the area is highly suggestive of an oceanic influence, but data constraints limit the ability to quantitatively assess this effect. For the two branches of Deception Ø, only the northern branch shows a retreat which coincides with an increase in melt while the southern branch has remained relatively stable. It should be noted, however, that neither of these two glaciers have been sufficiently mapped, and there are large uncertainties in our knowledge of bathymetry near their termini. For Polaric, the stability of the northern branch is similar to that of K.I.V. Steenstrup where a large submarine sill promotes stability via protection from oceanic changes at depth. The southern branch of Polaric, which lacks the same prominent sill structure, has conversely retreated although this retreat may not be from subsurface warming as the fjord is only a few 10's of meters below sea level – too shallow to be affected by Atlantic Water on the shelf.

Finally, at Kangerlussuaq Glacier, there is significant evidence that ocean warming has influenced the stability of the terminus. As ocean temperatures at depth increased near the end of the 1990's, the cumulative melt anomaly increased sufficiently to dislodge the glacier from its equilibrium position and induced a destabilization of the ice front. Subsequently, calving processes increased and the glacier retreated substantially with further increases in melt. It should be noted that the retreat of Kangerlussuaq has been previously been connected to warmer waters within the fjord by Christoffersen et al. [2011] using a different ocean model than that employed here, providing corroborating evidence for the ocean-induced retreat of this important glacier.

3.5.2 Geikie Plateau

The Geikie Plateau is a fin-shaped region between Kangerlussuaq Fjord and Scoresby Sound. There are several glaciers on the plateau which discharge ice from the main ice sheet including Nordfjord Glacier, Styrte Glacier, Courtauld Glacier, Frederiksborg Glacier, Sorgenfri Glacier, Kong Christian IV Glacier, Rosenborg Glacier, Kronborg Glacier, Borggraven Glacier, Sortebræ Glacier, Apuseeq Anittangasikkaajuk and its northern branch, Dendrit Glacier and its southern branch, and Torv Glacier and its southern branch.

Glacier Evolution The retreat of glaciers along the east coast of Greenland have been noted in several studies to be dependent on latitude, with glaciers above 69°N having minimal retreat and those below experiencing substantial retreat [e.g. Walsh et al. [2012], Seale et al. [2011]]. The observations within this study largely corroborate previous findings, yet there are several outliers to this trend. Starting with Kangerlussuaq Fjord, below 69°N, the retreats of Styrte, Courtauld and Frederiksborg have totaled 1.5 km, 0.5 km, and 0.5 km, respectively. Nordfjord is the only glacier within this fjord which has remained stable during this time, showing a minimal retreat of 0.25 km. North of Kangerlussuaq Fjord, Sorgenfri and Kong Christian IV have shown a minimal retreat of less than 0.5 km, but the adjacent Rosenborg, Kronborg, and Borggraven have retreated by 2.5 km, 1.5 km, and 4 km respectively.

Sortebræ glacier, north of Borggraven, represents a unique glacier history for any marine-terminating glacier in Greenland: the ice front underwent a substantial surge in 1994, advancing more than 9 km within the course of 1 year. The surge has been attributed to the hydrology of the glacier upstream [Murray et al., 2002], rather than changes in the local ocean conditions. After the retreat, the glacier then began a continuous retreat, losing 13 km of its ice front between 1996 and 2019. Apuseeq, located at 69°N, has two branches which have both retreated by more than 4 km since 1985. The northern branch has experienced sustained retreat over this time while the southern branch underwent a brief period of stability between 1992 and 2002, and then continued to retreat. The two branches of Dendrit Glacier underwent a similar progression, with the southern branch retreating continuously since 1985 and the northern branch retreating after 2002. The southern

branch of Torv Glacier is the only glacier on the Geikie Plateau outside of Scoresby Sound which remained stable during this time, as the main branch of Torv retreated by more than 1 km.

The Role of Ocean Melt The contrasting behavior of glaciers on either side of 69°N is hypothesized to be due to the different source currents. As the Irminger current advects onto the continental shelf in this region, and then flows south, there is a steady supply of heat to fjords below this parallel. In contrast, the glaciers north of this parallel are fed by relatively cold, fresh PW in the East Greenland Current and would not experience warming until later. Overall, the glaciers experiencing warming from the Irminger would be expected to begin their retreats first, while the glaciers fed by the EGC would retreat later. This effect is realized in the results presented here, but only to a small effect: the retreats at Sorgenfri, Apuseeq, and both branches of Dendrit are observed to occur at the same time that ice front undercutting began to increase on their termini, but other adjacently located glaciers either remained stable or have fjords so shallow that they would not be affected by intrusions of deep, warm Atlantic water. These shallow glaciers represent the majority of those on the northern flank of Kangerlussuaq Fjord and seaward side of the Geikie Plateau: Nordfjord, Styrte, Courtauld, Sorgenfri, Rosenborg, Kronborg, the northern branch of Apuseeq, and both branches of Torv. The two remaining glaciers (below 69°N) – Frederiksborg and Kong Christian IV – have remained stable, contrary to the overarching ocean-modulating hypothesis. These glaciers terminate in deeper fjords yet have calving-promoting bathymetry: a steep prograde slope and a sharp sill, respectively.

3.5.3 Scoresby Sound

Scoresby Sound is a wide inlet that cuts into the continent at around 70°N latitude. The sound encompasses several glaciers terminating on the northern boundary of the Geikie Plateau as well as several glaciers positioned deep in the fjord. These glaciers include Ostre Borg Glacier, Nakkaagajik Timerseq, Mone Glacier, Brede Glacier, Sydbrae Glacier, Magga Dan Glacier, Kista Dan Glacier and its western branch, Vestfjord Glacier, Rolige Bræ, Eielson Glacier, Daugaard-Jensen Glacier, Charcot Glacier, and F. Graae Glacier.

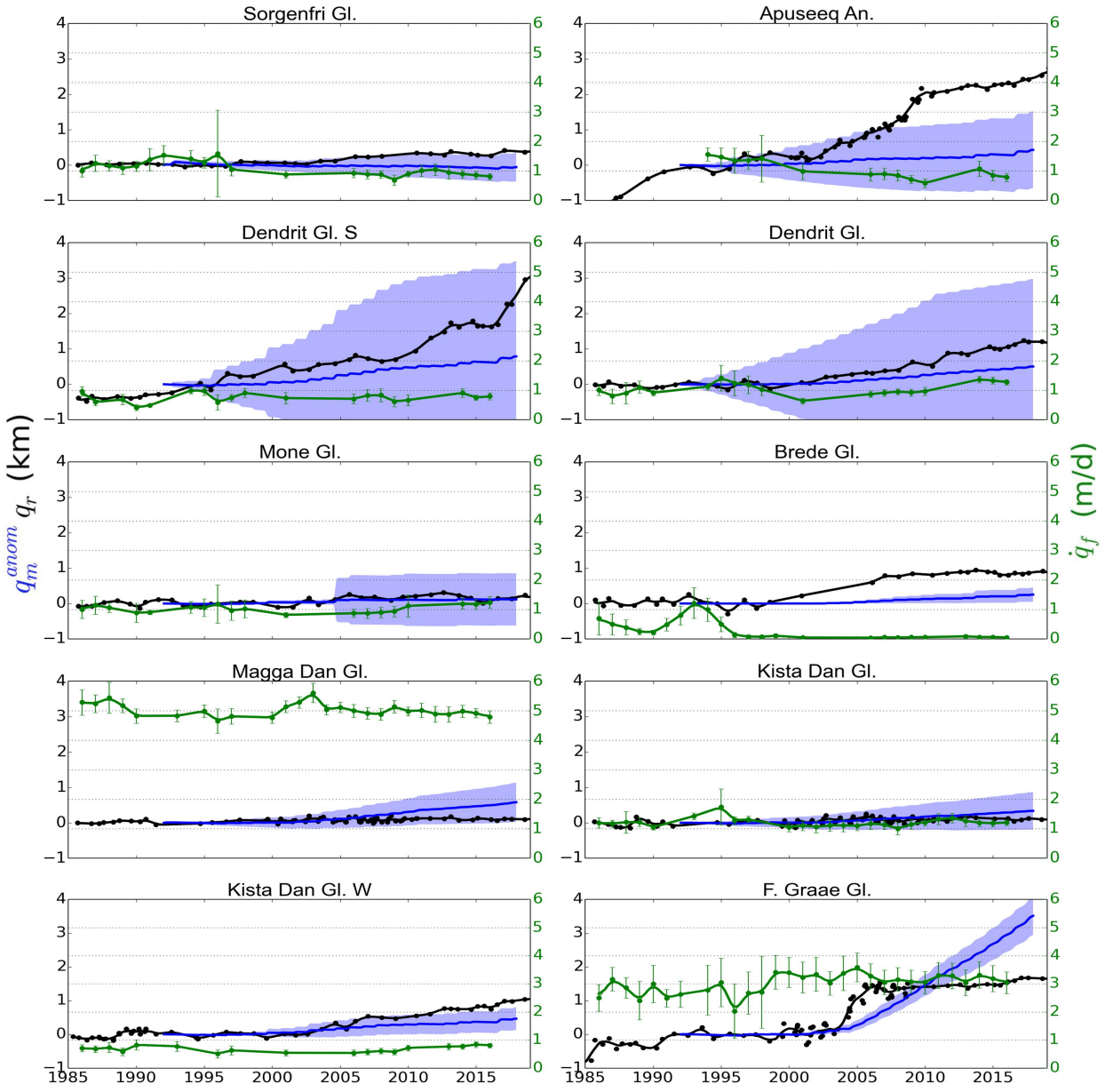

Figure 3.20: Geikie Plateau and Scoresby Sound Glacier Results

Summary of the ice front retreat (q_r), cumulative melt anomaly (q_m^{anom}), and ice velocity (q_f) for 6 glaciers in southwest Greenland.

Glacier Evolution Glaciers in Scoresby Sound have seen substantially less change than other glaciated regions of Greenland. Near the mouth of the sound, Ostre Borg and Nakkagajik retreated 1 km and 0.5, respectively, between 2000 and 2019 while the neighboring Mone Glacier has maintained a constant front position. Similar small retreats are observed at glaciers further into the sound, with Brede and Sydbræ retreating by less than 0.5 km, and Magga Dan and Kista Dan remaining stable. The western branch of Kista Dan, in contrast to the main branch, has retreated steadily over a distance of 1 km since the year 2000. Within the deeper network of fjords within Scoresby Sound, the ice front of Vestfjord has remained stable despite some evidence of small seasonally-created floating extensions, while Eielson and Rolige have seen only small changes totaling less than 0.5 km. The most substantial ice front changes are observed in the most northern fjord of Scoresby Sound with Daugaard-Jensen retreating 1.5 km between 2010 and 2019, and F. Graæ undergoing a 1.5 km step-wise retreat 2003-2004. Some retreat was observed at Charcot prior to 1992, but the ice front has remained stable since then.

The Role of Ocean Melt Within Scoresby Sound, there is substantial evidence that oceanic warming has played an important role in modulating the retreat of ice front positions. On the northern side of the Geikie Plateau, Mone, Brede, Magga Dan, Kista Dan, and Kista Dan W have all retreated concurrent with a positive anomaly in ocean melt. The retreats of these glaciers have been small and gradual in all cases except Brede which retreated in a more step-wise fashion coincident with an increase in melt. These glaciers provide evidence of very small changes in ocean conditions yielding small progressions of retreat in constrast to the large warming trends that triggering retreats of several kilometers in other regions of the ice sheet. In the same area, Nakkaagajik and Sydbræ terminate in shallow water while Mone Glacier is largely controlled by calf ice production as it terminates on a steep, prograde slope that promotes calving.

It is difficult to draw conclusions on the role of the ocean for the glaciers which terminate deeper within the Scoresby Sound as there have been relatively few measurements of bathymetry in this area on account of the large production of icebergs that tend to clog these fjords. The step-wise retreat of F. Graae shows evidence for an ocean-induced retreat as the timing of the melt anomaly on this glacier occurs simultaneously with the triggering of retreat after almost two decades of stability.

For Daugaard-Jensen, Rolige, and Vestfjord, on the other hand, increases in melt do not match with the long-term stability, implying these glaciers may be more controlled by calving processes than by melt. It should be noted, however, that there are very few CTD measurements available within this fjord, and the modulation of ocean waters between the sample area at the mouth of Scoresby Sound and the glacier terminus is likely misrepresented. For Charcot and Eielson, the current Bedmachine product indicates extremely shallow bathymetry leaving the impact of the ocean on these glaciers in doubt.

3.6 Northeast Greenland

The cold northeast sector of the ice sheet has the fewest (12) marine-terminating glaciers of any sector on the ice sheet, but the region still accounts of 32 Gt/yr or 6.4% of discharge from the ice sheet and 24% of the ice sheet by area. The NE sector can be broken down into three main regions: Scoresby Land (7 glaciers), the area around the Storstrømmen outlet (3 glaciers), and the Northeast Greenland Ice Stream (2 glaciers). The relatively high discharge rates from the NE sector are primarily controlled by the two large outlet glaciers which constitute the Northeast Greenland Ice Stream: Zachariæ Isstrøm (11.6 Gt/yr) and Nioghalvfjerdsfjorden (12 Gt/yr).

Due to the remote location of the NE in proximity to available harbors, persistent sea ice conditions for the majority of the year, and the deluge of icebergs carried along the coast through the East Greenland Current, bathymetry mapping and CTD measurements in this area have been relatively sparse. However, some measurements do exist near Waltershausen. The knowledge of bathymetry in NE Greenland is instead inferred from airborne gravity measurements from NASA's Operation Ice Bridge, encompassing Gerard de Geer Glacier, Nordenskiöld Glacier, Zachariæ Isstrøm, and Nioghalvfjerdsfjorden [Boghosian et al., 2015]. CTDs in this area are primarily provided as AXCTDs from the OMG campaign, and available after 2016.

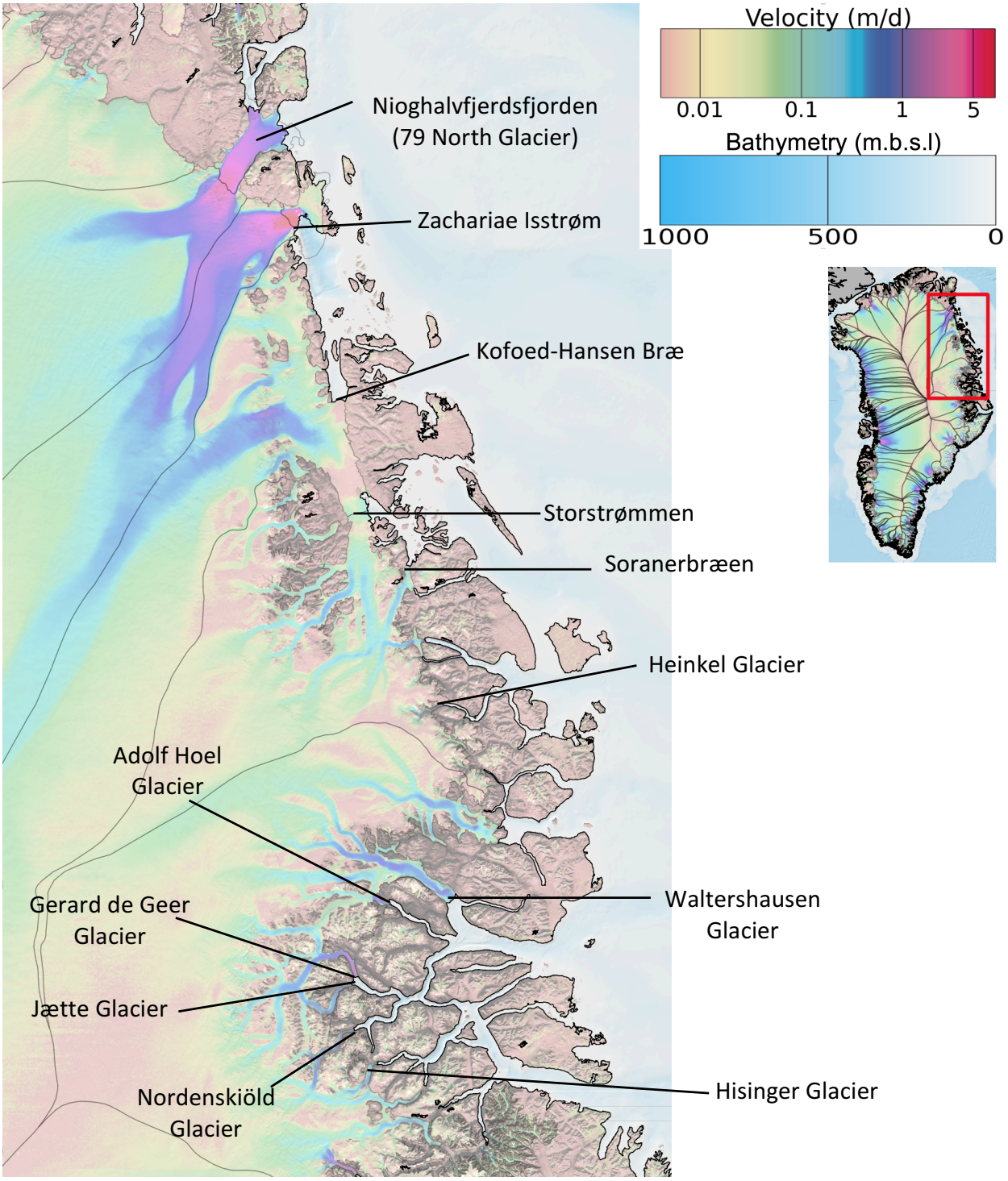

Figure 3.21: Map of Northeast Greenland Glaciers

Overview of NE Greenland glaciers.

3.6.1 Scoresby Land

Scoresby Land encompasses the region north of Scoreby Sound which is incised by fjords more than 100 km in length. There are 7 significant marine-terminating glaciers in the region including Hisinger Glacier, Nordenskiöld Glacier, Jætte Glacier, Gerard de Geer Glacier, Adolf Hoel Glacier, and Waltershausen Glacier. North of Scoresby Land, there is an additional smaller glacier named Heinkel Glacier.

Glacier Evolution In Scoresby Land, glacier retreat has been minimal since 1985 but as for the other regions of the ice sheet, a small retreat signal is observed to begin around the year 2000 for a few glaciers in the region. The retreat trends for Hisinger, Adolf Hoel, and Heinkel are nearly identical, undergoing a continuous 1 km retreat between 2000 and 2019 after 15 years of stability between 1985 and 2000. Jætte and Waltershausen have followed a similar trend with a retreat of approximately 0.5 km over the same time. Nordenskiöld and Gerard de Geer have maintained approximately stable ice front positions over the 1985 to 2000 time period.

The Role of Ocean Melt As bathymetric and oceanographic measurements are sparse in Scoresby Land, it is difficult to draw conclusions on the impact of ocean melt on the small retreats observed for these glaciers. For Hisinger, Adolf Hoel, and Heinkel, the BedMachine dataset indicates fjords which are only 1-5 meters deep on average. With the geometry, it is impossible to discern a record of thermal forcing from model output, and hence to draw conclusions on the role of ocean melt in inducing the small retreats observed at these glaciers. For the other four glaciers, the ice front depths of several 10's of meters provide an opportunity to assess the role of ocean melt. At Jætte and Waltershausen where melt rates are 0.25-0.5 m/d on average, there is a small undercutting anomaly accumulated following an increase in melt after 2005. This increase in melt is concurrent with the timing of ice front retreat, indicating ocean melt – as minimal as it is – likely plays a direct role in the small retreats observed at these two glaciers. At Nordenskiöld and Gerard de Geer on the other hand, melt rates have remained approximately consistent between the two time periods, consistent with the constant positions of the ice fronts. Thus, while melt rates

are low in this sector of the ice sheet, the small increase in thermal forcing over time has led to an increase in ice front undercutting and small observed retreats at the ice fronts. It should be noted that the heat provided to these fjords in the model output is not provided by the influx of deep, warm, AW as it is for other regions, but instead by the seasonal air-to-sea heat exchange associated with warmer air temperatures and the melting of sea ice within the fjords.

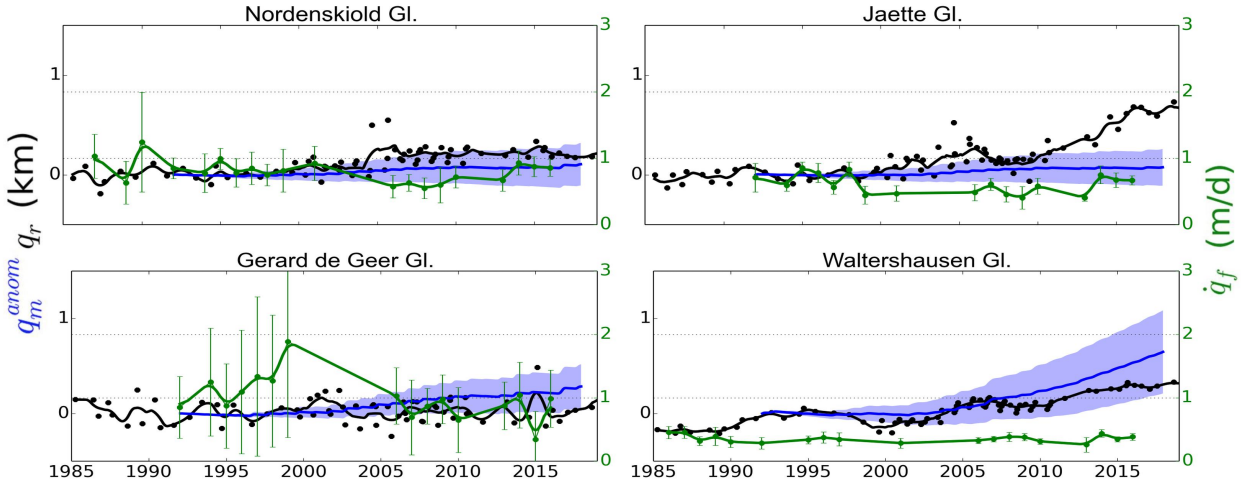

Figure 3.22: Northeast Greenland Glacier Results

Summary of the ice front retreat (q_r), cumulative melt anomaly (q_m^{anom}), and ice velocity (q_f) for 6 glaciers in southwest Greenland.

3.6.2 Storstrømmen Area

Storstorømmen is a large glacier system which encompasses the junction of two large floating extensions. In some literature, the southern branch is distinguished by the separate name L. Bistrup Bræ (e.g. [Mouginot et al., 2018]). The glacier Kofoed-Hansen Bræ terminates to its north while Soranerbræen is located on its southern boundary.

Glacier Evolution Soranerbræen, like the glaciers further south in Scoresby Land, has not undergone substantial change over the past 30 years. Since 2005, the ice front has undergone a slow retreat, with the majority of ice loss focused on its eastern flank. In contrast, Kofoed-Hansen Bræ and Storstømmen have seen substantial change. Kofoed-Hansen Bræ has retreated continuously a

total distance of 5 km since 1985, with rapid retreat between 1985 and 2000. The retreat has slowed since the year 2000, but has remained consistent. The retreat pattern at Kofoed-Hansen Bræ is notably different than most other glaciers in Greenland which experienced faster retreat in more recent years. Storstrømmen is a unique glacier in that it has a substantial floating section 10-20 km in length. The glacier ice front has retreated nearly 4 km since 2010 after 25 years of stability, yet this pales in contrast to the 12 km retreat of its grounding line between 1992 and 2016.

The Role of Ocean Melt As for glaciers in Scoresby Land, the lack of bathymetric measurements around Storstømmen greatly hinder the assessment of ocean melt on the evolution of the ice fronts in this region. In the BedMachine dataset, the ice front depths at Soranerbræen are between 0 and 5 m, which is too shallow to assess a reasonable value for ocean-induced melt. At Kofoed-Hansen Bræ, the fjord is between 60 and 100 m depth, and the ice front undercutting rates estimate here are approximately 0.1 m/d. While modeled melt rates are higher 1992-2005 than 2005-2017, concurrent with the retreat rate of the ice front, it is impossible to determine an accurate anomaly baseline because the ice front has undergone retreat during this entire period, similar to other examples such as Kjer Glacier in the NW sector. In other words, the baseline environmental parameters for stability at this glacier are not discernible from the present data. Finally, for Storstømmen, the melt rates between 1992 and 2017 rise from an average 0.1 m/d to 0.5 m/d with mild ocean warming during this time. While this melt anomaly accounts for the small ice front retreat around 2010, the melt rates are likely not representative of the glacier evolution. In fact, the terminus region of this glacier is known to depend highly on an interannual surge, and has been predicted to advance again with a surge between 2027 and 2033. In other words, the role of the ocean in controlling the evolution of this glacier is not clear.

3.6.3 Northeast Greenland Ice Stream

The Northeast Greenland Ice Stream represent a large flow of ice covering approximately 150,000 km^2. The stream terminates in two huge glaciers: Zachariæ Isstrøm and Nioghalvfjerdsfjorden. The latter glacier will be referred to its popular name of "79 North" arising from its terminus

location at 79°N latitude and the difficulty western scientists have in pronouncing its name.

Glacier Evolution The ice front of Zachariæ has undergone substantial, continued retreat since 2002, totaling nearly 600 km^2 of ice loss, or 27 km on average across the width of the fjord. At the same time, significant grounding line retreat has been observed, totaling nearly 7 km between 1996 and 2015 [Mouginot et al., 2015]. This loss of grounded ice has led to near doubling of discharge from the glacier. These changes are in contrast to 79 North, which has a much longer floating ice tongue than Zachariæ. The floating portion of 79 North lost an average 5 km from its floating extension in the form of large, tabular icebergs but little change has been observed at its grounding line located nearly 55 km upstream of the floating extension margin.

The Role of Ocean Melt On the floating extension geometry of Zachariæ and 79 North, basal melting underneath the ice is expected to play a more dominant role in the retreat of the grounding line and acceleration of ice from upstream. The parameterization for ocean melt used herein does not capture these processes, but Mouginot et al. [2015] note that basal melt has increased substantially at both glaciers, reaching an estimated 25 m/yr on Zachariæ and 13 m/yr on 79 North. In other words, the methods used in this study do not capture the ocean's role in modulating recent changes, but existing studies provide noteworthy evidence on the topic.

3.7 Northern Greenland

The cold, northern sector of the ice sheet extends over a wide swath of coastline where 28 varied glaciers terminate. The key regions of the N sector include Independence Fjord in the east (3 glaciers), the fjords fed by waters from the Lincoln Sea (8 glaciers), the Nares Straight (4 glaciers), and the Inglefeld Gulf (13 glaciers). Due to the long, narrow geometry and extremely cold waters in the fjords of this area of the ice sheet, several glaciers have developed long floating extensions within the past century, although many of these have broken up within the last few decades. In all, the N sector has lost the most ice by area at 1109 km^2, yet only about half of this ice loss (558 km^2) corresponds to grounded ice. While there are a multitude of glaciers in this region, the area

only discharges 27 Gt/yr – the lowest of any sector of the ice sheet. The most significant glaciers are Petermann Glacier and Ryder Glacier, where long (65 km and 27 km respectively) floating extensions have persisted until present day, and Humboldt Glacier, which is the widest glacier in Greenland at over 100 km.

Bathymetry data in the N sector is most complete in Inglefeld Gulf which has been surveyed by airborne gravity during NASA's Operation Ice Bridge [Boghosian et al., 2015]. OMG has also provided single-beam echo sounding data within Inglefeld in addition to an abundant collection of AXCTDs around the northern fjords starting in 2016.

3.7.1 Independence Fjord

Independence Fjord in the northeast region of the ice sheet has three main glaciers: Hagen Bræ, Academy Glacier, and Marie Sophie Glacier.

Glacier Evolution Despite their remote location relative to the distant source of heat from the Atlantic, the glaciers in Independence Fjord have seen significant changes in the past few decades. Hagen Bræ, in the southern branch of the fjord, previously had a 15 km floating extension which broke up in 2008 [Hill et al., 2018b], and has subsequently retreated 2 km. Academy glacier, in the northern branch of the fjord, has retreated continuously since the year 1990, but the retreat stabilized around 2009. Marie Sophie, north of Academy, experienced a minimal retreat of 1 km which occurred between 2001 and 2006.

The Role of Ocean Melt The break-up of Hagen Bræ's floating extension in 2008 came after substantial increases in ocean thermal forcing within Independence Fjord, suggesting increased basal melt processes likely played a key role in its collapse. However, as for previously mentioned glaciers with floating extensions that broke up within the last two decades, the melt parameterization utilized here does not capture circulation and melt processes underneath the shelf, and therefore cannot be used to draw conclusions on its demise. Similarly, the ongoing retreat of Academy makes it impossible to determine the impact of increased melt as this environmental signal is mixed with a

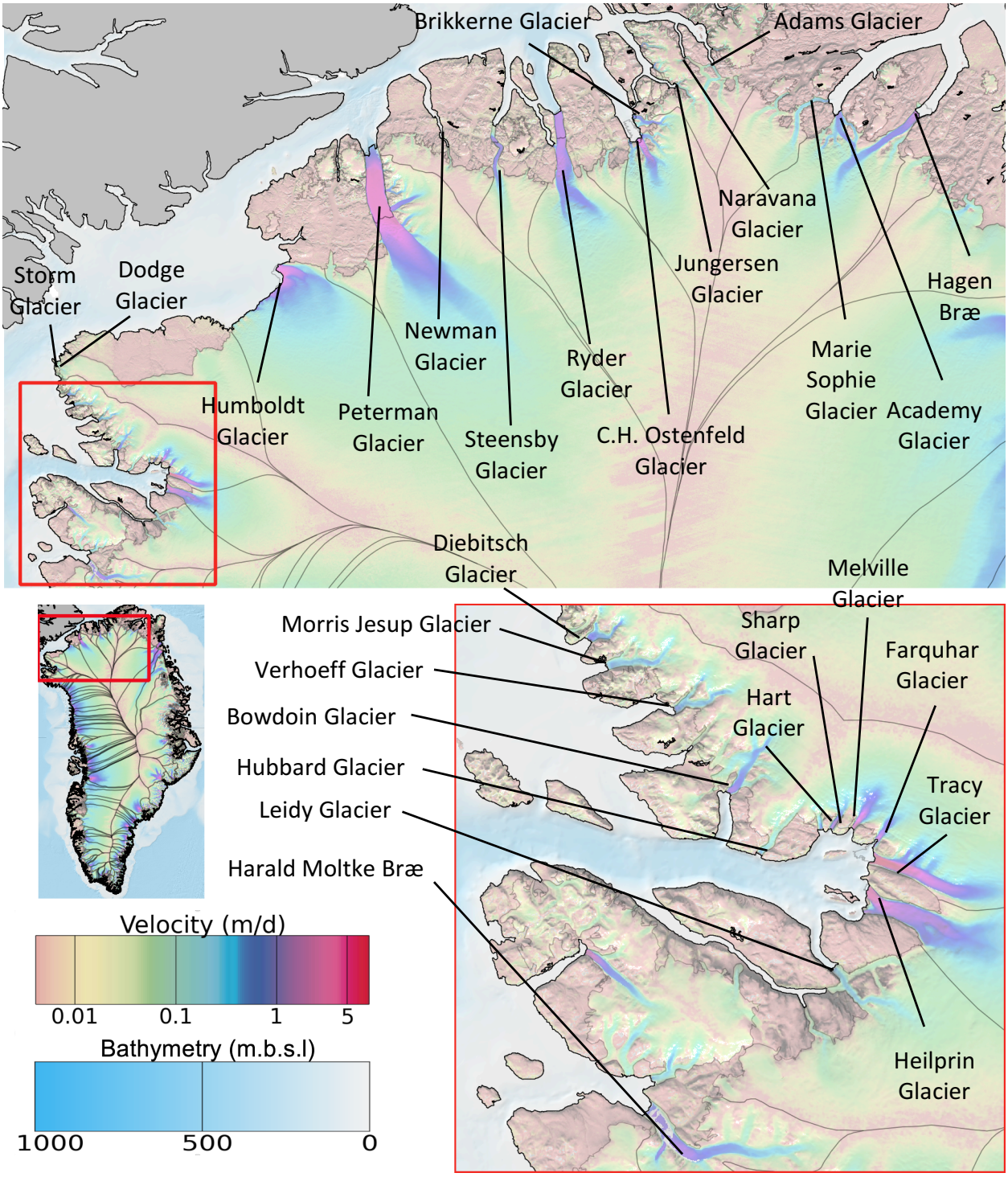

Figure 3.23: Map of Northern Greenland Glaciers

Overview of N Greenland Glaciers. The lower right panel reflects Inglefeld Gulf, which is indicated by the red box in the top panel.

pre-existing forcing that has destabilized the ice front. For Marie Sophie, the small retreat observed to begin around the year 2000 is attributed to increased ocean induced melt as the ice front began to retreat at the same time as the cumulative melt anomaly increased.

3.7.2 Lincoln Sea Region

The Lincoln Sea encompasses the northern boundary of the ice sheet which connects several fjords and inlets where 8 glaciers terminate. From east to west, these are Adams Glacier, Naravana Glacier, Jungersen Glacier, Brikkerne Glacier, C.H. Ostenfeld Glacier, Ryder Glacier, Steensby Glacier, and Newman Glacier.

Glacier Evolution On the eastern side of the Lincoln Sea Region, Adams, Naravana, and Jungersen have retreated by 1 km, 1.5 km, and 4km since the year 2000 when satellite observation are available. Data on the retreats of these glaciers is sparse, but the majority of retreat is observed after 2010. In C.H. Ostenfeld Fjord, the lateral Brikkerne has been remarkably stable over the past several decades while the main C.H. Ostenfeld glacier lost an extensive floating section which, at its longest point in 1991, was nearly 20 km in length. After the collapse of its ice tongue, C.H. Ostenfeld continued to retreat another several kilometers. Further west, Ryder and Steensby have both also supported floating ice extensions for more than 20 kilometers in length. Despite the adjacent location of these two glaciers, the evolution of their termini has been contrasting with the extension at Ryder staying intact, while that at Steesby broke up in the year 2012, leaving only a small floating extension of 1-3 kilometers in length. At Newman Glacier, west of Steensby, the ice front position has remained constant.

The Role of Ocean Melt Due to the remote location of these fjords in Greenland and the persistent sea ice preventing passage by boat, the majority of glacier regions here have not been surveyed to reveal their bathymetry. Thus, in the BedMachine dataset, the bathymetry of Adams, Naravana, Jungersen, Brikkerne, and Newman terminate in fjords which have a mean water depth which is less than 1 m meter below sea level on average. This shallow bathymetry, which is likely

due to a lack of measurements in the region, obscures the interpretation of their retreat relative to changing ocean conditions. For the three remaining glaciers with floating extensions, however, there is clear evidence that increased ocean thermal forcing in the region beginning after the year 2000 has played an important role in the recently observed evolution. At C.H. Ostenfeld, the final collapse of the remaining 9 km of its floating extension in 2002 occurred after a 1° increase in TF, leaving a vertical ice front that is more typical of glaciers further south in Greenland. The terminus of this glacier continued to retreat in subsequent years with a modeled increase in undercutting from 0.25 m/d to 0.5 m/d. At Ryder, the floating ice extension has been maintained but satellite measurements indicate that the grounding line has retreat upwards of 10 km between 1992 and 2017 coincident with an increase in melt from 0.3 m/d to 0.7 m/d.

3.7.3 Nares Straight

The Nares Straight is a narrow passage between northern Greenland and Ellesemere Island. Within this narrow region are the massive Petermann and Humboldt Glaciers as well as the smaller Dodge and Storm Glaciers.

Glacier Evolution Petermann glacier flows into a narrow fjord in Nares Straight where it terminates in the longest floating ice extension in Greenland at 65 kilometers in length. The front position at Petermann has been approximately constant over the past several decades except for a large, 25 kilometer calving event which transpired between 2010 and 2012. In recent years, the grounding line has retreat 1-2 kilometers after several decades of stability. At Humboldt, the largest changes have been observed on the northern flank where flow speeds are fastest and the ice front has retreated more than 5 km since 2000. However, when averaged over the entire length of the terminus, the retreat is more minimal at around 3 km between 2000 and 2018. Further south, at the end of Nares Straight, Dodge has undergone a small retreat of 1 km since 2000 while Storm has been relatively stable.

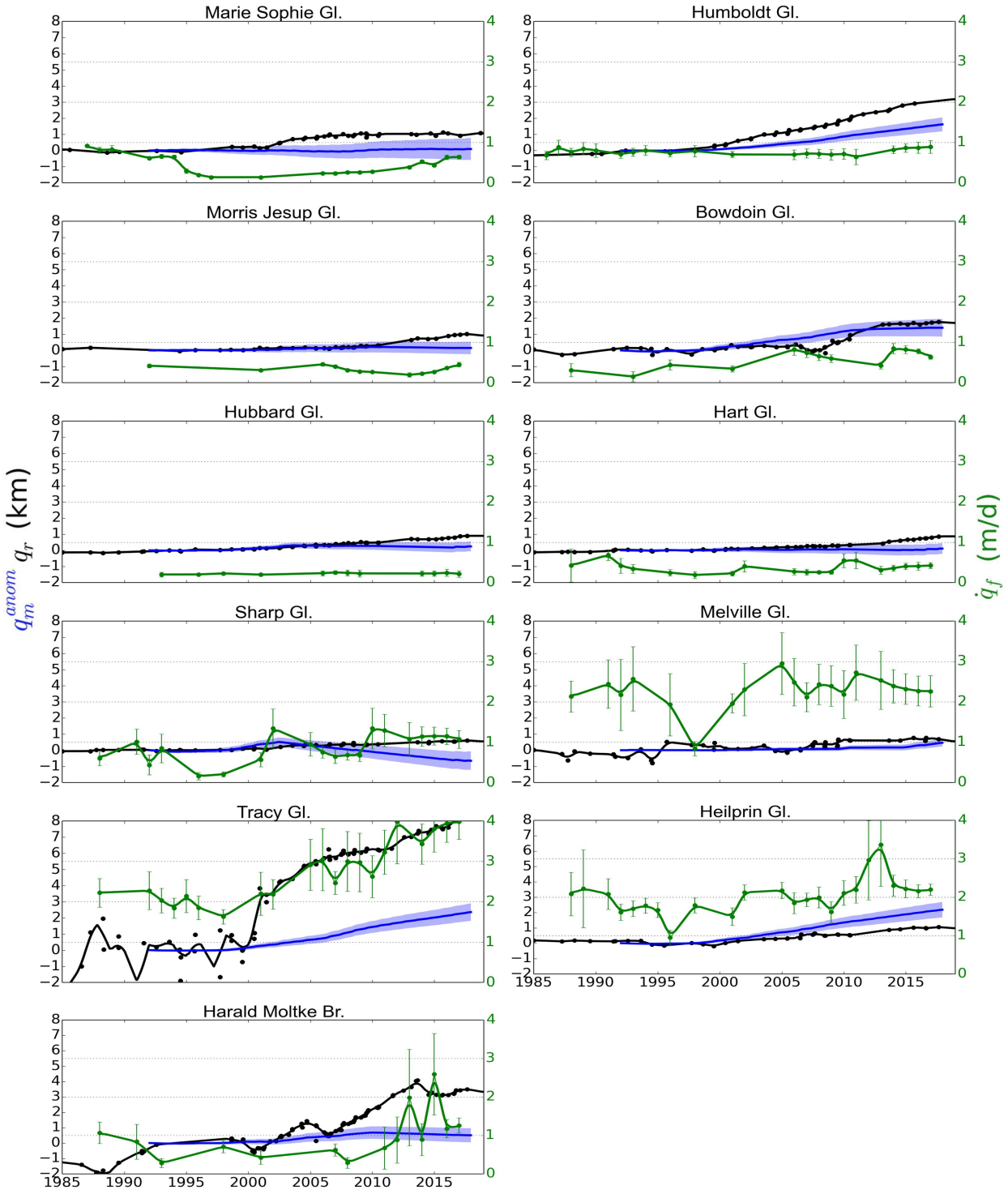

Figure 3.24: North Greenland Glacier Results

Summary of the ice front retreat (q_r), cumulative melt anomaly (q_m^{anom}), and ice velocity (q_f) for 6 glaciers in southwest Greenland.

The Role of Ocean Melt As discussed for other glaciers with long floating extensions, the undercutting model employed here does not capture circulation below ice shelves, and it is difficult to ascertain the role of the ocean on the large 2010 calving event from this approach. For Humboldt however, the modeled results reveal an increase in melt before the year 2000, leading to an increasing cumulative melt anomaly which mirrors the tend in ice front retreat. Undercutting rates are small, at 0.18 m/d on average with higher rates of 0.26 m/d observed in the 2008-2018 time period. For Dodge and Storm, the shallow bathymetry of less than 1 m below sea level on average (in the latest dataset) is too shallow to conduct an assessment of melt.

3.7.4 Inglefeld Gulf

Inglefeld Gulf is a glaciated bay between Nares Straight and Baffin Bay. There are 12 glaciers within the gulf, including Diebitsch Glacier, Morris Jesup Glacier, Verhoeff Glacier, Bowdoin Glacier, Hubbard Glacier, Hart Glacier, Sharp Glacier, Melville Glacier, Farquhar Glacier, Tracy Glacier, Heilprin Glacier, and Leidy Glacier. The glacier Harald Moltke Bræ is located south of Inglefeld Gulf.

Glacier Evolution The glaciers in Inglefeld Gulf have seen significant retreat over the past several years. On the northwest end of Inglefeld, Diebitsch glacier retreated 1.5 km starting in 2000 while the neighboring Morris Jesup retreated 1 km starting in 2008. Verhoeff, on the other hand, has not substantially changes over this time. Further into the fjord, Bowdoin underwent an abrupt retreat between 2009 and 2012, retreating by 1.5 km. Hubbard, Hart, and Sharp have all retreated nearly 1 km since the year 2000 after a 15 year period of stability. Melville has undergone substantial interannual variability between 1985 and 2019, with a net retreat distance of 0.5 km in total. Farquhar is a unique glacier in that it used to terminate directly into the lateral boundary of Tracy glacier to its south before Tracy retreated in 2001. Since this separation occurred, Farquhar has retreated 3 km from the prior boundary on Tracy. From 1995 to 2001, the extent of Tracy underwent significant seasonal and inter-annual oscillations, likely from the development of a 2-3 km floating section at its terminus. As the glacier retreated, the seasonal variation declined

significantly, and the ice front has retreated nearly 10 km since 2001. On Heilprin to the south of Tracy, the northern branch of the glacier has retreated further than the southern branch, leading to an average 1 km retreat observed over the entire ice front initiated in the year 2000. Leidy Glacier, the marine-terminating glacier within Inglefeld, has retreated approximately 1 km since its initiation in 2000. The glacier Harald Moltke Bræ, outside of Inglefeld, is a unique case for marine-terminating glaciers in that it has undergone several surge-like advances of approximately 1 km overlain on a long trend of retreat. The net front change at Harald Moltke has been 3 km since 1992.

The Role of Ocean Melt Several of the glaciers in Inglefeld have been discussed in previous literature that suggests the ocean plays a significant role in controlling their terminus locations. First, the smaller glaciers on the northern side of the gulf experienced short retreats coincident with small cumulative melt anomalies: Morris Jesup, Bowdoin, Hubbard, Hart, Sharp, and Meltville. Bowdoin, in particular, was observed to retreat after a large portion of its terminus started floating and eventually calved off [Sugiyama et al., 2015], providing corroborating evidence for large changes induced at the terminus. The two remaining glaciers on this side – Diebitsch and Verhoeff – have shallow bathymetry, yet the former has retreated by 1.5 km while the latter has remained stable.

The differing retreat distances at Tracy and Heilprin have been linked to differences in their bathymetry, with the larger retreat at Tracy due to its deeper fjord [Porter et al., 2014], allowing for greater access to deep, warm water. Further evidence for higher melt rates on Tracy vs Heilprin was highlighted by Willis et al. [2018], using a multitude of CTDs collected within the gulf in 2016. The results in the study herein support these previous conclusions with a higher undercutting rate calculated for Tracy, and an increase in the cumulative melt which coincides with the timing of glacier retreat.

Chapter 4

Synthesis

4.1 Glacier Retreat in Different Thermal Forcing Regimes

4.1.1 1992-1998: Low Thermal Forcing

From 1992 to 1998, the total loss in ice area from the fronts of marine-terminating glaciers was 295 km^2 – only 8% of the total area loss over the full 1992-2018 period investigated here. The majority of this area loss came from either portions of glaciers supporting floating ice shelves (225 km^2) and seven glaciers which were already in a sustained state of retreat (37 km^2). During this period of relative stability, temperature reconstructions reveal an ocean state which was cooler than subsequent periods: on average, the thermal forcing was 4.1°C for all regions as compared to the 4.3°C simulated for the entire study time period. Consequently, the average melt rate was also low at 0.49 m/d with a latitudinal gradient mirroring that of thermal forcing. Coincident with the lower undercutting rates and stable ice fronts, ice discharge was also lower than the subsequent values observed on these glaciers in the years after 1998. See Tables 4.1, 4.2, and 4.3 which depict the progression of each sector of the ice sheet during and after the stable period.

Table 4.1: Overview Statistics for the 1992-1998 Stable Period

Sector	**Undercutting Rate Mean (m/d)**	**Thermal Forcing Mean (°C)**	**Areal Ice Loss Grounded (km^2)**	**Total (km^2)**	**Ice Discharge (Gt/yr)**
NW	0.43	3.4	-5	-5	88
CW	0.62	4.1	9	-3	65
SW	0.81	6.7	5	5	30
SE	1.01	6.6	26	26	141
CE	0.35	3.5	6	6	79
NE	0.10	2.4	68	178	31
N	0.10	2.1	68	87	22
Mean	**0.49**	**4.1**	**25**	**42**	**65**
Total	–	–	**177**	**295**	**455**

Statistics for the ocean state, melt, retreat, and discharge during the 1992-1998 stable period when ocean thermal forcing was lower than in subsequent years.

4.1.2 1998-2008: Regional Warming

After 1997, heat anomalies from the North Atlantic Ocean entrained in the Irminger and West Greenland currents spread additional ocean heat around the continent, yielding an increase in thermal forcing for all seven sectors of the ice sheet. The most substantial warming occurred in Baffin Bay boosting the thermal forcing by 1.6°C and 1.84°C for the NW and CW sectors, respectively. Overall, thermal forcing increased 0.11 °C/year, or the equivalent of 1.1°C on average during this time. Accordingly, the modeled undercutting rates at the glaciers around Greenland increased in all sectors, and a widespread trend in ice front retreat was observed. In total, there was a total ice loss of 1,404 km^2 with the biggest losses observed in the NW and the NE sectors. While the ice loss area is comparable for these two regions, the loss of ice in the NW was nearly all from grounded glaciers while that in the NE was largely from floating extensions at Zachariæ Isstrøm, Nioghalvfjerdsfjorden, and Storstrømmen. Thus, the loss of ice in the NW had a more substantial impact on the mass balance of the ice sheet, with a small 4 Gt/yr increase in discharge in the NW on average, compared to the negligible change in the NE. The loss of ice during this time period of warming ocean waters was nearly 5 fold higher than the cooler period which proceeded it.

Table 4.2: Overview Statistics for the 1998-2008 Warming Period

Sector	Undercutting Rate	Thermal Forcing		Areal Ice Loss		Ice
	Mean (m/d)	Mean (°C)	Trend (°C/yr)	Grounded (km^2)	Total (km^2)	Discharge (Gt/yr)
NW	0.76	4.06	0.16	360	360	91
CW	0.92	4.83	0.19	95	187	77
SW	0.97	7.17	0.11	19	19	30
SE	1.24	6.92	0.05	162	162	154
CE	0.45	3.88	0.06	110	110	83
NE	0.14	2.64	0.07	134	358	30
N	0.19	2.48	0.14	229	209	21
Mean	**0.67**	**4.57**	**0.11**	**158**	**201**	**70**
Total	–	–	–	**1109**	**1404**	**486**

Statistics for the ocean state, melt, retreat, and discharge during the 1998-2008 warming period when glacier retreat was initiated.

4.1.3 2008-2018: Regional Cooling

The warming of ocean waters reached an apex around 2008, at which point ocean temperatures started to cool around Greenland. The magnitude of cooling was nearly comparable to that of warming in the previous period: on average waters cooled at a rate of 0.08°. However, in contrast to the widespread response to warming, the response to cooling was not as straight-forward. In fact, the loss of ice was greater in all sectors of the ice sheet except for the southeast: glaciers lost a total 1210 km^2 from their terminus regions which was nearly 10% higher than the loss observed in the warming period. Much of this loss can be explained by undercutting rates which remained above average levels in the 1992-1998 period which maintain glacier equilibrium positions. Moreover, the distribution of glacier retreat between glaciers: in the warming period, many glaciers began to retreat after the onset of warm water increased melt on their termini and dislodged them from their previous positions. After this initial perturbation, many glaciers restabliized in upstream positions. However, a few glaciers continued to undergo long-term retreat that continued even after the initial forcing was applied. Much of this progression is related to the shape of the bed upstream, with wider and/or deeper fjords promoting larger retreats.

Table 4.3: Overview Statistics for the 2008-2018 Cooling Period

Sector	Undercutting Rate	Thermal Forcing		Areal Ice Loss		Ice
	Mean (m/d)	Mean (°C)	Trend (°C/yr)	Grounded (km^2)	Total (km^2)	Discharge (Gt/yr)
NW	0.74	4.07	-0.07	394	394	110
CW	0.94	4.81	-0.15	109	109	88
SW	1.00	6.85	-0.07	22	22	31
SE	1.11	6.52	-0.1	145	145	160
CE	0.45	4.02	-0.09	116	116	87
NE	0.16	3.02	-0.02	175	314	34
N	0.21	2.96	-0.06	250	835	24
Mean	**0.66**	**4.60**	**-0.08**	**173**	**277**	**76**
Total	–	–	–	**1210**	**1936**	**534**

Statistics for the ocean state, melt, retreat, and discharge during the 2008-2018 cooling period after glacier retreat had already been initiated.

4.2 Categorization of Glacier Response to Ocean Temperature Variability

In the previous chapter assessing glaciers in the 7 sectors of the ice sheet, substantial evidence was presented highlighting the role of ice front undercutting in the retreat of Greenland's glaciers over the past several decades. However, there were several circumstances which obscured the calculation or interpretation of model results. Here, five categories are delineated to describe these circumstances, providing a foundation to outline the contributions this study has made to our knowledge of the impact ocean warming has played in the recent evolution of the ice sheet. These categories include glaciers which are Melt-Dominated (MD), Calving-Dominated (CD), undergoing Sustained Retreat (SR), containing a Floating Extension (FE), and terminating in Shallow Bathymetry (SB). The categorization scheme is shown in Figure 4.1, and each category is described in the successive subsections and depicted schematically in Figure 4.3.

4.2.1 Shallow Bathymetry

As described in Section 1.2, heat anomalies from the North Atlantic Ocean are transported to the Greenland coastline through a network of currents including the Irminger Current, the West

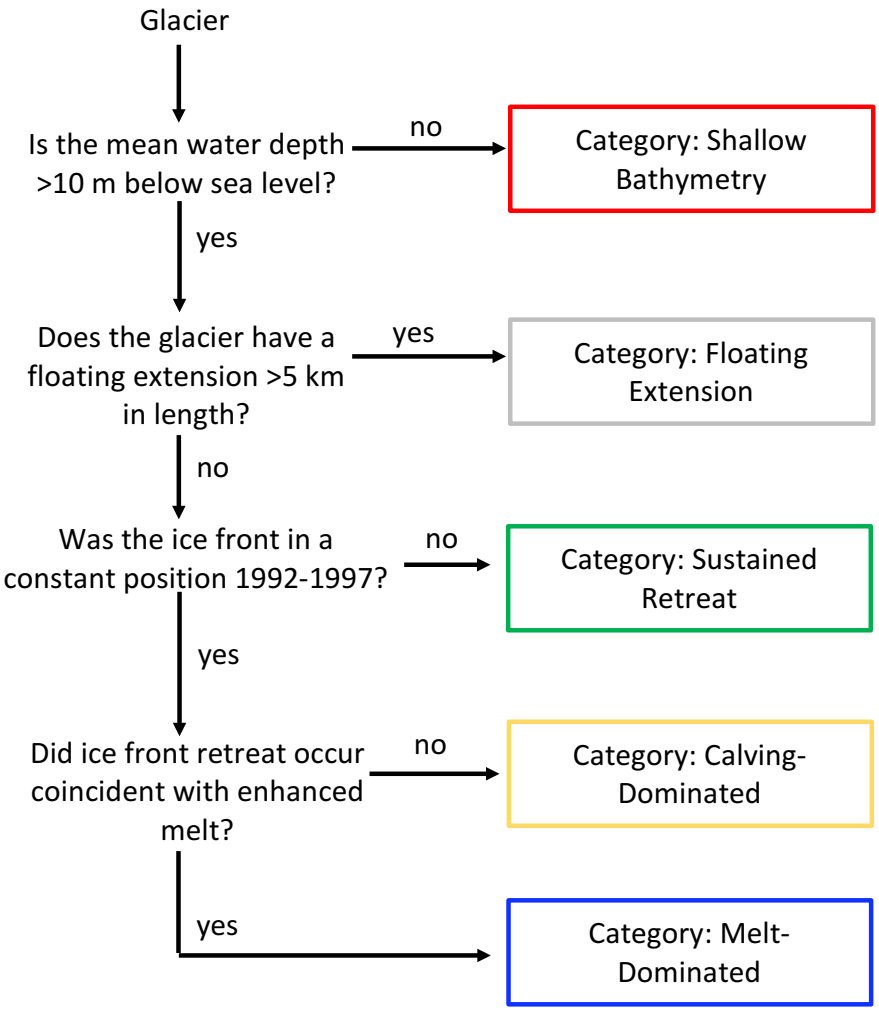

Figure 4.1: Glacier Categorization Flowchart

Procedure to categorize glaciers based on their geometry and recent progression of retreat.

Greenland Current, and East Greenland Current. Within these pathways, warm water from the Atlantic (AW) is more dense than waters from the Arctic Ocean and surface waters that have been mixed with runoff from the ice sheet. Consequently, this denser water is subducted to the deeper portion of the water column, and AW is found typically below 200 m depth. Thus, warming from the Altantic is not expected to influence glaciers which terminate in shallow water.

There are 50 glaciers which terminate in fjords that, in the BedMachine dataset, have ice front depths which are less than 10 m below sea level – far too shallow for warm AW to infiltrate their fjords and cause melting at their grounding lines. With this geometry, the glaciers would instead be influenced by oceanic heat anomalies associated with seasonal air-sea heat exchange. The quantity of heat added to the fjord depends greatly on latitude as fjords in the northern regions maintain a seasonal sea ice layer for a greater portion of the year, preventing warmer atmospheric conditions from transmitting heat into fjord waters. See, for example, the ocean thermal forcing, water depths, inferred undercutting rates and retreat histories at Sortebræ in the CE sector, Sermilik Bræ in the SW sector and Diebitsch Glacier in the N sector, as shown in Figure 4.2. For Sortebræ, the glacier underwent a surge in 2004, advancing into deeper water, and then a rapid retreat back to shallow water of only 1-2 meters. A similar situation is observed at Sermilik Bræ and Diebitsch: prior to their ice front retreats into an upstream position, the ice fronts terminated in waters 10-20 m in depth, on average, where they were exposed to seasonal fluctuations in ocean temperature. As retreat continued, the ice fronts reached portions of the bed which were no long in contact with the ocean. In effect, the glaciers became land-terminating.

However, in observing these glaciers in satellite imagery, it is clear that these glaciers are still largely in contact with the local ocean environment. Thus, the problem with this assessment – and the entire calculation of ocean thermal forcing and ice front undercutting for these glaciers – is that the BedMachine dataset does not accurately reflect the geometry of the fjord where these glacier terminate. This issue is not reflective of errors in the methods by which the BedMachine dataset has been formulated, but rather the fact that these fjords have never been surveyed by echo sounders on boats, airborne gravity, or otherwise. In fact, the story is the same for nearly 90% of the glaciers which fit into this category: there is a lack of data within many of the fjords on the

ice sheet. By number, these glaciers make up a substantial portion of the 226 marine-terminating glaciers on the ice sheet, but by flux, they are make up a relatively small percentage at 18 Gt/yr in all – only 3% of the total flux from the ice sheet. Moreover, these glaciers have constituted 176 km^2 of areal ice loss – only 5% of the total observed ice loss. Nonetheless, these glaciers make up important sections of the coastline, and future field work to map bathymetry within Greenland's fjords should be focused on these regions. For reference, the locations of these fjords are indicated in Figure 4.7.

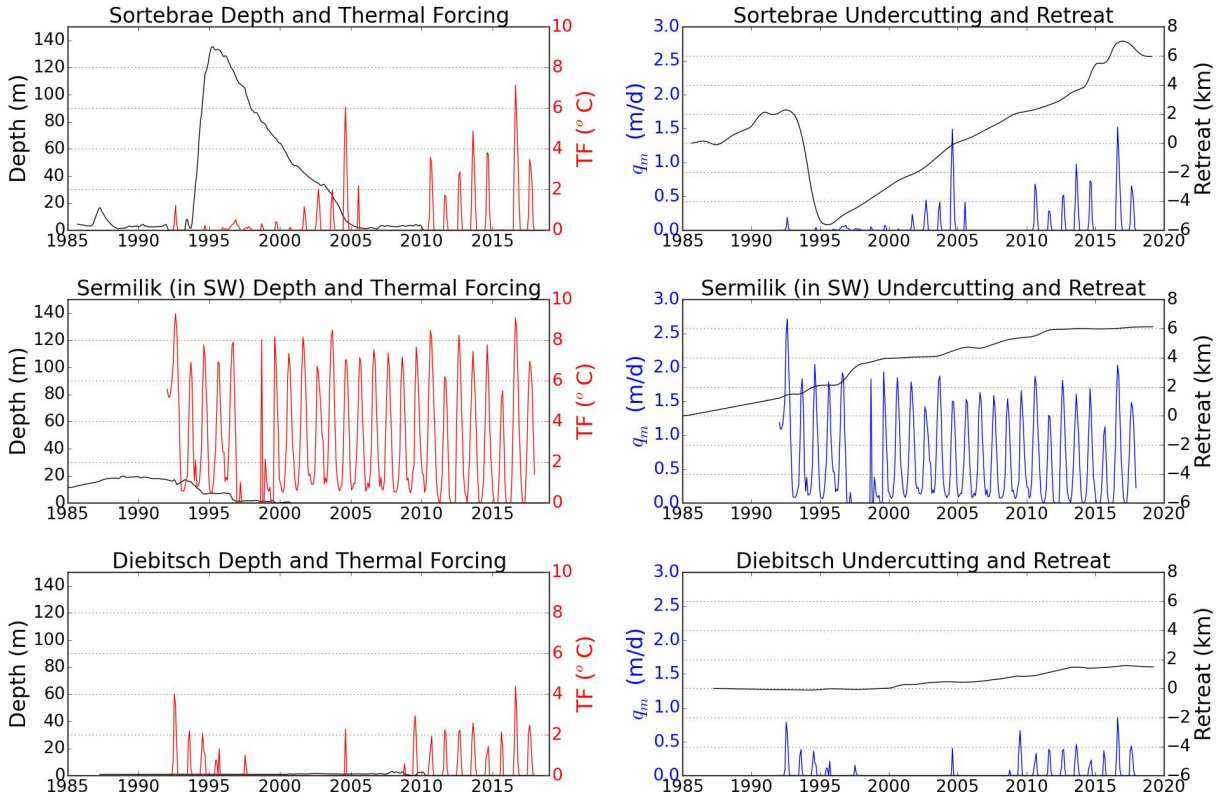

Figure 4.2: Glacier Categorization Flowchart

Examples of glaciers classified as having shallow bathymetry.

4.2.2 Floating Ice Extensions

The majority of glaciers in Greenland have at least a small section of their terminus which is afloat, resulting from the undercutting processes depicted in Figure 2.1. These small floating sections

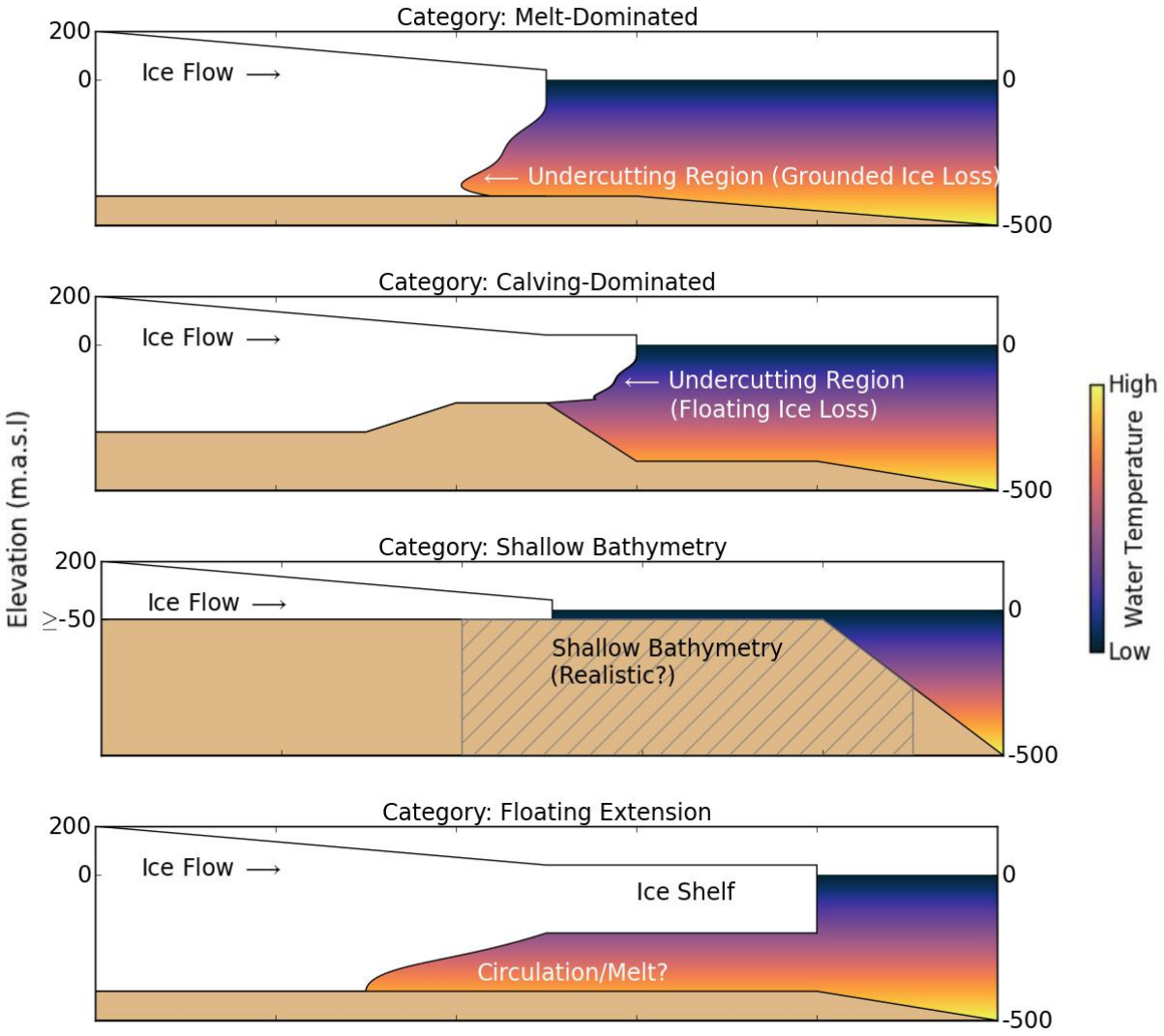

Figure 4.3: Schematic Depictions of Glacier Categorizations

Examples of glacier categories.

have been observed in glacier faces scanned by multi-beam echo sounders [Fried et al., 2015, Rignot et al., 2015] and are predicted by fjord circulation models of melt within discharge plumes Xu et al. [2012, 2013], Rignot et al. [2016]. These floating extensions are not expected to provide significant buttressing to the glacier upstream and are anticipated to shed off of the ice face quickly after formation.

Floating extensions which extend for several kilometers in front of the glacier grounding line and maintain contact with fjords walls, on the other hand, play a significant role in the stability of glaciers. For example, when Jakobshavn Isbræ lost its floating extension in 2003, the ice speed at its terminus more than doubled over the course of a decade. Modeling studies on Petermann Glacier similarly predict a large acceleration of ice if a substantial portion of the ice tongue calves, but insignificant acceleration if only a small portion of the floating extension is lost [Hill et al., 2018a]. As glaciers with floating extensions are typically large and discharge a high quantity of ice, the influence of ocean melt on their grounding lines is a high priority for understanding recent mass loss from the ice sheet. Indeed, these glaciers constitute some of the best-studied glaciers on the ice sheet and there has been some effort to parameterize melting below these floating extensions to anticipate their breakup (e.g. Cai et al. [2017]). However, existing parameterizations do not accurately capture melt on the grounding line. The model used in this study is insufficient to capture such melt as it encapsulates an estuarine-like circulation pattern in front of a vertical ice face which does not accurately capture processes controlling circulation within an ice shelf cavity.

In this study, 10 glaciers are identified which currently maintain a substantial floating extension ($>$ 5 km in length) bounded by a long, narrow fjord (Nioghalvfjerdsfjorden, Ryder Glacier, Steensby Glacier, and Petermann Glacier) or which lost a floating extension within the past decade (Alison Glacier, Jakobshavn Isbræ, Storstrømmen, Zachariæ Isstrøm, Hagen Bræ, and C.H. Ostenfeld). For the issues pertaining to the application of the ice front undercutting model described above, this work does not attempt to quantify the role of ocean melt in controlling the evolution of these glaciers. Rather, records of ice front positions and grounding lines are provided with the hope that future studies will take up the effort to explain the role of ocean melt in modulating change from these glaciers. Historical images for 9 of these glaciers are provided with their grounding line

positions in Figure 4.4 for reference.

4.2.3 Sustained Retreat

As described in Section 2.4 and highlighted through Chapter 3, the method used to deduce the impact of enhanced ice front undercutting on the retreat of Greenland's marine-terminating glaciers is determined by calculating the anomaly in melt relative to a baseline value in the 1992-1997 time period. The rationale for this baseline time period was that the majority of glaciers on the ice sheet were stable during this time, as deduced from records of ice front positions and ice velocity fields. In effect, this approach is not valid for glaciers which were not stable during this time period. The response of these glaciers to increases in thermal forcing and ice front undercutting after 1997 are mixed with a pre-existing response to forcing which was induced before the model time period began.

In this study, there are 7 glaciers identified which were already in a state of sustained retreat: Kjer Glacier, the southern-most branch of Upernavik Isstrøm, Midgård Glacier, the northern branch of Apuseeq Anittangasikkaajuk, Kaarale Glacier, Kofoed-Hansen Bræ, and Academy Glacier. The retreat records for these glaciers are shown in Figure 4.5. Note that glaciers which were additionally categorized as having shallow bathymetry or a floating extension are not included in this category, as depicted in the categorization schematic in Figure 4.1. For example, Sermilik Bræ in Figure 4.2 shows a history of retreat prior to and during the 1992-1997 period, but it is classified as SB. While the glaciers which were already retreating have undergone significant mass loss and retreat, their impact on the full assessment of retreat and the mass balance of the ice sheet is minimal: their total 180 km^2 areal ice loss only constitutes 5% of the total loss, and their 6 Gt/yr discharge is approximately 1% of the discharge from the ice sheet as a whole.

4.2.4 Calving-Dominated Glaciers

As described for nearly every ice sheet sector described in Chapter 3, there are several examples of glaciers which remained stable despite substantial increases in the modelled ice front undercutting.

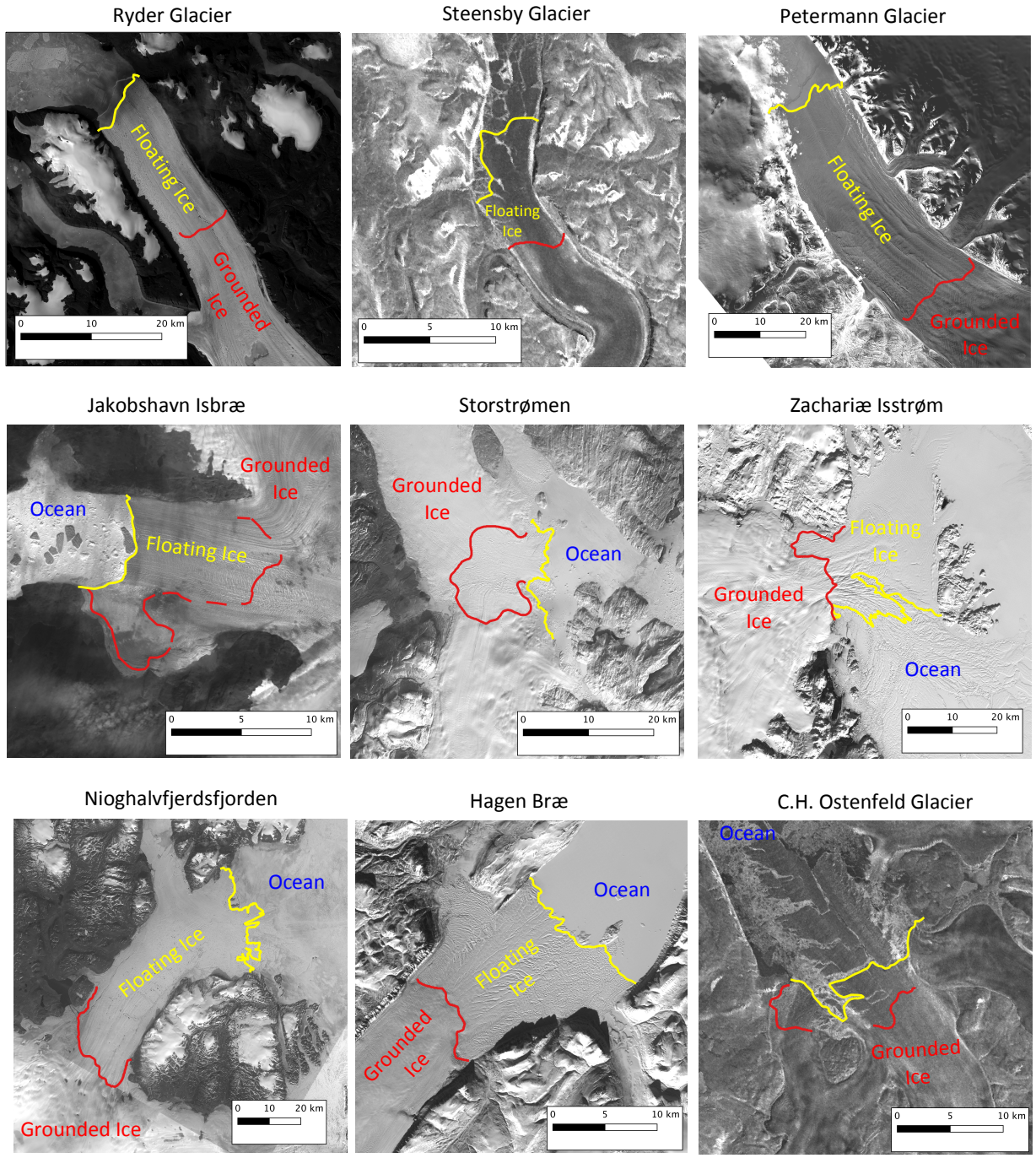

Figure 4.4: Examples of Glaciers with Floating Extensions

Satellite images showing the floating extensions of 9 glaciers around Greenland. Images for Steensby, Petermann, and C.H. Ostenfeld are from ERS-1/2 while the remainder are from Landsat 5. The grounding line is shown in red and the ice front position is shown in yellow. Note that Alison Glacier, the 10^{th} glacier which had a floating extension, is not depicted in this figure.

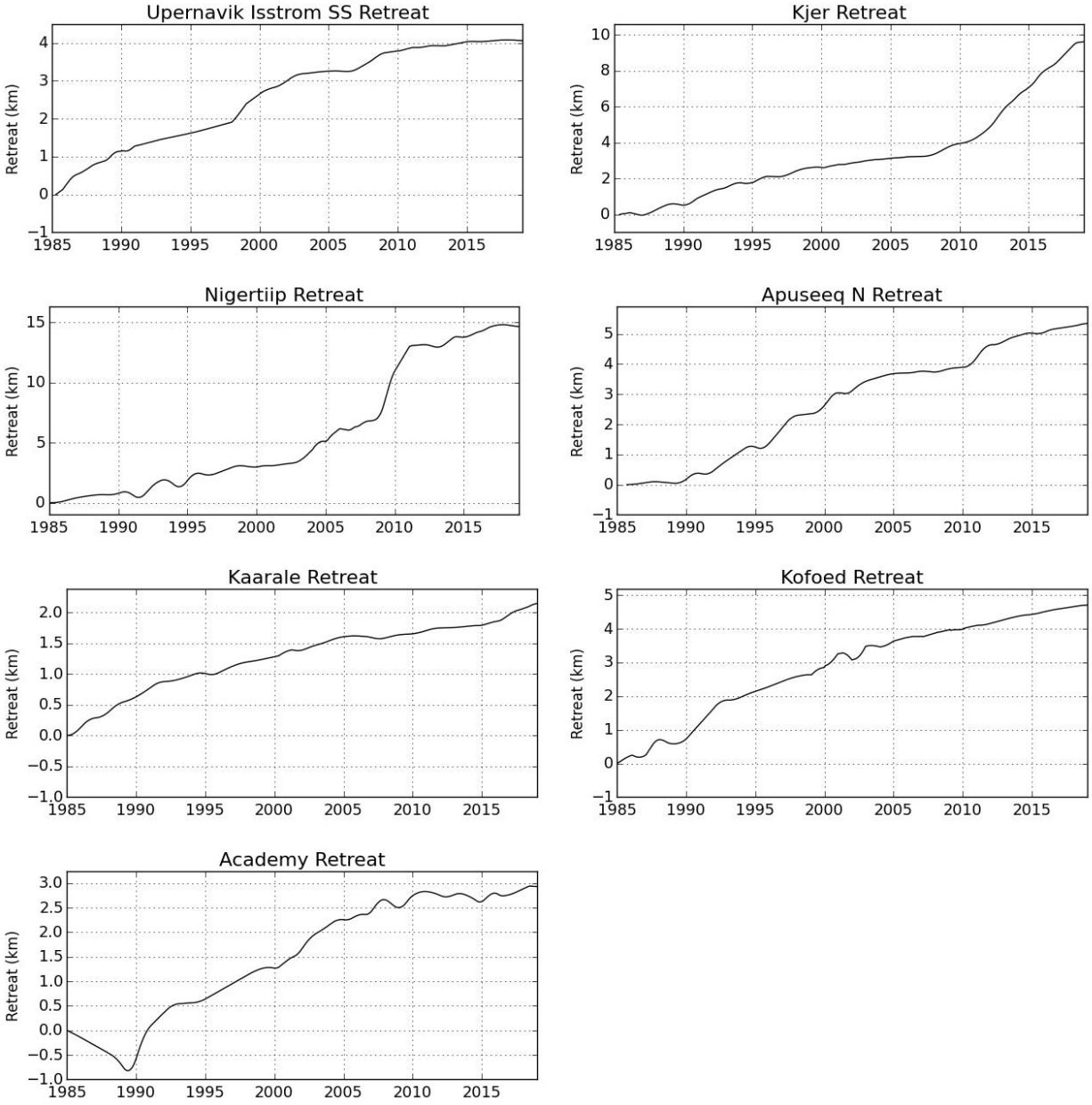

Figure 4.5: Examples of Glaciers with Sustained Retreat 1992-1998

Glaciers undergoing continued retreat in the 1992-1998 time period.

In this investigation, the stability of the ice front in the face of enhanced ocean melt is attributed to a unique geometry of the calving face that prohibits undercutting from reducing the buttressing at the grounding line and changing the stress balance of the terminus region to cause retreat. These glaciers terminate in shallow sill regions and within constrictions or "neckings" between fjord walls that diminished the effect of removing ice at the deepest part of the glacier ice front. As ice is advected from upstream, pushing the ice front past these sills and constrictions, the ice front is naturally undercut as it reaches hydrostatic equilibrium and detaches from the bed. When the plume of subglacial discharge is emitted at these locations, the effect of melt is to undercut ice which is already afloat. As with portions of ice undercut by ocean melt, these floating sections will eventually calve off of the glacier ice front, leaving the stress balance of the terminus largely unchanged. See, for example, the second panel of Figure 4.3 which depicts a calving front which has advected over a shallow sill. This situation is analogous to Store Glacier in the CW sector, which is depicted with other examples of calving-dominated glaciers in Figure 4.6.

In this study, we identify 34 glaciers which exhibit this calving-dominated behavior, with examples provided in Figure 4.6 and described in Chapter 3. Many of these glaciers represent substantial discharge rates from the ice sheet, and the stability of their ice fronts has helped keep these fluxes constant: at the 34 glaciers categorized as calving-dominated, there was only an 2.1% increase in discharge between their 1992 and 2018 rates. This is only a fraction of the 25.5% increase in ice discharge observed on the Greenland Ice Sheet is a whole, indicating the stability of these glacier are key modulators of mass loss from the continent.

4.2.5 Melt-Dominated Glaciers

In assessing the impact of ocean temperature variability on the evolution of 226 glaciers from the ice sheet, it is impossible to conclude on 67 glaciers because of small bathymetry or other residual errors in the bed shape, the presence of floating sections, and ice fronts which were already in a sustained state of retreat when ocean model data is available. For another 34 glaciers, shallow sills and residual errors in bathymetry prevent undercutting from having an impact on the stability of the ice terminus location. In total, these glaciers account for 198 Gt/yr of ice discharge and 969

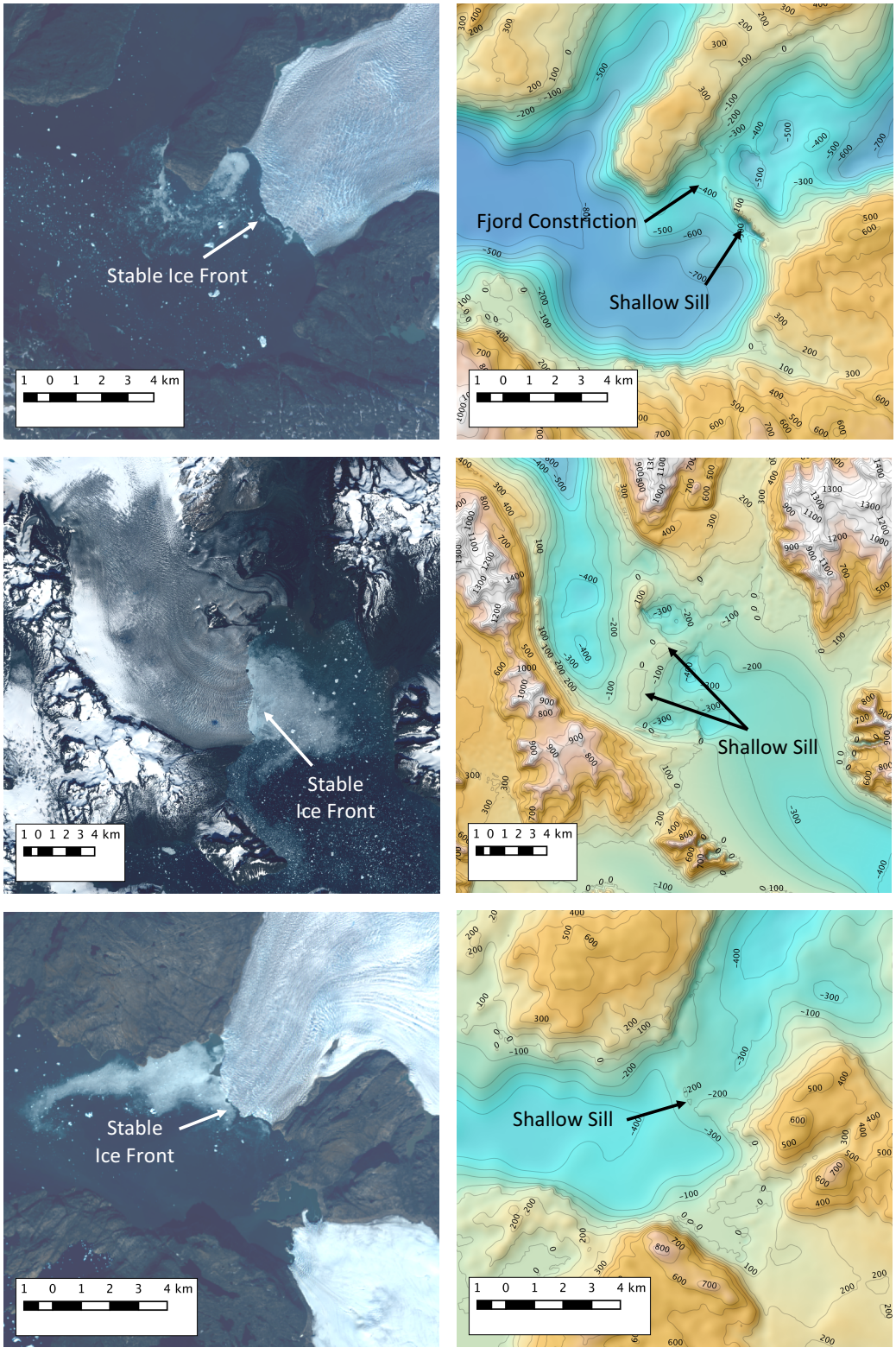

Figure 4.6: Examples of Bathymetry for Calving-Dominated Glaciers

Examples of glaciers which are categorized as calving-dominated. The left panel shows a Landsat image of the glacier position, and the right shows the bathymetry/bed in BedMachine Version 3 [Morlighem et al., 2017]

Table 4.4: Overview of Glacier Categorizations

Category	Mean Ice Discharge (Gt/yr)	Tidewater Glaciers (#)	Areal Ice Loss Grounded (km^2)	Areal Ice Loss Total (km^2)
Shallow-Bathymetry	18	50	176	176
Floating Extension	81	10	534	1725
Sustained Retreat	6	7	180	180
Calving-Dominated	93	34	56	56
Melt-Dominated	279	125	1465	1465
Total	**477**	**226**	**2481**	**3602**

Breakdown of the discharge and retreat magnitudes by the categorizations delineated in Section 4.2

km^2 of ground ice loss – the equivalent of 41% of the total ice discharge and 40% of the total ice area loss from the ice sheet between 1992 and 2018. The remainder of the ice discharge and retreat area is attributed to glaciers which are melt-dominated – the most significant glaciers on the ice sheet.

In total, there are 125 glaciers in this study which were identified as melt-dominated. These glaciers are characterized as having a stable ice front position between 1985 and the late 1990's, and then a progression of retreat which ensues around the turn of the millennium when thermal forcing around the ice sheet increased. The retreat distance of these glaciers typically corresponds closely with their melt anomaly during the period of increased thermal forcing between 1997 and 2008. As thermal forcing started to decline after 2008, some glaciers restabilized while others continued to retreat. During this subsequent cooling period, retreat records do not closely correspond to the melt anomaly for the majority of glaciers. The rationale for this mismatch is that the initial increase in melt was sufficient to undercut the ice front to detach a substantial portion of the grounded terminus, alter the stress balance in the terminus region, decrease the buttressing force on the ice upstream, and cause an acceleration of ice. Indeed, surface thinning and ice acceleration are observed at nearly all of the marine terminating glaciers [Mouginot et al., 2019]. In fact, marine terminating glaciers constituted an 29.2% increase in discharge which was more than the total 25.5% increase in total for all glaciers on the ice sheet. In terms of retreat, the melt-dominated glaciers accounted for 1,465 km^2 of ice loss between 1992 and 2018.

4.2.6 Summary

Figure 4.8 provides an overview of the retreat rates for each of the categorizations outlined above over three different time periods, while Figure 4.7 provides a map delineating the regional positions of glaciers in each category. Table 4.4 provides a statistical overview of each categorization.

Melt-dominated glaciers constitute the highest proportion of glaciers by both total number and total discharge from the ice sheet. In terms of ice area loss on the periphery of the continent, the 134 MD glaciers are second only to the areal loss by glaciers with floating extensions. However, as revealed by the progression of grounding lines mapped from double-difference interferograms, the majority of ice loss from glaciers with floating extensions is comprised of floating ice rather than grounded ice. This is an important distinction because the loss of grounded ice represents a more significant buttressing force counteracting the flow of ice upstream. In other words, the loss of grounded ice is typically associated with accelerated discharge from the ice sheet, and a contribution to global sea level rise. When compared with the grounded ice loss rates, the retreat of melt-dominated glaciers is revealed to be a more substantial component of areal ice loss. This is viewed in the larger increase in acceleration at melt-dominating glaciers than their FE counterparts. As expected for CD glaciers, retreat rates are negligible at these locations, with only small perturbations observed in select locations. For SR glaciers, the small number of glaciers (7 in total) play little role in the total retreat rate for all glacier in Greenland. Finally, while the glaciers with shallow bathymetry make up a critical number of glaciers in Greenland, their retreat rate is actually quite small overall. It should be noted that the net advance of SB glaciers in the 1992-1998 time period is entirely from the anomalous surge observed at Sortebræ in the CE sector, which is likely from circumstances unrelated to the oceanic regime in the area.

4.3 Impact of Melt on Ice Sheet Evolution

In this section, total quantities of melted ice are compared to advection, calving, and retreat rates.

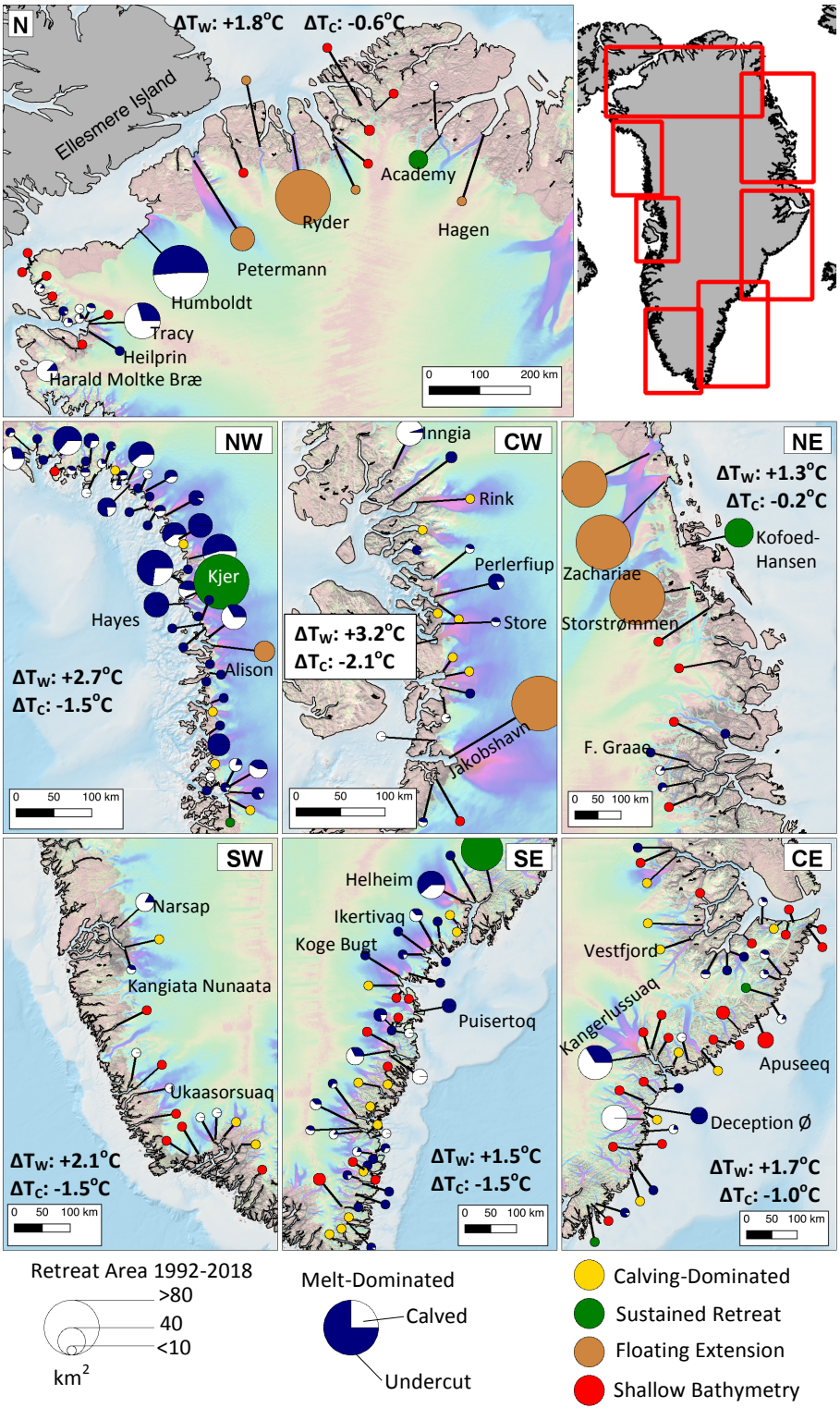

Figure 4.7: Glacier Categorization Map

Map depicting the locations, retreat rates, and categorizations of glaciers around the ice sheet.

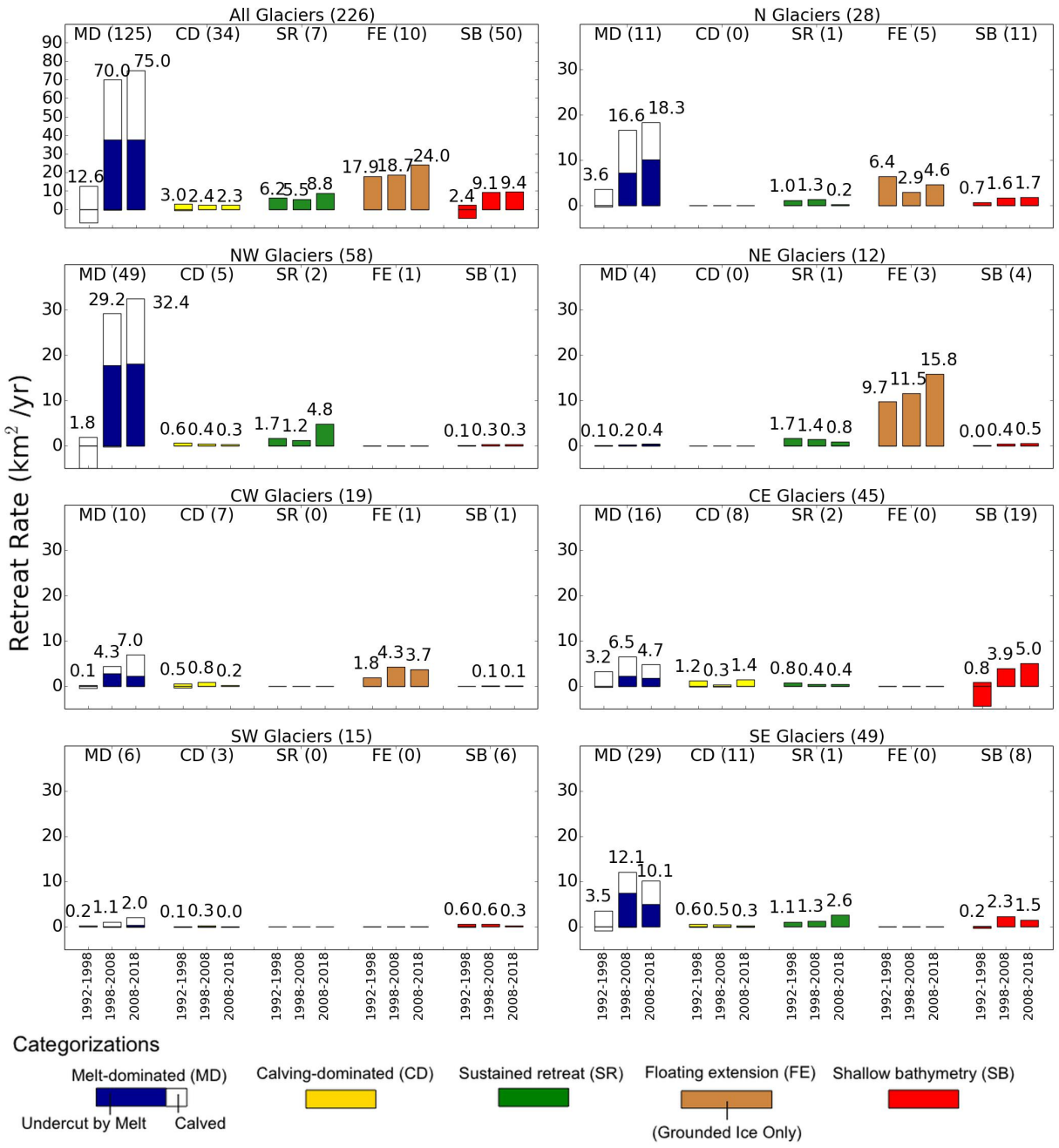

Figure 4.8: Retreat Rates by Categorization and Sector

Break down of retreat by region, time period and classification. Note that the vertical axes for the top panels are scaled differently for clarity.

4.3.1 Ice Front Undercutting vs. Dry Calving

Dry calving – the processes by which ice blocks break off from the fronts of marine terminating glaciers induced by the propagation of surface cracks [Nick et al., 2009] or other processes – has evaded a universal description either analytically or by deterministic models. As described in Section 2.1 the dry calving rates in this investigation are deduced as the residual of the mass balance equation 2.1, i.e.

$$q_c = q_f - q_m - q_r \tag{4.1}$$

With the records generated here, it is possible to determine the relative importance of q_m and q_c in causing mass loss from the ice sheet. However, for the reasons depicted in the preceding section describing the categorization of glaciers and their corresponding melt rates, this assessment is only valid for glaciers which are MD or SR. The SB and FE glaciers cannot be appropriately captured with the modelled variables, and estimates of CD glaciers yield results which are not representative of melt which induces significant ablation. Thus, the results provided in this section correspond to MD and SR glaciers, which constitute 61% of the flux and 69% of the retreat from the ice sheet between 1992 and 2018.

Ice front melt and undercutting constitutes a wide range of fractional ablation values, from relatively little influence observed at Tracy Glacier in the N sector for which melt constituted 9% of the total ablation and Saqqarliup Sermia for which melt constituted almost 100% of the ablation. By region, the CW region shows the highest ratios between melt and ablation with 33.2% of ablation attributable to melt, and the NE section has the lowest at just 7.7% of ablation from melt. In total, for all MD glaciers on the ice sheet, approximately 25.5% of the ablation on glacier termini is attributable to ocean melt. Figure 4.9 depicts the relative proportions of calving and melting compared to total ablation on the ice sheet.

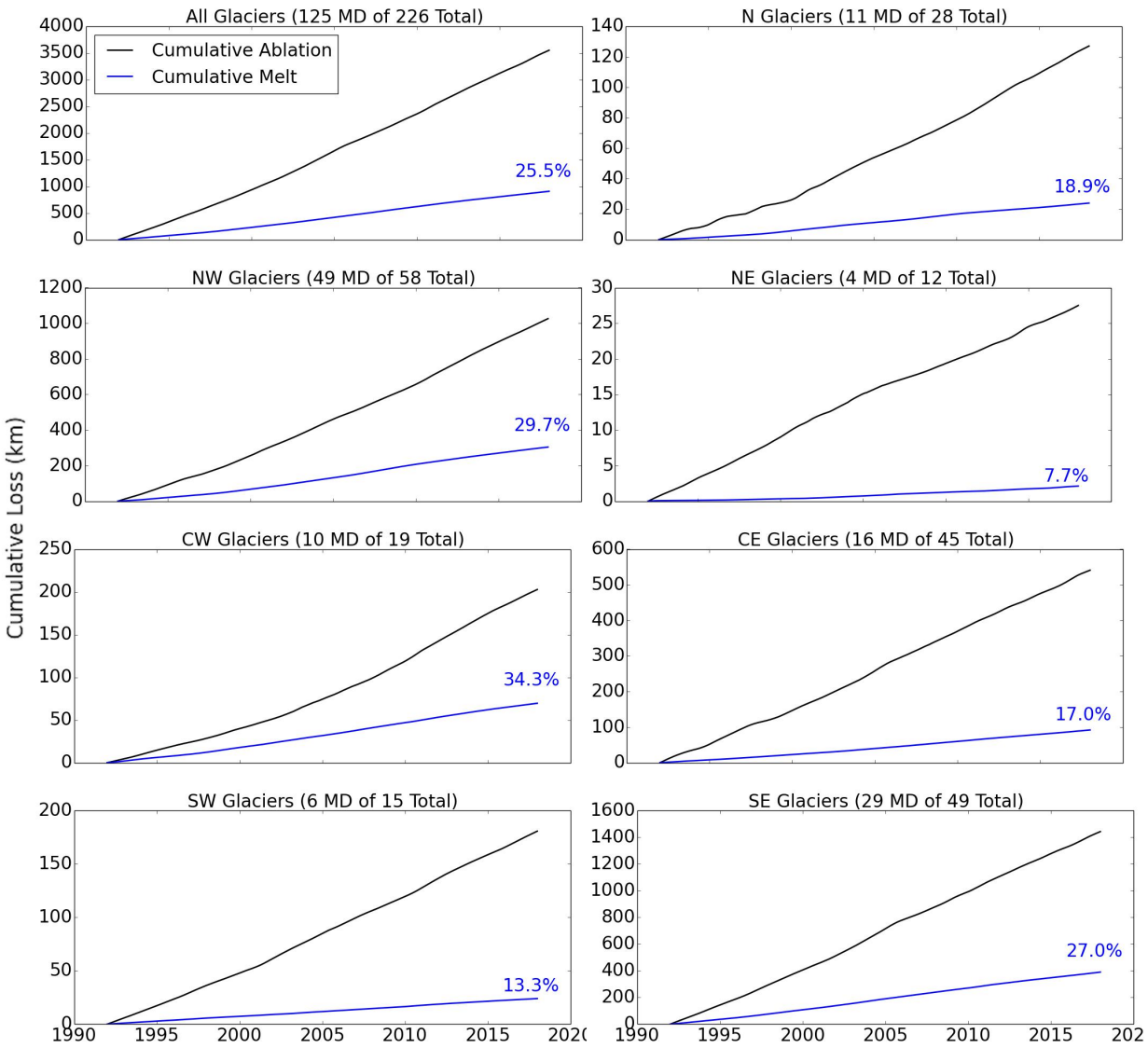

Figure 4.9: Cumulative Melt vs. Cumulative Ablation

The cumulative melt compared to the total ablation for each sector of the ice sheet. Note that these statistics only pertain to glaciers which are categorized as MD because the estimate of melt for other glaciers are either misleading or inaccurate. The total ablation is deduced as the sum of advection and ice loss via retreat.

4.3.2 The Influence of Melt on Retreat and Acceleration

On the regional average, the influence of melt is relatively small as compared to the inferred magnitude of ice loss by calving – a statistic which might suggest that melt plays a relatively small role in the evolution of glaciers on the ice sheet. However, this comparison does not take into account the effect that small changes in melt can, in turn, have on the retreat and subsequent acceleration of glaciers. As described in Section 2.4, the study herein observed accumulated melt *anomalies* in comparison to the retreat values. Figure 4.10 provides a regional view of the total undercutting anomaly in comparison to retreat for each sector of the ice sheet. Until around 2008, there is a striking comparison between the magnitude of M^{anom} and ice front retreat R. After 2008, these lines begin to substantially diverge as retreat ensues further. This progression of retreat in comparison to increased melt is suggestive of ocean melt acting as a forcing agent on the periphery of the ice sheet, causing ice front retreat. When the ice front is dislodged from its stable position, the inferred calving rates increase, consistent with calving acting as a response to regional climate forcing, in line with suggestions by Truffer and Motyka [2016]

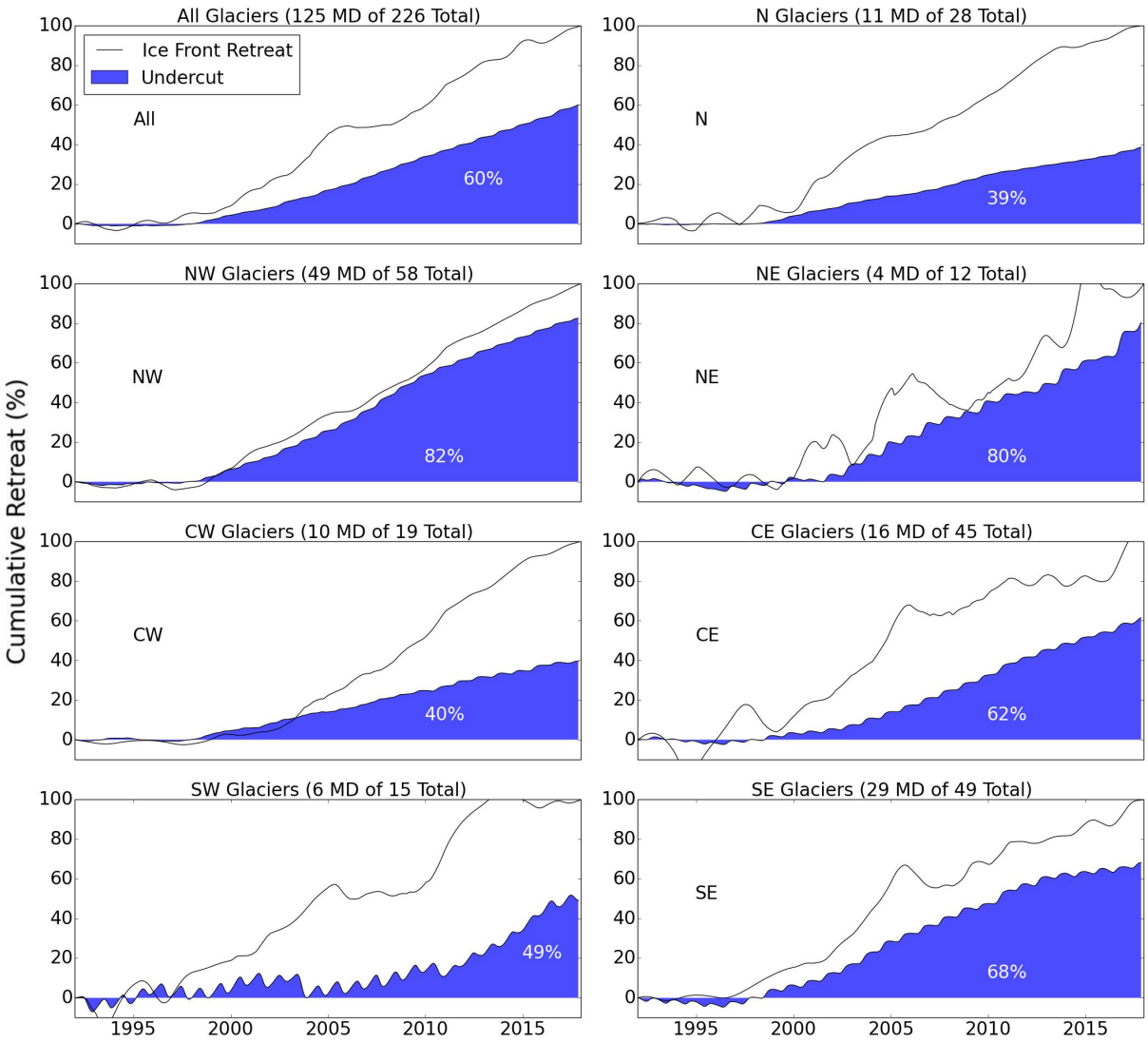

Figure 4.10: Comparison of Cumulative Melt Anomalies and Retreat Distances by Sector

Comparison between the cumulative ice front retreat distances and the cumulative melt rate anomalies averaged for each sector.

Chapter 5

Conclusions

5.1 Impact of Temperature Variability on Ice Sheet Mass Balance

The investigation herein establishes a quantitative link between regional ocean warming around Greenland, and the retreat of glacier ice margins. The subsequent acceleration and thinning of glaciers after margin retreat further implicates ocean temperature variability in causing long term changes in mass loss, and in turn, sea level rise.

This study has identified three broad-scale regimes of ocean temperature and glacier retreat: a 1992-1998 cold period when retreat was minimal, a 1998-2008 warming period when glacier retreat was substantial, and a 2008-2018 cooling period when some glaciers were continuing to retreat and others restabilized. During the 1992-1998 time period, the ocean state around Greenland was relatively cold and the total ice loss was 295 km^2 and primarily controlled by a select number of glaciers which were undergoing retreat and a few regions where floating ice extensions were present. As oceans temperatures warmed after 2008, substantial changes were observed at the majority of tidewater glaciers, leading to an 1,404 km^2 areal mass loss over this time. After 2008, as the ocean state experienced moderate cooling, many sectors of the ice sheet saw a restabilization of ice fronts. However, retreat continued for many other regions, particularly in the northwest sector. In total, the areal ice loss was 3,603 km^2 over the 1992-2018 period, which includes the break-up of several

ice tongues.

In all, 134 glaciers have clear evidence of enhanced ice front undercutting playing a dominant role in their retreat: from 1992 to 2018, melt anomalies accounted for 60.2% of ice front retreat while the remainder was the result of enhanced calving after retreat was initiated. Moreover, the timing of increased melt corresponds closely with the timing of glacier retreat after the period of quiescence in the first half of the 1990's. For another 25 glaciers, unique fjord geometries with abrupt, shallow sills and fjord constrictions prevent undercutting processes from having a significant impact on the loss of ice at the terminus, leaving the glacier front position largely impervious to the effect of increase ocean temperatures. These calving-dominated glaciers control approximately 17.7% of ice discharge from the ice sheet. Finally, it is difficult to draw conclusions for the remaining 67 glaciers because of residual deficiencies in our mapping of the fjords around Greenland (50 glaciers), the presence of floating ice extensions for which we lack a generalized melt model (10 glaciers), and cases where the glacier was already responding to forcing outside of the timespan of our oceanographic records. These 67 glaciers constitute only 37.5% of the grounded ice area lost and 3.7% of the ice discharge from glaciers on the ice sheet. On the other hand, this study implicates the ocean in causing changes on glaciers which control 60.4% of the ice sheet flux and contributed to 60.2% of its area loss between 1992 and 2018. As related to the mass balance of the ice sheet, these glaciers have contributed to 62.8% of the negative mass balance 1992-2018 – an equivalent of 6.1 mm of sea level rise.

5.2 Implications and Outlook

From the results herein, the Greenland Ice Sheet and its contribution to sea level rise are linked to the ocean temperature trends around the continent. As ocean temperatures are expected to rise in the coming century, future glacier retreat and associated mass losses will yield continuing contributions to global sea level rise. The amount of future ocean warming, and in turn, the sea level contribution from Greenland will depend greatly on progressions of greenhouse gas (GHG) emissions in the coming century. Figure 5.1 provides an outlook for ocean temperature around

Greenland under two common scenarios: a moderate scenario in which GHG emissions are curbed within the next several decades (RCP 4.5), and a more extreme scenario in which the emissions of GHGs follow a "business as usual" approach, increasing through time (RCP 8.5).

The amount of mass loss from the ice sheet, however, is still very much an open question which is greatly hindered by model deficiencies. While uncertainties in various surface processes and the cost of running high resolution models are known areas for improvements in ice sheet models, the results indicated in this study outline a critical component missing from all existing projections of ice sheet mass loss: the ocean boundary conditions and associated melting at glacier ice fronts. As of this writing, there are currently no ice sheet-wide simulations which have been run with an ocean forcing on the boundary that captures the ice front melt processes sufficient to drive inland migration of ice fronts and the subsequent acceleration of ice that leads to sea level rise. And there are certainly no configurations which attempt to couple ice models to ocean models at the ice sheet scale – experiments which would capture potential feedbacks in the ice-ocean system that may enhance or dampen the ice sheet response to sea level rise.

While ice sheet-wide modeling which includes an ocean forcing has not yet been attempted on an ice sheet scale, there are several notable regional studies that capture these processes. For example, Choi et al. [2017] found that, under enhanced ablation at rates of 5 m/d, Zachariæ Isstrøm in the NE sector of the ice sheet would retreat more than 30 km and accelerate substantially, leading to a 16.2 mm rise in sea level from this glacier alone. This same approach was expanded in a regional study by Morlighem et al. [2019], which found that for a portion of the NW sector of the ice sheet, increased thermal forcing of 3°C would lead to a sea level rise of 10-30 mm from the retreat of 23 glaciers. These studies provide a framework by which ice sheet-wide estimates of sea level rise can be driven by increased thermal forcing on the periphery of the ice sheet in an ice-sheet wide model. With the development of these simulations, ocean warming projections can be linked to changes on the ice and subsequent sea level rise.

Pending further advances in modeling, a recent study by Slater et al. [2019] has provided estimates of ice front retreat based on correlation factors between records of ice front retreat and regional ocean forcings. In this study, it was found that under the RCP4.5 scenario depicted above, glacier retreat

will be minimal in the coming century, while under the RCP8.5 scenario, ice margin retreat will be substantial. This study quantitatively corroborates the implications here, that future warming is expected to cause widespread retreat and continued mass loss during the coming century.

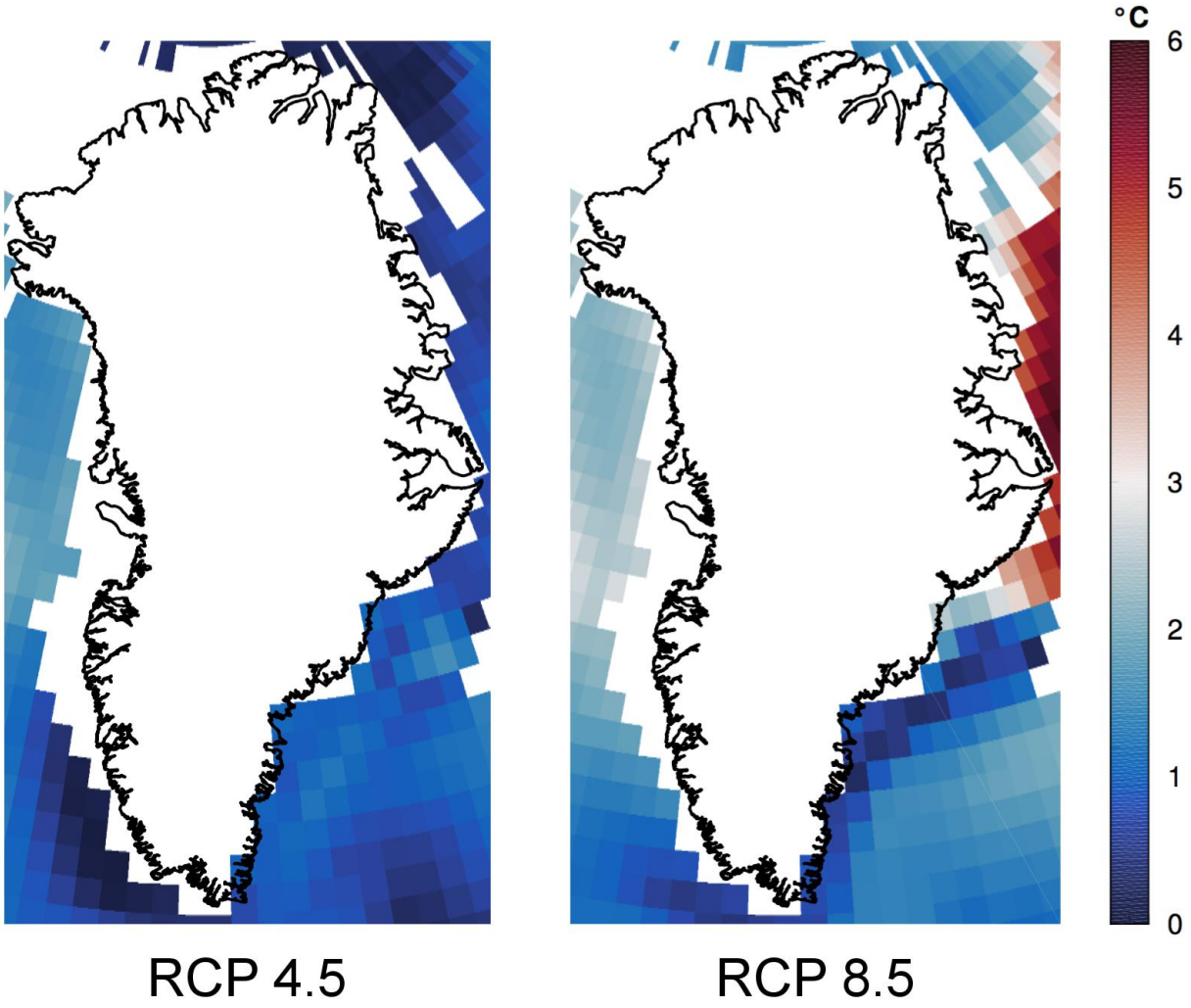

Figure 5.1: Future Ocean Warming Scenarios Around Greenland

Comparison of two ocean warming scenarios for a moderate (RCP4.5) and significant (RCP8.5) rise in greenhouse gases emissions above current values.

5.3 Recommendations for Future Advancements

In the course of this investigation, the full assessment of ocean temperature variability and corresponding changes in ice front melt on the recent evolution of Greenland's marine terminating glaciers has been hindered by several factors which should be pursued in subsequent studies to improve our understanding of this complex system. These can be broadly broken down into four main categories: improved observations, consistent ocean state estimates, processes at the ice-ocean interface, and ice sheet modelling.

Observational Improvements While NASA's Ocean's Melting Greenland campaign has made significant advances in mapping the fjord geometries and water properties around Greenland, there are still areas for which observations are lacking.

In terms of bathymetry, this study has highlighted 50 glaciers for which the bed shape is likely too shallow in the current version of the BedMachine product. These glaciers reflect regions where future mapping should be concentrated as the majority of these examples are in fjords where no measurements currently exist, leading to synthetically derived bathymetry values within these fjords. The central east, northeast, and northern sectors of the the ice sheet contain the most amount of these glaciers but even in the southwest where there are annual oceanographic surveys conducted by the Danish Meteorological Institute, there are several glacier fjords which remain un-mapped. Many of the glaciers with floating ice shelves represent areas where mapping should be improved as well. Bathymetry mapping by boat is often difficult and dangerous in the terminus regions of fjords where iceberg calving may occur at any moment and the surface waters are full of brash ice which is largely impassible by ship. In these areas, the use of autonomous underwater vehicles equipped with multibeam echo sounders may be required to accurately map the underwater fjord environment.

For the oceanographic measurements, the vast quantity of CTDs provided by OMG has greatly improved our understanding of the circulation and modulation of waters around Greenland, but these measurements provide a relatively small snapshot in time. As glacial changes persist on the

ice sheet, similar oceanographic measurements should be made, both on the continental shelf and inside the fjords. There have been substantial recent advancements in the quantity and quality of autonomous floats deploys in the global oceans, and these may provide some measurements around Greenland in the coming decades. However, these floats operate by traversing the water column and transmitting measurements back to research centers via satellite. In Greenland, where sea ice conditions may persist for more than half of the year, enormous floating icebergs circulate around the peripheral waters, and fjords are choked with ice mélange, these autonomous floats will not be able to provide consistent measurements because they will not be able to access the surface to transmit the collected data. Even in the OMG campaign, a few autonomous ALAMO floats were deployed without a single measurement. Thus, an ongoing effort to conduct CTDs by either boat or plane will be necessary to continue measuring water properties around Greenland.

Ocean State Estimates Much of this dissertation (e.g. Section 2.3.3) has been dedicated to the description and calibration of ocean state estimates for use in the understanding changes on the periphery of the Greenland Ice Sheet. The two estimates used here – the 4 km Solution and the LLC270 Solution – offer very different pictures of the ocean state (e.g. Figure 2.6) which resulted primarily from their resolution and the ways in which they incorporated existing measurements into the modelled state. The 4 km Solution was superior in the transfer of heat through narrow passages such as the Davis Straight, but without consistent assimilation of existing data, the model solution has the potential to drift away from the potential real ocean state. Future modelling efforts should be focused on high resolution configurations, particularly in regions which require the resolution of eddies to obtain accurate heat transport. As high computational costs often keep model resolutions relatively low, future advancements in ocean modelling should be aimed at "nesting" higher resolution regimes into lower resolution models to capture eddies and other smaller-scale phenomena. In addition to eddies on the continental shelf and other bathymetric constrictions, substantial effort should be dedicated to the modulation of water properties within the fjords. Even the eddy-resolving 4 km resolution employed here was not sufficient to observe the transfer of heat across the continental shelf and into the fjords, leaving the modulation of water profiles across this domain to be inferred by CTDs taken from within the fjords. The resolution

of circulation within these fjords could be tackled using the same "nested" methodology suggested above. With more accurate ocean models that capture fine-scale processes and encapsulate the vast quantity of available oceanographic observations, the assessment of current and future temperature variability on the retreat of Greenland's glaciers will be vastly improved.

Ice-Ocean Interactions While substantial work has been pursued to characterize and quantify processes at the ice-ocean interface, substantial uncertainty exists in the how these processes vary across different fjords and ice front geometries. One of the major types of glaciers which remains unresolved in parameterized models is those with floating extensions. Little is known about how water enters and leaves the sub-ice tongue cavity, the circulation within these areas, and the pattern of melt and possible refreeze on the ice itself. These uncertainties lead to questions in the extent to which ocean temperature variability affects the stability of floating ice extensions and their influence on ice from upstream. Future modeling efforts should be focused on identifying simple methods for quantifying ice tongue melt and thresholds for their break-up. Using parameterizations such as those provided by Cai et al. [2017], ice sheet models seeking to provide estimates of future mass loss and sea level rise can capture the small number but significant contribution of these glaciers as outlined in this study.

Ice Sheet Modeling As reflected in Section 5.2, developments in ice sheet modeling still require substantial improvements to fully capture the progression of the ice sheet under future warming scenarios. First, it is recommended that ice sheet models are run in a configuration in which parameterized ice front melt – with the Rignot et al 2016 parameterization, for example – can be applied to investigate the retreat distance of the glaciers margins, and the subsequent ice acceleration and mass loss from the ice sheet. These experiments will provide an improved estimate of ice sheet mass loss by encapsulating processes which have historically been omitted from such projections. However, to fully encapsulate processes on the ice-ocean interface, effort should be dedicated toward the coupling of ice and ocean models. This will facilitate the investigation of feedbacks that may diminish or enhance the effect of melt on retreat. One successful example of this application is from Seroussi et al. [2017] who coupled the Ice Sheet System Model [Larour et al., 2012] to the MIT

General Circulation Model [Marshall et al., 1997] to investigate the retreat of Thwaites glacier – an experiment that, in this example, showed melt is overestimated without the influence of cold, fresh meltwater associated with the melting processes. Applying this approach in an entire ice sheet and regional ocean simulation would be exceedingly computationally expensive, but would provide the most accurate numerical view of the ice sheet evolution in the future.

References

Lu An, Eric Rignot, Jeremie Mouginot, and Romain Millan. A century of stability of Avannarleq and Kujalleq glaciers, west Greenland, explained using high-resolution airborne gravity and other data. *Geophysical research letters*, 45(7):3156–3163, 2018.

Lu An, Eric Rignot, Romain Millan, Kirsty Tinto, and Josh Willis. Bathymetry of northwest Greenland using Ocean Melting Greenland (OMG) high-resolution airborne gravity and other data. *Remote Sensing*, 11(2):131, 2019.

Etienne Berthier, Helene Vadon, David Baratoux, Yves Arnaud, C Vincent, Kurt L Feigl, F Remy, and Benoit Legresy. Surface motion of mountain glaciers derived from satellite optical imagery. *Remote Sensing of Environment*, 95(1):14–28, 2005.

Anders Anker Bjørk, LM Kruse, and PB Michaelsen. Brief communication: Getting Greenland's glaciers right–a new data set of all official Greenlandic glacier names. *The Cryosphere*, 9(6): 2215–2218, 2015.

Alexandra Boghosian, Kirsty Tinto, James R Cochran, David Porter, Stefan Elieff, Bethany L Burton, and Robin E Bell. Resolving bathymetry from airborne gravity along Greenland fjords. *Journal of Geophysical Research: Solid Earth*, 120(12):8516–8533, 2015.

Charlie Bunce, J Rachel Carr, Peter W Nienow, Neil Ross, and Rebecca Killick. Ice front change of marine-terminating outlet glaciers in northwest and southeast Greenland during the 21st century. *Journal of Glaciology*, 64(246):523–535, 2018.

Cilan Cai, Eric Rignot, Dimitris Menemenlis, and Yoshihiro Nakayama. Observations and modeling of ocean-induced melt beneath Petermann glacier ice shelf in northwestern Greenland. *Geophysical Research Letters*, 44(16):8396–8403, 2017.

Nolwenn Chauche. Ph.D. Thesis: Glacier-ocean interaction at Store glacier (west Greenland). 2016.

Y Choi, M Morlighem, E Rignot, J Mouginot, and M Wood. Modeling the response of Nioghalvfjerdsfjorden and Zachariae Isstrøm glaciers, Greenland, to ocean forcing over the next century. *Geophysical Research Letters*, 44(21):11–071, 2017.

Poul Christoffersen, Ruth Mugford, Karen J Heywood, Ian Joughin, Julian A Dowdeswell, James PM Syvitski, Adrian Luckman, and Toby J Benham. Warming of waters in an east greenland fjord prior to glacier retreat: mechanisms and connection to large-scale atmospheric conditions. *The Cryosphere*, 5(3):701–714, 2011.

Ellyn M Enderlin and Ian M Howat. Submarine melt rate estimates for floating termini of Greenland outlet glaciers (2000–2010). *Journal of Glaciology*, 59(213):67–75, 2013.

Mark Fahnestock, Ted Scambos, Twila Moon, Alex Gardner, Terry Haran, and Marin Klinger. Rapid large-area mapping of ice flow using Landsat 8. *Remote Sensing of Environment*, 185: 84–94, 2016.

Denis Felikson, Timothy C Bartholomaus, Ginny A Catania, Niels J Korsgaard, Kurt H Kjær, Mathieu Morlighem, Brice Noël, Michiel van den Broeke, Leigh A Stearns, Emily L Shroyer, et al. Inland thinning on the Greenland ice sheet controlled by outlet glacier geometry. *Nature Geoscience*, 10(5):366–369, 2017.

Ian Fenty, Josh K Willis, Ala Khazendar, Steven Dinardo, René Forsberg, Ichiro Fukumori, David Holland, Martin Jakobsson, Delwyn Moller, James Morison, et al. Oceans Melting Greenland: Early results from nasa's ocean-ice mission in Greenland. *Oceanography*, 29(4):72–83, 2016.

Mason J Fried, Ginny A Catania, Timothy C Bartholomaus, Daniel Duncan, Marcy Davis, Leigh A Stearns, Jonathan Nash, Emily Shroyer, and David Sutherland. Distributed subglacial discharge drives significant submarine melt at a greenland tidewater glacier. *Geophysical Research Letters*, 42(21):9328–9336, 2015.

Emily Hill, Hilmar Gudmundsson, J Rachel Carr, and Chris Stokes. Velocity response of Petermann glacier, northwest Greenland, to past and future calving events. *The Cryosphere*, 12(12):3907–3921, 2018a.

Emily A Hill, J Rachel Carr, Chris R Stokes, and Hilmar Gudmundsson. Dynamic changes in outlet glaciers in northern Greenland from 1948 to 2015. *The Cryosphere*, 12(10):3243–3263, 2018b.

David M Holland, Robert H Thomas, Brad De Young, Mads H Ribergaard, and Bjarne Lyberth. Acceleration of Jakobshavn Isbrae triggered by warm subsurface ocean waters. *Nature geoscience*, 1(10):659, 2008.

Ian Howat. MEaSURES Greenland ice velocity: Selected glacier site velocity maps from optical images, version 1. 2016. doi: https://doi.org/10.5067/EYV1IP7MUNSV.

Ian M Howat, Ian Joughin, Mark Fahnestock, Benjamin E Smith, and Ted A Scambos. Synchronous retreat and acceleration of southeast Greenland outlet glaciers 2000–06: Ice dynamics and coupling to climate. *Journal of Glaciology*, 54(187):646–660, 2008.

Ian M Howat, A Negrete, and Ben Smith. The Greenland Ice Mapping Project (GIMP) land classification and surface elevation data sets. *The Cryosphere*, 8(4):1509–1518, 2014.

Martin Jakobsson, Larry Mayer, Bernard Coakley, Julian A Dowdeswell, Steve Forbes, Boris Fridman, Hanne Hodnesdal, Riko Noormets, Richard Pedersen, Michele Rebesco, et al. The international bathymetric chart of the Arctic Ocean (IBCAO) version 3.0. *Geophysical Research Letters*, 39(12), 2012.

Ian Joughin, Ron Kwok, and Mark Fahnestock. Estimation of ice-sheet motion using satellite radar interferometry: method and error analysis with application to Humboldt glacier, Greenland. *Journal of Glaciology*, 42(142):564–575, 1996.

Ian Joughin, Ben E Smith, Ian M Howat, Ted Scambos, and Twila Moon. Greenland flow variability from ice-sheet-wide velocity mapping. *Journal of Glaciology*, 56(197):415–430, 2010.

Ian Joughin, Richard B Alley, and David M Holland. Ice-sheet response to oceanic forcing. *Science*, 338(6111):1172–1176, 2012.

Ala Khazendar, Ian G Fenty, Dustin Carroll, Alex Gardner, Craig M Lee, Ichiro Fukumori, Ou Wang, Hong Zhang, Hélène Seroussi, Delwyn Moller, et al. Interruption of two decades of Jakobshavn Isbrae acceleration and thinning as regional ocean cools. *Nature Geoscience*, page 1, 2019.

Eric Larour, Helene Seroussi, Mathieu Morlighem, and Eric Rignot. Continental scale, high order, high spatial resolution, ice sheet modeling using the Ice Sheet System Model (ISSM). *Journal of Geophysical Research: Earth Surface*, 117(F1), 2012.

Sydney Levitus et al. The world ocean database. *Data Science Journal*, 12:WDS229–WDS234, 2013.

John Marshall, Alistair Adcroft, Chris Hill, Lev Perelman, and Curt Heisey. A finite-volume, incompressible navier stokes model for studies of the ocean on parallel computers. *Journal of Geophysical Research: Oceans*, 102(C3):5753–5766, 1997.

Christoph Mayer, Niels Reeh, Frederik Jung-Rothenhäusler, Philippe Huybrechts, and Hans Oerter. The subglacial cavity and implied dynamics under Nioghalvfjerdsfjorden glacier, ne Greenland. *Geophysical Research Letters*, 27(15):2289–2292, 2000.

Dorota Medrzycka, Douglas I Benn, Jason E Box, Luke Copland, and James Balog. Calving behavior at Rink Isbræ, west Greenland, from time-lapse photos. *Arctic, Antarctic, and Alpine Research*, 48(2):263–277, 2016.

Mark Meier and Austin Post. Fast tidewater glaciers. *Journal of Geophysical Research: Solid Earth*, 92(B9):9051–9058, 1987.

Sebastian H Mernild and Bent Hasholt. Observed runoff, jökulhlaups and suspended sediment load from the Greenland ice sheet at Kangerlussuaq, west Greenland, 2007 and 2008. *Journal of Glaciology*, 55(193):855–858, 2009.

Romain Millan, Eric Rignot, Jeremie Mouginot, Michael Wood, Anders Anker Bjørk, and Mathieu Morlighem. Vulnerability of southeast Greenland glaciers to warm Atlantic water from Operation IceBridge and Ocean Melting Greenland data. *Geophysical research letters*, 2018.

Twila Moon and Ian Joughin. Changes in ice front position on Greenland's outlet glaciers from 1992 to 2007. *Journal of Geophysical Research: Earth Surface*, 113(F2), 2008.

Mathieu Morlighem, Chris N Williams, Eric Rignot, Lu An, Jan Erik Arndt, Jonathan L Bamber, Ginny Catania, Nolwenn Chauché, Julian A Dowdeswell, Boris Dorschel, et al. Bedmachine v3: Complete bed topography and ocean bathymetry mapping of Greenland from multibeam echo sounding combined with mass conservation. *Geophysical Research Letters*, 44(21):11–051, 2017.

Mathieu Morlighem, Michael Wood, Hélène Seroussi, Youngmin Choi, and Eric Rignot. Modeling the response of northwest Greenland to enhanced ocean thermal forcing and subglacial discharge. *The Cryosphere*, 13(2):723–734, 2019.

John Mortensen, Kunuk Lennert, Jorgen Bendtsen, and Soren Rysgaard. Heat sources for glacial melt in a sub-Arctic fjord (Godthåbsfjord) in contact with the Greenland ice sheet. *Journal of Geophysical Research: Oceans*, 116(C1), 2011.

Roman J Motyka, Ryan Cassotto, Martin Truffer, Kristian K Kjeldsen, Dirk Van As, Niels J Korsgaard, Mark Fahnestock, Ian Howat, Peter L Langen, John Mortensen, et al. Asynchronous behavior of outlet glaciers feeding Godthåbsfjord (Nuup Kangerlua) and the triggering of Narsap Sermia's retreat in sw Greenland. *Journal of Glaciology*, 63(238):288–308, 2017.

Jeremie Mouginot, Eric Rignot, Bernd Scheuchl, Ian Fenty, Ala Khazendar, Mathieu Morlighem, Arnaud Buzzi, and John Paden. Fast retreat of Zachariæ Isstrøm, northeast Greenland. *Science*, 350(6266):1357–1361, 2015.

Jeremie Mouginot, Eric Rignot, Bernd Scheuchl, and Romain Millan. Comprehensive annual ice sheet velocity mapping using Landsat-8, Sentinel-1, and RADARSAT-2 data. *Remote Sensing*, 9(4):364, 2017.

Jeremie Mouginot, Anders Anker Bjørk, Romain Millan, Bernd Scheuchl, and Eric Rignot. Insights on the surge behavior of Storstrømmen and L. Bistrup Bræ, northeast Greenland, over the last century. *Geophysical Research Letters*, 45(20):11–197, 2018.

Jérémie Mouginot, Eric Rignot, Anders A Bjørk, Michiel van den Broeke, Romain Millan, Mathieu Morlighem, Brice Noël, Bernd Scheuchl, and Michael Wood. Forty-six years of Greenland ice sheet mass balance from 1972 to 2018. *Proceedings of the National Academy of Sciences*, page 201904242, 2019.

Tavi Murray, Tazio Strozzi, Adrian Luckman, Hamish Pritchard, and Hester Jiskoot. Ice dynamics during a surge of Sortebrae, east Greenland. *Annals of Glaciology*, 34:323–329, 2002.

Tavi Murray, Kilian Scharrer, TD James, SR Dye, Edward Hanna, Adam Booth, Nick Selmes, Adrian Luckman, Adriene Hughes, Sue Cook, et al. Ocean regulation hypothesis for glacier dynamics in southeast Greenland and implications for ice sheet mass changes. *Journal of Geophysical Research: Earth Surface*, 115(F3), 2010.

Tavi Murray, Kilian Scharrer, Nick Selmes, AD Booth, TD James, Suzanne Bevan, Jenny Bradley, Sue Cook, Laura Cordero Llana, Yoann Drocourt, et al. Extensive retreat of Greenland tidewater glaciers, 2000–2010. *Arctic, Antarctic, and Alpine Research*, 47(3):427–447, 2015. doi: https://doi.org/10.1657/AAAR0014-049.

Faezeh M Nick, Andreas Vieli, Ian M Howat, and Ian Joughin. Large-scale changes in Greenland outlet glacier dynamics triggered at the terminus. *Nature Geoscience*, 2(2):110, 2009.

Brice Noël, Willem J Van De Berg, Erik Van Meijgaard, Peter Kuipers Munneke, Roderik Van De Wal, and Michiel R Van Den Broeke. Evaluation of the updated regional climate model RACMO2.3: summer snowfall impact on the Greenland ice sheet. *The Cryosphere*, 9(5):1831–1844, 2015.

Brice Noël, Willem Jan Van De Berg, Horst Machguth, Stef Lhermitte, Ian Howat, Xavier Fettweis, and Michiel R Van Den Broeke. A daily, 1 km resolution data set of downscaled Greenland ice sheet surface mass balance (1958-2015). *Cryosphere*, 10(5):2361–2377, 2016.

OMG. OMG mission: Bathymetry (sea floor depth) data from the ship-based bathymetry survey. Ver. 0.1. *OMG SDS, CA, USA*, 2016a.

OMG. Omg mission: Conductivity, Temperature and Depth (CTD) data from the ocean survey. Ver. 0.1. *OMG SDS, CA, USA*, 2016b.

Steffan Podlech and Anker Weidick. Catastrophic break-up of the front of Jakobshavn Isbræ, West Greenland, 2002/03. *J. Glaciol.*, 50(168):153–154, 2004.

David F Porter, Kirsty J Tinto, Alexandra Boghosian, James R Cochran, Robin E Bell, Serdar S Manizade, and John G Sonntag. Bathymetric control of tidewater glacier mass loss in northwest Greenland. *Earth and Planetary Science Letters*, 401:40–46, 2014.

Austin Post. Preliminary hydrography and historic terminal changes of Columbia glacier, Alaska. 1975.

Eric Rignot and Pannir Kanagaratnam. Changes in the velocity structure of the Greenland ice sheet. *Science*, 311(5763):986–990, 2006.

Eric Rignot and Jeremie Mouginot. Ice flow in Greenland for the international polar year 2008–2009. *Geophysical Research Letters*, 39(11), 2012.

Eric Rignot, Michele Koppes, and Isabella Velicogna. Rapid submarine melting of the calving faces of west Greenland glaciers. *Nature Geoscience*, 3(3):187, 2010.

Eric Rignot, Ian Fenty, Dimitris Menemenlis, and Yun Xu. Spreading of warm ocean waters around Greenland as a possible cause for glacier acceleration. *Annals of Glaciology*, 53(60):257–266, 2012.

Eric Rignot, Ian Fenty, Yun Xu, Cilan Cai, and Chris Kemp. Undercutting of marine-terminating glaciers in west Greenland. *Geophysical Research Letters*, 42(14):5909–5917, 2015.

Eric Rignot, Yun Xu, Dimitris Menemenlis, Jeremie Mouginot, Bernd Scheuchl, Xin Li, Mathieu Morlighem, Helene Seroussi, Michiel van den Broeke, Ian Fenty, et al. Modeling of ocean-induced ice melt rates of five west Greenland glaciers over the past two decades. *Geophysical Research Letters*, 43(12):6374–6382, 2016.

Anthony Seale, Poul Christoffersen, Ruth I Mugford, and Martin O'Leary. Ocean forcing of the Greenland ice sheet: Calving fronts and patterns of retreat identified by automatic satellite monitoring of eastern outlet glaciers. *Journal of Geophysical Research: Earth Surface*, 116(F3), 2011.

H Seroussi, M Morlighem, E Rignot, A Khazendar, E Larour, and J Mouginot. Dependence of century-scale projections of the Greenland ice sheet on its thermal regime. *Journal of Glaciology*, 59(218):1024–1034, 2013.

Helene Seroussi, Yoshi Nakayama, Eric Larour, Dimitris Menemenlis, Mathieu Morlighem, Eric Rignot, and Ala Khazendar. Continued retreat of Thwaites glacier, west Antarctica, controlled by bed topography and ocean circulation. *Geophysical Research Letters*, 44(12):6191–6199, 2017.

Donald Slater, Fiamma Stanero, Denis Felikson, Chris Little, Heiko Goelzer, Xavier Fettweis, and James Holte. Past and future response of Greenland's tidewater glaciers to submarine melting. *The Cryosphere*, 2019.

Donald A Slater, Fiamma Straneo, Sarah B Das, Clark G Richards, Till JW Wagner, and Peter W Nienow. Localized plumes drive front-wide ocean melting of a Greenlandic tidewater glacier. *Geophysical Research Letters*, 45(22):12–350, 2018.

Fiammetta Straneo and Patrick Heimbach. North atlantic warming and the retreat of Greenland's outlet glaciers. *Nature*, 504(7478):36, 2013.

Fiammetta Straneo, David A Sutherland, David Holland, Carl Gladish, Gordon S Hamilton, Helen L Johnson, Eric Rignot, Yun Xu, and Michele Koppes. Characteristics of ocean waters reaching Greenland's glaciers. *Annals of Glaciology*, 53(60):202–210, 2012.

Shin Sugiyama, Daiki Sakakibara, Shun Tsutaki, Mihiro Maruyama, and Takanobu Sawagaki. Glacier dynamics near the calving front of Bowdoin glacier, northwestern Greenland. *Journal of glaciology*, 61(226):223–232, 2015.

David A Sutherland and Fiammetta Straneo. Estimating ocean heat transports and submarine melt rates in Sermilik fjord, Greenland, using lowered acoustic doppler current profiler (LADCP) velocity profiles. *Annals of Glaciology*, 53(60):50–58, 2012.

Martin Truffer and Roman J Motyka. Where glaciers meet water: Subaqueous melt and its relevance to glaciers in various settings. *Reviews of Geophysics*, 54(1):220–239, 2016.

KM Walsh, IM Howat, Y Ahn, and EM Enderlin. Changes in the marine-terminating glaciers of central east Greenland, 2000–2010. *The Cryosphere*, 6(1):211–220, 2012.

Josh K Willis, Dustin Carroll, Ian Fenty, Gurjot Kohli, Ala Khazendar, Matthew Rutherford, Nicole Trenholm, and Mathieu Morlighem. Ocean-ice interactions in inglefield gulf: Early results from NASAs Oceans Melting Greenland mission. *Oceanography*, 31(2):100–108, 2018.

Michael Wood, Eric Rignot, Ian Fenty, Dimitris Menemenlis, Romain Millan, Mathieu Morlighem, Jeremie Mouginot, and Helene Seroussi. Ocean-induced melt triggers glacier retreat in northwest Greenland. *Geophysical Research Letters*, 45(16):8334–8342, 2018.

Yun Xu, Eric Rignot, Dimitris Menemenlis, and Michele Koppes. Numerical experiments on subaqueous melting of Greenland tidewater glaciers in response to ocean warming and enhanced subglacial discharge. *Annals of Glaciology*, 53(60):229–234, 2012.

Yun Xu, Eric Rignot, Ian Fenty, Dimitris Menemenlis, and Mar Flexas. Subaqueous melting of Store glacier, west Greenland from three-dimensional, high-resolution numerical modeling and ocean observations. *Geophysical Research Letters*, 40(17):4648–4653, 2013.

Hong Zhang, Dimitris Menemenlis, and Ian Fenty. ECCO LLC270 ocean-ice state estimate. 2018.

Appendix A

Summary Tables

Table A.1: Overview of NW Glaciers in the Melville Bay Region during 1992-2018

Glacier	Cateogry	Depth	$\overline{q_m}$	R		F	$F+R$	M	M^{anom}	$M/(F+R)$	M^{anom}/R
		(m)	(m/d)	(km^2)	(km)	(km)	(km)	(km)	(km)	(%)	(%)
Savissuaq Gl. WWWW	MD	134	0.25	25.9	5.3	7.7	13.0	2.4	1.46	18.5	27.5
Savissuaq Gl. WWW	MD	139	0.29	7.9	2.6	5.4	8.0	2.7	1.77	33.8	68.1
Savissuaq Gl. WW	MD	119	0.54	5.2	1.7	4.6	6.3	5.2	1.75	82.5	>100
Savissuaq Gl. W	MD	174	0.50	5.2	0.9	7.1	8.1	4.7	2.58	58.0	>100
Savissuaq Gl.	MD	164	0.68	32.0	4.8	9.5	14.3	6.5	3.08	45.5	64.2
Helland Gl. W	SB	4	–	5.8	2.2	–	–	–	–	–	–
Helland Gl.	MD	93	0.29	6.3	1.5	3.8	5.4	2.8	0.61	51.9	40.7
Helland Gl. E	MD	93	0.63	3.1	1.3	6.1	7.5	6.0	0.67	80.0	51.5
Yngvar Nielsen Gl. W	MD	109	0.52	0.5	0.3	17.9	18.2	5.0	0.45	27.5	>100
Yngvar Nielsen Gl.	MD	207	0.66	16.8	4.2	18.3	22.5	6.2	2.97	27.6	70.7
Mohn Gl.	MD	54	0.53	10.2	0.8	–	–	–	-0.53	–	–
Carlos Gl. W	MD	5	0.09	3.7	1.6	7.7	9.3	0.8	0.46	8.6	28.7
Carlos Gl.	MD	207	0.59	8.6	2.2	23.6	25.8	5.6	2.06	21.7	93.6
Gade Gl.	CD	269	–	1.7	0.3	32.2	32.5	7.7	–	23.7	–
Morell Gl. W	MD	102	0.38	6.8	4.5	7.5	11.9	3.6	2.35	30.3	52.2
Morell Gl.	MD	107	0.41	10.1	4.6	14.1	18.7	3.9	1.00	20.9	21.7
Docker Smith Gl. W	MD	282	0.94	28.2	6.8	24.3	31.0	8.9	4.12	28.7	60.6
Docker Smith Gl.	MD	290	0.87	20.6	3.8	12.8	16.6	8.3	2.91	50.0	76.6
Docker Smith Gl. E	MD	122	0.46	1.1	0.4	14.5	14.9	4.3	1.30	28.9	>100
Rink Gl. W	MD	85	0.52	1.6	1.1	4.7	5.8	4.9	-0.11	84.5	–
Rink Gl.	MD	215	0.64	14.4	3.6	16.3	19.8	6.1	2.10	30.8	58.3
Rink Gl. S	MD	176	0.65	1.8	0.8	48.9	49.7	6.2	3.39	12.5	>100
Issuusarsuit Se.	MD	233	0.88	6.3	1.1	17.3	18.4	8.3	2.79	45.1	>100
Kong Oscar Gl. NN	MD	233	0.69	7.0	2.2	12.1	14.3	6.6	2.82	46.2	>100
Kong Oscar Gl. N	MD	104	0.44	12.5	3.5	16.4	19.9	4.2	1.90	21.1	54.3
Kong Oscar Gl.	MD	553	1.24	16.6	4.2	63.7	67.9	11.8	3.83	17.4	91.2

Summative statiscs for 26 glaciers in the Melville Bay region. Categories correspond to Melt-Dominated (MD), Calving-Dominated (CD), Sustained Retreat (SR), Floating Extension (FE), and Shallow Bathymetry (SB) glaciers (see Section 4.2). R is glacier retreat, F is the total ice advection, M is the total ice melted, M^{anom} is the total ice melted above the baseline melt rate, M/F is the fraction of advected ice which was melted, M^{anom}/R is the fraction of retreat attributable to the melt anomaly. See section 3.1.1 for a descriptive interpretation of these results.

Table A.2: Overview of NW Glaciers in the Kullorsuaq Region during 1992-2018

Glacier	Cateogry	Depth (m)	$\overline{q_m}$ (m/d)	R (km^2)	R (km)	F (km)	$F+R$ (km)	M (km)	M^{anom} (km)	$M/(F+R)$ (%)	M^{anom}/R (%)
Nordenskiold Gl. N	MD	89	0.48	1.9	0.6	15.8	16.4	4.6	0.08	28.0	13.3
Nordenskiold Gl.	MD	207	0.65	26.6	5.2	12.5	17.7	6.2	3.16	35.0	60.8
Nansen Gl.	MD	213	0.68	26.7	2.8	22.3	25.1	6.4	3.19	25.5	>100
Nansen Gl. S	CD	118	–	1.5	0.2	9.8	10.0	4.4	–	44.0	–
Sverdrup Gl.	MD	264	0.93	37.0	5.8	36.1	41.9	8.8	3.20	21.0	55.2
Dietrichson Gl.	MD	250	0.69	7.7	2.5	26.3	28.8	6.5	3.38	22.6	>100
Steenstrup Gl.	MD	212	0.57	39.9	4.0	22.3	26.3	5.4	2.96	20.5	74.0
Kjer Gl. N	MD	178	0.52	20.7	4.4	8.6	13.0	5.0	2.06	38.5	46.8
Kjer Gl.	AR	167	–	62.3	8.0	21.3	29.3	5.1	–	17.4	–
Hayes Gl. North	MD	139	0.50	27.9	1.7	14.5	16.2	4.8	2.86	29.6	>100
Hayes Gl.	MD	339	0.70	7.7	1.6	45.9	47.5	6.7	3.13	14.1	>100
Hayes Gl. NN	MD	397	0.83	4.3	1.1	14.8	15.9	7.8	1.43	49.1	>100
Hayes Gl. N	MD	237	0.64	6.1	2.0	15.5	17.4	6.1	3.01	35.1	>100
Hayes Gl. M	MD	334	0.82	4.7	0.8	42.1	42.9	7.8	2.82	18.2	>100
Hayes Gl. SS	MD	263	0.66	27.4	6.2	6.5	12.7	6.2	2.06	48.8	33.2
Alison Gl.	FE	605	–	68.8	15.8	–	–	–	–	–	–

Summative statiscs for 16 glaciers in the Kullorsuaq region. Categories correspond to Melt-Dominated (MD), Calving-Dominated (CD), Sustained Retreat (SR), Floating Extension (FE), and Shallow Bathymetry (SB) glaciers (see Section 4.2). R is glacier retreat, F is the total ice advection, M is the total ice melted, M^{anom} is the total ice melted above the baseline melt rate, M/F is the fraction of advected ice which was melted, M^{anom}/R is the fraction of retreat attributable to the melt anomaly. See section 3.1.2 for a descriptive interpretation of these results.

Table A.3: Overview of NW Glaciers in the Upernavik Region during 1992-2018

Glacier	Cateogry	Depth	$\overline{q_m}$	R		F	$F+R$	M	M^{anom}	$M/(F+R)$	M^{anom}/R
		(m)	(m/d)	(km^2)	(km)	(km)	(km)	(km)	(km)	(%)	(%)
Illullip Se.	MD	325	0.87	6.1	1.3	50.0	51.3	8.3	3.65	16.2	>100
Cornell Gl. N	MD	115	0.81	2.3	1.1	4.2	5.3	7.7	1.44	145.3	>100
Cornell Gl.	MD	177	0.73	5.0	0.9	10.2	11.1	6.9	3.07	62.2	>100
Ussing Br. N	MD	263	0.79	4.0	0.8	21.0	21.8	7.5	3.74	34.4	>100
Ussing Br.	CD	242	–	1.9	0.5	31.1	31.6	7.8	–	24.7	–
Qeqertarsuup Se.	MD	167	0.77	6.2	1.4	13.5	14.9	7.3	3.00	49.0	>100
Kakivfaat Se.	MD	355	0.91	24.1	2.5	27.7	30.1	8.7	3.40	28.9	>100
Nunatakassaap Se.	CD	205	–	0.3	0.1	31.1	31.1	7.5	–	24.1	–
Akullikassaap Se. W	MD	58	0.73	1.3	0.9	3.2	4.1	6.9	-0.05	168.3	–
Akullikassaap Se.	MD	107	0.65	1.5	1.0	1.1	2.1	6.2	4.43	295.2	>100
Akullikassaap Se. E	MD	110	0.58	3.9	2.3	3.3	5.5	5.5	1.90	100.0	82.6
Upernavik Isstrom NW	MD	292	1.08	14.8	5.3	14.3	19.7	10.3	1.09	52.3	20.6
Upernavik Isstrom N	MD	411	1.16	20.9	7.0	49.6	56.5	11.0	2.90	19.5	41.4
Upernavik Isstrom C	MD	468	1.09	13.5	3.9	50.8	54.7	10.4	3.25	19.0	83.3
Upernavik Isstrom S	MD	258	1.01	4.8	1.1	49.6	50.8	9.6	3.25	18.9	>100
Upernavik Isstrom SS	AR	183	–	7.0	2.7	8.9	11.7	7.5	–	64.1	–

Summative statiscs for 16 glaciers in the Upernavik region. Categories correspond to Melt-Dominated (MD), Calving-Dominated (CD), Sustained Retreat (SR), Floating Extension (FE), and Shallow Bathymetry (SB) glaciers (see Section 4.2). R is glacier retreat, F is the total ice advection, M is the total ice melted, M^{anom} is the total ice melted above the baseline melt rate, M/F is the fraction of advected ice which was melted, M^{anom}/R is the fraction of retreat attributable to the melt anomaly. See section 3.1.3 for a descriptive interpretation of these results.

Table A.4: Overview of CW Glaciers during 1992-2018

Glacier	Cateogry	Depth	$\overline{q_m}$	R		F	$F+R$	M	M^{anom}	$M/(F+R)$	M^{anom}/R
		(m)	(m/d)	(km^2)	(km)	(km)	(km)	(km)	(km)	(%)	(%)
Inngia Isbrae	MD	148	0.90	29.2	9.0	20.6	29.6	8.5	0.43	28.7	4.8
Umiammakku Isbrae	MD	231	1.00	12.6	3.8	26.8	30.7	9.5	4.58	30.9	>100
Rink Isbrae	CD	568	–	5.2	1.2	88.6	89.7	15.0	–	16.7	–
Kangerlussuup Se.	CD	193	–	0.4	0.1	45.8	45.9	8.0	–	17.4	–
Kangerluarsuup Se.	MD	81	0.41	3.2	1.1	4.8	5.9	3.9	1.04	66.1	94.5
Perlerfiup Se.	MD	139	0.71	9.2	3.4	10.3	13.7	6.8	1.43	49.6	42.1
Sermeq Silarleq	MD	243	1.13	18.0	5.1	39.7	44.8	10.8	4.20	24.1	82.4
Kangilleq	MD	88	0.94	0.4	0.1	29.0	29.1	8.9	0.51	30.6	>100
Sermilik	MD	65	0.62	0.2	0.1	22.0	22.1	5.9	-0.20	26.7	–
Lille Gl.	MD	98	0.64	3.1	1.4	10.6	12.0	6.1	0.66	50.8	47.1
Store Gl.	CD	302	–	-0.3	-0.1	105.4	105.4	11.0	–	10.4	–
Sermeq Avannarleq	CD	186	–	0.7	0.1	48.2	48.3	7.2	–	14.9	–
Sermeq Kujalleq	CD	268	–	4.2	0.8	60.5	61.3	7.7	–	12.6	–
Kangilernata Se.	MD	194	0.62	10.9	2.7	24.4	27.1	5.9	4.17	21.8	>100
Eqip Se.	MD	64	1.01	8.9	2.1	20.7	22.8	9.6	0.15	42.1	7.1
Sermeq Avannarleq	MD	41	0.39	10.5	3.3	7.7	11.0	3.7	-0.06	33.6	–
Jakobshavn Isbrae	FE	533	–	170.9	16.9	–	–	–	–	–	–
Alangorliup Se.	SB	10	–	1.2	0.5	–	–	–	–	–	–
Saqqarliup Se.	MD	85	0.52	5.2	1.0	4.2	5.2	4.9	0.47	94.2	47.0

Summative statiscs for 19 glaciers. Categories correspond to Melt-Dominated (MD), Calving-Dominated (CD), Sustained Retreat (SR), Floating Extension (FE), and Shallow Bathymetry (SB) glaciers (see Section 4.2). R is glacier retreat, F is the total ice advection, M is the total ice melted, M^{anom} is the total ice melted above the baseline melt rate, M/F is the fraction of advected ice which was melted, M^{anom}/R is the fraction of retreat attributable to the melt anomaly. See section 3.2 for a descriptive interpretation of these results.

Table A.5: Overview of SW Glaciers during 1992-2018

Glacier	Cateogry	Depth (m)	$\overline{q_m}$ (m/d)	R (km^2)	R (km)	F (km)	$F+R$ (km)	M (km)	M^{anom} (km)	$M/(F+R)$ (%)	M^{anom}/R (%)
Narsap Se.	MD	143	0.88	20.9	5.0	39.3	44.4	8.4	0.85	18.9	17.0
Akullersuup Se.	MD	43	0.70	0.6	0.2	28.9	29.1	6.6	0.28	22.7	>100
Kangiata Nunaata Se.	MD	119	0.89	7.2	1.8	96.7	98.5	8.5	0.73	8.6	40.6
Nakkaasorsuaq	SB	1	–	0.5	0.5	–	–	–	–	–	–
Avannarleq Br.	MD	57	0.75	-0.2	-0.1	38.2	38.0	7.2	-2.51	18.9	–
Nigerlikasik	SB	1	–	1.4	1.1	–	–	–	–	–	–
Ukaasorsuaq	MD	91	1.18	0.2	0.1	–	–	–	-0.62	–	–
Sermiligaarsuup Br.	SB	1	–	0.0	0.0	–	–	–	–	–	–
Sermilik Br.	SB	2	–	7.7	4.9	–	–	–	–	–	–
Naajat Se.	SB	1	–	1.9	1.2	–	–	–	–	–	–
Eqalorutsit Killiit Se.	MD	43	0.97	3.6	3.0	–	–	–	-1.16	–	–
Eqalorutsit Killiit Se. E	MD	59	0.82	1.8	2.2	–	–	–	-0.12	–	–
Eqalorutsit Kangilliit Se.	CD	407	–	-0.9	-0.3	63.4	63.2	30.2	–	47.8	–
Qooqqup Se.	CD	195	–	2.1	1.3	36.3	37.6	20.0	–	53.2	–
Sermeq	SB	1	–	0.9	0.9	–	–	–	–	–	–

Summative statiscs for 15 glaciers. Categories correspond to Melt-Dominated (MD), Calving-Dominated (CD), Sustained Retreat (SR), Floating Extension (FE), and Shallow Bathymetry (SB) glaciers (see Section 4.2). R is glacier retreat, F is the total ice advection, M is the total ice melted, M^{anom} is the total ice melted above the baseline melt rate, M/F is the fraction of advected ice which was melted, M^{anom}/R is the fraction of retreat attributable to the melt anomaly. See section 3.3 for a descriptive interpretation of these results.

Table A.6: Overview of SE Glaciers in the South King Christian IV Coast Region during 1992-2018

Glacier	Cateogry	Depth	$\overline{q_m}$	R		F	$F+R$	M	M^{anom}	$M/(F+R)$	M^{anom}/R
		(m)	(m/d)	(km^2)	(km)	(km)	(km)	(km)	(km)	(%)	(%)
Mogens Heinesen Gl. N	MD	323	1.52	12.2	6.7	51.2	57.9	14.5	2.55	25.0	38.1
Mogens Heinesen Gl. C	MD	251	1.32	6.7	3.8	32.6	36.5	12.6	1.68	34.5	44.2
Mogens Heinesen Gl. S	MD	280	1.47	8.4	4.0	81.8	85.8	14.0	0.55	16.3	13.8
Mogens Heinesen Gl. SS	MD	46	0.04	1.2	0.4	10.6	11.1	0.3	0.02	2.7	5.0
Mogens Heinesen Gl. SSS	MD	66	0.86	2.1	1.0	39.6	40.5	8.1	-1.05	20.0	–
Puisortoq Gl. N	MD	344	2.05	6.2	3.1	34.9	38.0	19.5	2.11	51.3	68.1
Puisortoq Gl. C	MD	291	1.38	6.4	3.5	14.5	17.9	13.2	0.70	73.7	20.0
Puisortoq Gl. S	MD	336	1.63	4.1	2.1	36.2	38.2	15.5	2.36	40.6	>100
Napasorsuaq Gl. N	MD	233	1.23	2.1	1.5	18.6	20.1	11.7	2.46	58.2	>100
Napasorsuaq Gl. C	MD	146	1.08	0.2	0.1	7.4	7.5	10.2	0.60	136.0	>100
Napasorsuaq Gl. S	SB	62	–	4.9	2.7	–	–	–	–	–	–
Napasorsuaq Gl. SS	SB	3	–	2.1	1.2	–	–	–	–	–	–
Anorituup Kangerlua Gl. N	MD	466	2.21	8.7	3.8	48.7	52.5	21.0	2.94	40.0	77.4
Anorituup Kangerlua Gl. S	MD	177	1.41	1.5	0.9	21.1	22.1	13.4	1.09	60.6	>100
Herluf Trolle Gl. N	MD	274	1.41	1.6	0.8	45.7	46.5	13.4	2.69	28.8	>100
Herluf Trolle Gl. S	MD	359	1.82	3.3	2.7	30.0	32.7	17.3	3.76	52.9	>100
Kangerluluk Gl.	SB	164	–	13.9	10.0	–	–	–	–	–	–
Danell Gl.	MD	136	0.63	0.0	0.0	39.4	39.4	6.0	0.10	15.2	>100
Danell Gl. S	MD	187	0.80	2.0	1.6	9.9	11.4	7.6	1.44	66.7	90.0
Danell Gl. SS	CD	266	–	1.6	1.4	9.7	11.1	12.8	–	115.3	–
Danell Gl. SSS	CD	120	–	0.5	0.7	12.5	13.2	15.3	–	115.9	–

Summative statiscs for 21 glaciers in the South King Christian IV Coast region. Categories correspond to Melt-Dominated (MD), Calving-Dominated (CD), Sustained Retreat (SR), Floating Extension (FE), and Shallow Bathymetry (SB) glaciers (see Section 4.2). R is glacier retreat, F is the total ice advection, M is the total ice melted, M^{anom} is the total ice melted above the baseline melt rate, M/F is the fraction of advected ice which was melted, M^{anom}/R is the fraction of retreat attributable to the melt anomaly. See section 3.4.1 for a descriptive interpretation of these results.

Table A.7: Overview of SE Glaciers in the North King Christian IV Coast Region during 1992-2018

Glacier	Cateogry	Depth	$\overline{q_m}$	R		F	$F+R$	M	M^{anom}	$M/(F+R)$	M^{anom}/R
		(m)	(m/d)	(km^2)	(km)	(km)	(km)	(km)	(km)	(%)	(%)
Puisertoq Gl.	MD	113	1.76	16.0	3.2	31.5	34.7	16.7	3.36	48.1	>100
Graulv Gl. E	SB	1	–	1.4	0.8	–	–	–	–	–	–
Graulv Gl.	MD	376	2.54	5.3	2.1	73.9	76.0	24.2	2.98	31.8	>100
Gyldenlove Gl. N	MD	230	2.05	14.5	2.8	37.2	40.0	19.5	2.22	48.8	79.3
Gyldenlove Gl. S	MD	31	0.32	10.3	3.3	14.3	17.6	3.1	-0.15	17.6	–
Fimbul Gl.	SB	34	–	10.3	3.8	–	–	–	–	–	–
A.P. Bernstorf Gl.	MD	219	0.69	19.3	5.2	79.7	84.9	6.6	1.70	7.8	32.7
Maelkevejen Gl.	MD	46	0.00	16.7	6.3	38.8	45.1	0.0	0.01	0.0	0.2
Thrym Gl.	SB	2	–	1.8	0.8	–	–	–	–	–	–
Skinfaxe Gl.	CD	240	–	0.6	0.2	53.0	53.2	9.4	–	17.7	–
Rimfaxe Gl.	CD	214	–	0.2	0.1	49.5	49.6	10.5	–	21.2	–
Heimdal Gl.	CD	175	–	-0.4	-0.2	59.3	59.1	7.9	–	13.4	–
Tingmiarmiut Gl.	MD	369	2.04	9.6	4.1	104.3	108.4	19.4	2.78	17.9	67.8

Summative statiscs for 13 glaciers in the North King Christian IV Coast region. Categories correspond to Melt-Dominated (MD), Calving-Dominated (CD), Sustained Retreat (SR), Floating Extension (FE), and Shallow Bathymetry (SB) glaciers (see Section 4.2). R is glacier retreat, F is the total ice advection, M is the total ice melted, M^{anom} is the total ice melted above the baseline melt rate, M/F is the fraction of advected ice which was melted, M^{anom}/R is the fraction of retreat attributable to the melt anomaly. See section 3.4.2 for a descriptive interpretation of these results.

Table A.8: Overview of SE Glaciers in the Northern SE Region during 1992-2018

Glacier	Cateogry	Depth	$\overline{q_m}$	R		F	$F+R$	M	M^{anom}	$M/(F+R)$	M^{anom}/R
		(m)	(m/d)	(km^2)	(km)	(km)	(km)	(km)	(km)	(%)	(%)
Midgard Gl.	AR	96	–	45.1	14.0	50.5	64.5	16.9	–	26.2	–
Fenris Gl.	MD	212	2.37	8.9	3.3	36.8	40.1	22.5	5.09	56.1	>100
Helheim Gl.	MD	471	2.72	30.4	5.7	156.9	162.5	25.9	3.48	15.9	61.1
Heim Gl.	MD	83	0.45	2.0	0.6	10.2	10.8	4.3	-0.05	39.8	–
Heim Gl. S	CD	71	–	1.0	0.4	6.8	7.2	7.9	–	109.7	–
Ikertivaq Gl. NNN	MD	205	1.02	2.4	1.7	20.1	21.8	9.7	2.23	44.5	>100
Ikertivaq Gl. NN	MD	263	1.10	14.5	4.1	53.9	58.1	10.5	1.53	18.1	37.3
Ikertivaq Gl. N	MD	158	1.11	3.5	0.9	36.3	37.1	10.6	1.84	28.6	>100
Ikertivaq Gl. M	MD	375	1.35	8.0	1.7	46.9	48.6	12.9	1.69	26.5	99.4
Ikertivaq Gl. S	MD	316	0.94	5.6	1.6	46.2	47.8	8.9	1.25	18.6	78.1
Koge Bugt Gl. N	MD	178	0.60	3.4	1.0	36.0	37.1	5.8	0.99	15.6	99.0
Koge Bugt Gl. C	MD	231	1.31	5.0	1.5	82.0	83.6	12.5	1.77	15.0	>100
Koge Bugt Gl. S	CD	267	–	4.0	0.7	61.9	62.6	11.9	–	19.0	–
Koge Bugt Gl. SS	SB	1	–	3.2	1.1	–	–	–	–	–	–
Koge Bugt Gl. SSS	SB	2	–	0.5	0.1	–	–	–	–	–	–

Summative statiscs for 15 glaciers in the Northern SE region. Categories correspond to Melt-Dominated (MD), Calving-Dominated (CD), Sustained Retreat (SR), Floating Extension (FE), and Shallow Bathymetry (SB) glaciers (see Section 4.2). R is glacier retreat, F is the total ice advection, M is the total ice melted, M^{anom} is the total ice melted above the baseline melt rate, M/F is the fraction of advected ice which was melted, M^{anom}/R is the fraction of retreat attributable to the melt anomaly. See sections 3.4.3 and 3.4.4 for a descriptive interpretation of these results.

Table A.9: Overview of CE Glaciers in the Sermiligaaq to Kangerlussuaq Region during 1992-2018

Glacier	Cateogry	Depth	$\overline{q_m}$	R		F	$F+R$	M	M^{anom}	$M/(F+R)$	M^{anom}/R
		(m)	(m/d)	(km^2)	(km)	(km)	(km)	(km)	(km)	(%)	(%)
Kangerlussuaq Gl.	MD	501	0.93	37.1	7.3	120.6	127.9	8.8	2.51	6.9	34.4
Polaric Gl.	MD	179	0.75	2.6	0.3	27.9	28.2	7.1	1.98	25.2	>100
Polaric Gl. S	SB	34	–	6.7	1.6	–	–	–	–	–	–
Sondre Parallel Gl.	SB	4	–	4.3	1.8	–	–	–	–	–	–
Deception O Gl. CN	MD	145	1.57	18.8	5.4	60.0	65.4	14.9	7.19	22.8	>100
Deception O Gl. CS	CD	227	–	2.8	1.1	62.5	63.6	18.9	–	29.7	–
Uunartit Gl.	MD	144	1.39	28.0	7.0	68.9	75.9	13.3	-1.36	17.5	–
Kruuse Gl.	MD	15	0.30	5.2	2.3	44.5	46.9	2.8	0.52	6.0	22.6
Laube Gl. N	SB	5	–	0.2	0.1	–	–	–	–	–	–
Laube Gl.	SB	1	–	1.9	1.6	–	–	–	–	–	–
Laube Gl. S	MD	261	1.06	1.5	1.0	42.3	43.2	10.1	2.47	23.4	>100
K.I.V. Steenstrup Nordre Br.	CD	166	–	3.5	0.8	48.8	49.7	8.2	–	16.5	–
Knud Rasmussen Gl.	MD	108	1.92	1.9	0.9	9.8	10.7	18.3	0.74	171.0	82.2
Knud Rasmussen Gl. W	SB	19	–	0.5	0.3	–	–	–	–	–	–
Kaarale Gl.	AR	79	–	2.4	1.2	4.6	5.8	15.1	–	260.3	–

Summative statiscs for 15 glaciers in the Sermiligaaq to Kangerlussuaq region. Categories correspond to Melt-Dominated (MD), Calving-Dominated (CD), Sustained Retreat (SR), Floating Extension (FE), and Shallow Bathymetry (SB) glaciers (see Section 4.2). R is glacier retreat, F is the total ice advection, M is the total ice melted, M^{anom} is the total ice melted above the baseline melt rate, M/F is the fraction of advected ice which was melted, M^{anom}/R is the fraction of retreat attributable to the melt anomaly. See section 3.5.1 for a descriptive interpretation of these results.

Table A.10: Overview of CE Glaciers in the Geikie Plateau Region during 1992-2018

Glacier	Cateogry	Depth (m)	$\overline{q_m}$ (m/d)	R (km^2)	R (km)	F (km)	$F+R$ (km)	M (km)	M^{anom} (km)	$M/(F+R)$ (%)	M^{anom}/R (%)
Torv Gl. S	SB	1	–	2.3	0.8	–	–	–	–	–	–
Torv Gl. SS	SB	2	–	0.4	0.1	–	–	–	–	–	–
Dendrit Gl.	MD	52	0.50	7.8	1.2	9.8	11.0	4.7	0.50	42.7	41.7
Dendrit Gl. S	MD	10	0.19	6.6	2.8	7.4	10.2	1.8	0.79	17.6	28.2
Apuseeq An. N	AR	17	–	10.5	4.8	16.4	21.2	0.9	–	4.2	–
Apuseeq An.	MD	20	0.15	7.6	2.6	9.8	12.4	1.4	0.43	11.3	16.5
Sortebrae Gl.	SB	18	–	17.3	4.3	–	–	–	–	–	–
Borggraven Gl.	SB	15	–	14.6	3.3	–	–	–	–	–	–
Kronborg Gl.	SB	2	–	2.9	1.4	–	–	–	–	–	–
Rosenborg Gl.	SB	4	–	5.6	2.3	–	–	–	–	–	–
Kong Christian IV Gl.	CD	248	–	1.8	0.2	41.2	41.5	6.3	–	15.2	–
Sorgenfri Gl.	MD	46	0.07	1.2	0.4	9.5	9.9	0.7	-0.06	7.1	–
Frederiksborg Gl.	CD	47	–	0.9	0.4	31.4	31.7	0.9	–	2.8	–
Courtauld Gl.	SB	10	–	0.9	0.5	–	–	–	–	–	–
Styrte Gl.	SB	6	–	2.3	1.4	–	–	–	–	–	–
Nordjord Gl.	SB	3	–	0.5	0.3	–	–	–	–	–	–

Summative statiscs for 16 glaciers in the Geikie Plateau region. Categories correspond to Melt-Dominated (MD), Calving-Dominated (CD), Sustained Retreat (SR), Floating Extension (FE), and Shallow Bathymetry (SB) glaciers (see Section 4.2). R is glacier retreat, F is the total ice advection, M is the total ice melted, M^{anom} is the total ice melted above the baseline melt rate, M/F is the fraction of advected ice which was melted, M^{anom}/R is the fraction of retreat attributable to the melt anomaly. See section 3.5.2 for a descriptive interpretation of these results.

Table A.11: Overview of CE Glaciers in the Scoresby Sound Region during 1992-2018

Glacier	Cateogry	Depth	$\overline{q_m}$	R		F	$F+R$	M	M^{anom}	$M/(F+R)$	M^{anom}/R
		(m)	(m/d)	(km^2)	(km)	(km)	(km)	(km)	(km)	(%)	(%)
F. Graae Gl.	MD	276	0.40	3.9	1.7	29.1	30.8	3.8	3.51	12.3	>100
Charcot Gl.	SB	1	–	0.4	0.3	–	–	–	–	–	–
Daugaard-Jensen Gl.	CD	393	–	7.9	1.5	81.3	82.8	6.4	–	7.7	–
Eielson Gl.	SB	2	–	1.2	0.4	–	–	–	–	–	–
Rolige Br.	CD	165	–	1.4	0.5	19.2	19.7	4.0	–	20.3	–
Vestfjord Gl.	CD	119	–	3.7	1.1	51.2	52.3	0.1	–	0.2	–
Kista Dan Gl. W	MD	17	0.08	3.3	1.0	6.2	7.1	0.7	0.46	9.9	46.0
Kista Dan Gl.	MD	124	0.18	0.5	0.2	11.7	11.9	1.7	0.34	14.3	>100
Magga Dan Gl.	MD	123	0.17	0.7	0.2	47.0	47.1	1.6	0.58	3.4	>100
Sydbrae Gl.	SB	3	–	1.8	0.4	–	–	–	–	–	–
Brede Gl.	MD	53	0.03	3.0	0.8	1.7	2.4	0.3	0.25	12.5	31.2
Mone Gl.	MD	12	0.03	0.1	0.1	9.7	9.7	0.2	0.11	2.1	>100
Nakkaagajik Timerseq	SB	1	–	1.5	0.7	–	–	–	–	–	–
Ostre Borg Gl.	SB	5	–	2.2	1.0	–	–	–	–	–	–

Summative statiscs for 14 glaciers in the Scoresby Sound region. Categories correspond to Melt-Dominated (MD), Calving-Dominated (CD), Sustained Retreat (SR), Floating Extension (FE), and Shallow Bathymetry (SB) glaciers (see Section 4.2). R is glacier retreat, F is the total ice advection, M is the total ice melted, M^{anom} is the total ice melted above the baseline melt rate, M/F is the fraction of advected ice which was melted, M^{anom}/R is the fraction of retreat attributable to the melt anomaly. See section 3.5.3 for a descriptive interpretation of these results.

Table A.12: Overview of NE Glaciers during 1992-2018

Glacier	Cateogry	Depth (m)	$\overline{q_m}$ (m/d)	R (km^2)	R (km)	F (km)	$F+R$ (km)	M (km)	M^{anom} (km)	$M/(F+R)$ (%)	M^{anom}/R (%)
Nioghalvfjerdsbrae (79 North)	FE	162	–	153.5	4.8	–	–	–	–	–	–
Zachariae Isstrom	FE	481	–	600.6	27.2	–	–	–	–	–	–
Kofoed-Hansen Brae	AR	76	–	31.9	3.0	0.4	3.4	0.3	–	8.8	–
Storstrommen	FE	162	–	49.9	3.3	–	–	–	–	–	–
Soranerbraeen	SB	2	–	1.4	0.4	–	–	–	–	–	–
Heinkel Gl.	SB	2	–	1.6	0.9	–	–	–	–	–	–
Waltershausen Gl.	MD	91	0.11	3.5	0.3	3.1	3.5	1.0	0.65	28.6	>100
Adolf Hoel Gl.	SB	2	–	2.9	0.9	–	–	–	–	–	–
Gerard de Geer Gl.	MD	28	0.06	0.5	0.1	10.4	10.5	0.5	0.28	4.8	>100
Jaette Gl.	MD	55	0.02	1.3	0.6	5.5	6.0	0.2	0.08	3.3	13.3
Nordenskiold Gl.	MD	41	0.03	0.4	0.2	7.3	7.5	0.3	0.11	4.0	55.0
Hisinger Gl.	SB	1	–	2.4	1.2	–	–	–	–	–	–

Summative statiscs for 12 glaciers. Categories correspond to Melt-Dominated (MD), Calving-Dominated (CD), Sustained Retreat (SR), Floating Extension (FE), and Shallow Bathymetry (SB) glaciers (see Section 4.2). R is glacier retreat, F is the total ice advection, M is the total ice melted, M^{anom} is the total ice melted above the baseline melt rate, M/F is the fraction of advected ice which was melted, M^{anom}/R is the fraction of retreat attributable to the melt anomaly. See section 3.6 for a descriptive interpretation of these results.

Table A.13: Overview of N Glaciers during 1992-2018

Glacier	Cateogry	Depth (m)	$\overline{q_m}$ (m/d)	R (km^2)	R (km)	F (km)	$F+R$ (km)	M (km)	M^{anom} (km)	$M/(F+R)$ (%)	M^{anom}/R (%)
Hagen Br.	FE	76	–	190.6	16.4	–	–	–	–	–	–
Academy Gl.	AR	191	–	20.8	2.5	6.7	9.2	4.2	–	45.7	–
Marie Sophie Gl.	MD	193	0.34	3.9	1.0	3.1	4.1	3.2	0.09	78.0	9.0
Adams Gl.	SB	1	–	3.3	1.3	–	–	–	–	–	–
Naravana Gl.	SB	1	–	5.9	2.6	–	–	–	–	–	–
Jungersen Gl.	SB	0	–	11.9	4.4	–	–	–	–	–	–
Brikkerne Gl.	SB	37	–	2.6	0.6	–	–	–	–	–	–
C.H. Ostenfeld Gl.	FE	189	–	15.4	2.0	–	–	–	–	–	–
Ryder Gl.	FE	539	–	64.6	7.6	–	–	–	–	–	–
Steensby Gl.	FE	112	–	62.9	15.8	–	–	–	–	–	–
Newman Gl.	SB	1	–	1.1	0.7	–	–	–	–	–	–
Petermann Gl.	FE	825	–	363.6	23.0	–	–	–	–	–	–
Humboldt Gl.	MD	146	0.18	280.0	3.2	7.1	10.3	1.7	1.62	16.5	50.6
Dodge Gl.	SB	3	–	2.3	0.7	–	–	–	–	–	–
Storm Gl.	SB	2	–	0.7	0.4	–	–	–	–	–	–
Diebitsch Gl.	SB	1	–	5.3	1.6	–	–	–	–	–	–
Morris Jesup Gl.	MD	27	0.06	3.0	1.0	3.2	4.2	0.5	0.15	11.9	15.0
Verhoeff Gl.	SB	2	–	1.5	0.5	–	–	–	–	–	–
Bowdoin Gl.	MD	158	0.36	4.0	1.6	5.0	6.6	3.5	1.40	53.0	87.5
Hubbard Gl.	MD	40	0.07	2.3	1.0	2.1	3.0	0.7	0.24	23.3	24.0
Hart Gl.	MD	35	0.14	1.6	0.8	3.1	3.9	1.4	0.11	35.9	13.7
Sharp Gl.	MD	87	0.54	0.9	0.6	7.8	8.3	5.1	-0.65	61.4	–
Melville Gl.	MD	41	0.06	1.7	1.1	21.0	22.1	0.5	0.46	2.3	41.8
Farquhar Gl.	SB	185	–	6.9	3.3	–	–	–	–	–	–
Tracy Gl.	MD	251	0.32	39.1	8.0	25.9	33.9	3.0	2.36	8.8	29.5
Heilprin Gl.	MD	192	0.31	8.7	0.9	18.8	19.6	3.0	2.18	15.3	>100
Leidy Gl.	SB	45	–	3.5	0.9	–	–	–	–	–	–
Harald Moltke Br.	MD	54	0.14	23.4	3.8	7.1	10.9	1.3	0.50	11.9	13.2

Summative statiscs for 28 glaciers. Categories correspond to Melt-Dominated (MD), Calving-Dominated (CD), Sustained Retreat (SR), Floating Extension (FE), and Shallow Bathymetry (SB) glaciers (see Section 4.2). R is glacier retreat, F is the total ice advection, M is the total ice melted, M^{anom} is the total ice melted above the baseline melt rate, M/F is the fraction of advected ice which was melted, M^{anom}/R is the fraction of retreat attributable to the melt anomaly. See section 3.7 for a descriptive interpretation of these results.